Thermal mass and thermal bridging effects on transient thermal performance of walls and energy performance of office buildings

Benyamin Salehpour

A Thesis

in

The Department

of

Building, Civil, and Environmental Engineering

Presented in Partial Fulfillment of the Requirements

for the Degree of Master of Applied Science (Building Engineering) at

Concordia University

Montreal, Quebec, Canada

April 2022

CONCORDIA UNIVERSITY

School of Graduate Studies

This is to certify that the thesis prepared

By: Benyamin Salehpour

Entitled: Thermal mass and thermal bridging effect on transient thermal performance of walls and energy performance of office buildings

and submitted in partial fulfillment of the requirements for the degree of

Master of Applied Science (Building Engineering)

complies with the regulations of the University and meets the accepted standards with respect to originality and quality.

Signed by the final Examining Committee:

_____ Chair

Dr. Radu Zmeureanu

_____ Examiner

Dr. Bruno Lee

_____ Examiner

Dr. Radu Zmeureanu

_____ Supervisor(s)

Dr. Hua Ge, Dr. Mehdi Ghobadi

Approved by _____

Dr. Ashutosh Bagchi Chair of Department

_____ 2022 _____

Dr. Mourad Debbabi Dean of Faciliy

ABSTRACT

Thermal mass and thermal bridging effects on transient thermal performance of walls and energy performance of office buildings

Benyamin Salehpour

The increased requirements of buildings to reduce energy use has highlighted the importance of accounting for all factors that influence energy use in buildings. Thermal performance of the walls, as part of the building envelope systems, can contribute to the overall energy use and greenhouse gas emissions of the buildings. In this research, effects of thermal mass and thermal bridges on transient thermal performance of walls were assessed. Specifically, the impact of different placements of material layers within wall assemblies on the transient thermal performance of the concrete-based walls, and the energy performance of an office building, were investigated. Three case study sinusoidal outside temperature profiles, representative of heating-dominated, cooling-dominated, and temperate climates, were considered for studying the thermal performance of the walls. It was concluded that placing the thermally massive component in the middle layer of walls led to the lowest amplitudes of heat fluxes and indoor surface temperatures, as well as the lowest decrement factor and the longest time required to reach quasi-steady state conditions. On the other hand, weather conditions of three cities, Montreal, Miami, and Denver, were taken into account for the assessment of energy performance of an office building. It was concluded that the wall whose thermally massive layers are exposed to the indoor and outdoor weather conditions had the best performance amongst the cases studied. The second part of this research was devoted to presenting a method for taking into consideration the effects of steel and wood studs, as the thermal bridging elements, on dynamic thermal behavior of the walls. Three sinusoidal outside temperature conditions were assumed, and thermal performances of two case study walls under these conditions were assessed: a steel stud wall and a wood-frame wall. It was concluded that the maximum deviation between the instantaneous surface heat fluxes of the original steel stud wall and those of the corresponding equivalent wall was less than 5% while the deviations were dependent on the climate conditions for the wood-frame wall case.

Acknowledgements

To my mother, father, and brother, who I missed the most. They endlessly supported me whenever I encountered a new challenge both in my personal and professional life. Until the very last moment of my life, I am thankful of such a great family. They changed my life forever and made my life meaningful.

To my supervisors, Dr. Ge, Dr. Ghobadi, and Mr. Moore, who guided me throughout my master's journey. I could not be at the place I am right now without their useful pieces of advice. They trained a young professional in the most appropriate manner, and I am truly thankful of them because of the lessons they taught me.

To my colleagues at National Research Council (Canada), who added excellence to my research by such fruitful discussions. The opportunity of working at NRC was the best starting point of my professional career, which I will not forget for the rest of my life.

To my friends, who were my family in Canada, and as Joey says in "Friends" series: "nothing is more important in the whole world than family". They made my problems look much easier than they actually were. They make my life colorful; they add joy and passion to my existence. Specifically, my deepest appreciations go to Setiya Javadpour, Mohammad Vaseghi, Mehdi Dehghani, and Sina Tavassoli, who were there for me during my happiest and toughest times.

The Author would like to acknowledge the financial support from NRC, NSERC Discovery Grant, and Concordia Gina Cody School of Engineering and Computer Science throughout this investigation.

Table of contents

List of figures

List of tables

CHAPTER 1: Introduction and Motivation

1.1. Background

Energy use is of great importance when considering the economic growth of countries and environmental footprints. Global economy growth has forced governments to make proper policies to address the obstacles of energy supply and to develop novel methods for decreasing the environmental impacts of industries. Energy intensity factor (E/GDP) is globally accepted as an indication of countries' performance in managing the energy consumption. Canada, as a member of the G20, plays an important role in determining the aspects of energy efficiency and measures required to be taken to decrease the energy use. Canada's energy efficiency is significant to the worldwide energy use [1,2,3].

Another consideration is the rising costs of energy resources worldwide and especially in Canada. According to statistics Canada [3] the costs of electricity in September 2021 increased by nearly 30% compared to those of September 2010, and by nearly 80% compared to those of September 2000. Although the COVID-19 outbreak initially led to a drastic decrease in the energy source prices, the costs of energy sources have started to considerably increase, again [4]. For example, from April 2020 to September 2020, the costs of crude energy products have been almost doubled according to Statistics Canada [4].

As a measure to reduce the energy consumption and environmental footprints in Canada, a recent clean growth and climate change framework developed by the Canadian government [5] has set the goal of reducing the Greenhouse Gas (GHG) emissions by 45% until 2030 compared to the amount emitted in 2005. On the other hand, buildings' heating, cooling, and lighting are responsible for nearly 28% of total energy consumption in Canada [6], which signifies the importance of finding new ways for improving the energy performance of the buildings. In addition, according to the results of a survey published by National Resources of Canada (NRCan) [7], nearly 20% of total buildings' energy consumption in Canada is devoted to offices.

1.2. Problem statement

According to the International Energy Agency (IEA) [8], climate conditions, Heating, Ventilation, and Air Conditioning (HVAC) systems, building envelope, interior design, operation and maintenance, and occupancy behavior are the six parameters affecting the energy consumption of

the buildings. Components of a building envelope, as well as their configurations can affect the overall energy performance of the buildings. Thermal mass and thermal bridges are amongst the factors that can contribute to the overall thermal performance of the building envelope and the energy consumption of the buildings. Thermal mass is the ability of the components to store heat, which can affect the energy demand of the buildings and the thermal comfort of the occupants [9]. Employing materials with a high capacity for storing heat leads to the potential energy demand reduction and improving the thermal comfort of the occupants [3,11-14].

On the other hand, thermal bridges are parts of a building envelope where the uniformity of thermal resistance is considerably affected. For example, wherever a material with a different thermal conductivity fully or partially penetrates through a building envelope, or there is a change in the thickness of a fabric or a junction between two components of the building envelope, thermal bridges occur [15]. Higher heat flows can be identified at these places compared to the neighboring spots. They are a bypass for heat flow, and the more the insulation level without the thermal bridging element is, the higher the thermal bridging effect will be due to the existence of a thermal bridge [16]. Places with the highest potential for thermal bridging effect are shown in Figure 1. Thermal bridges affect the energy performance and durability of the buildings. They increase the heat losses during winter time and heat gains during summer time [17,18].

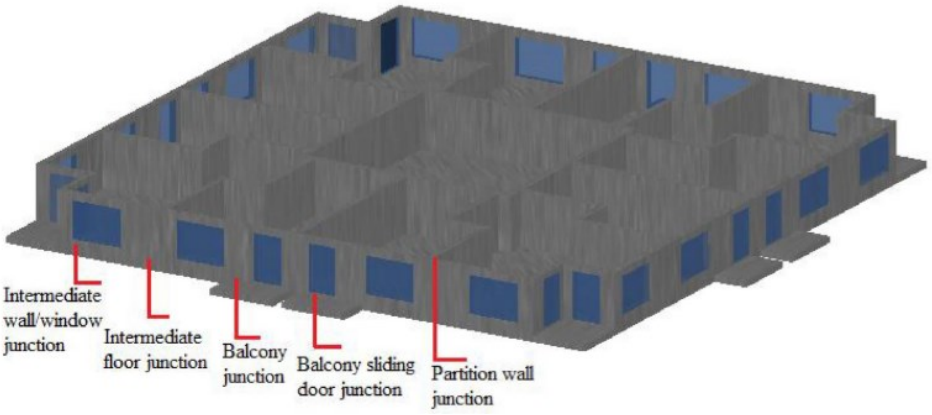

Figure 1. Examples of thermal bridges [19]

One of the other thermal bridging elements can be found within steel stud and wood-frame walls, where the frames can be the potential sources of higher heat losses due to their higher thermal conductivities [20,21]. Also, regarding the fact that steel stud walls are usually considered as assemblies with low thermal mass, the effects of thermal bridges on the thermal performance of

these walls, as well as on the energy performance of buildings that contain these walls as part of their building envelope, are more tangible [22].

Assessing the thermal performance of the envelope systems of the buildings are divided into two stages, namely thermal performance of envelope components themselves without investigating their contribution to overall energy performance of the buildings; and the impact of envelope design parameters on overall energy use of buildings. In terms of assessing the thermal behavior of the building envelope components, different methodologies can be utilized including analytical methods (such as the calculations of the steel and wood stud thermal bridges presented in ASHRAE Fundamentals Handbook [23]), experimental methods (such as Guarded Hot Box models), and numerical methods (such as heat transfer assessment in COMSOL Multiphysics © software) [24-31]. On the other hand, analytical methods are not capable of considering all components that can contribute to the energy demand of the buildings when assessing the thermal performance of the buildings. In addition, although some investigations were performed [32-34], experimental methods for real buildings are rather rare, and usually numerical methods are preferred. Developing Resistance-Capacitance (RC) models and numerically solving the governing equations, and using whole building energy simulation tools, are the most common methods used for evaluating the thermal performance of the buildings [11, 35, 36].

1.3. Objectives and scope

The main purposes of this research are as follows:

- Assessing the effects of thermal mass of the walls, and the placement of thermally massive layer within wall assemblies, on the transient thermal performance of the walls, as well as the energy demand of the buildings
- Evaluating the effects of steel and wood studs on the transient thermal performance of wall assemblies
- Presenting a method for taking into account the effects of thermal bridges on the transient thermal performance of stud walls, which can affect the energy performance of buildings containing studs walls as part of their building envelopes

This study contains two stages, namely simulating the thermal performance of the walls as separate elements by the means of heat transfer simulations in COMSOL Multiphysics © software, and the

assessment of the energy demand of a typical office building using EnergyPlus © and OpenStudio © whole building energy simulation software tools. Specifically, the impact of placement of thermally massive layer within the wall assemblies (i.e. different wall configurations) on the transient thermal performance of the walls and the energy performance of the buildings were assessed. Different climate conditions representing heating-dominated, cooling-dominated, and temperate climates were considered, and the simulations were performed. As for the effects of thermal mass, the results of the thermal performance assessments of the walls were compared to those of the whole building energy simulations. On the other hand, the effects of thermal bridges on the transient thermal performance of the stud walls were assessed, and a method was presented for taking into account the effects of thermal bridges on the transient thermal performance of the walls. Currently, common whole building energy simulation tools are not capable of considering the effects of thermal bridges occurred within stud walls, which may result in misleading heating and cooling demands. The presented method can be used to correctly simulate the performance of stud walls when assessing the energy performance of a building that contain stud wall assemblies.

1.4. Thesis outline

Chapter 2 is devoted to a literature review on two main topics: (i) effects of thermal mass and thermally massive layer placement on transient thermal performance of walls, as well as energy performance of buildings; and (ii) thermal bridging effect in stud walls.

Chapter 3 outlines methods used for this investigation. Instead of presenting details and design specifications of case studies, this chapter gives a general understanding of the problems and the procedures that this investigation follows for solving these problems.

In chapter 4, firstly, design parameters and specifications of our case studies are presented for each section of this investigation. Next, results of our analysis, as well as a thorough discussion on these results, are given.

Chapter 5 concludes the main findings of this investigation, and suggests the potential future work in this field.

CHAPTER 2: Literature Review

This chapter aims to review the available literature considering the following topics:

- The effects of thermal mass on the thermal performance of the walls and the energy consumption of the buildings
- The effects of thermally massive layer placement within the wall assemblies on the thermal performance of the walls, as well as the energy performance of the buildings
- Methodologies used to account for the thermal bridging effect
- Available standards which take into consideration the thermal bridging effect
- Equivalent wall method

Considering the thermal mass effect, the literature was categorized based on the climate conditions, under which the investigations were performed. Other key parameters for categorizing the literature were the methods used and the performance indicators considered for assessing the performance of case studies. On the other hand, as for the thermal bridging effect, available standards and codes considering thermal bridges were initially presented. Then, other articles and papers were reviewed and the comparisons were made. Finally, different methods for proposing an "equivalent wall" were presented and compared.

The main purpose of this section is to describe the fundamentals of assessing the thermal mass and thermal bridging effects and different methods for such an assessment, as well as comparing the results and finding, which contributes to identifying knowledge gaps and proposing feasible solutions. Available literature regarding both the thermal performance of the wall assemblies and the energy performance of the case study buildings were reviewed and the comparisons were made. In what follows, the reviewed literature, along with the results of the comparisons and a conclusion, will be presented.

2.1. Thermal mass effect

2.1.1. Materials' sequence effect

Amongst the essential design parameters of envelopes containing thermally massive walls, the possibility of improving the energy performance and thermal comfort of the buildings as a result of the choice of wall layers' configuration (i.e. sequencing of layers) has been a topic of interest for many papers. In the following sections, the available literature categorized based on the climate conditions, under which the investigations were performed, will be reviewed, and their results and conclusions will be compared and discussed.

2.1.1.1. Heating-dominated climate

Assessing the thermal performance of the walls with different configurations and insulation layer thicknesses and performing a cost analysis to find the optimum insulation layer thickness under the climate conditions of Elazig City, Turkey, was the objective of a work done by Ozel [37]. They found that the case of having an outside insulation layer of 8.2cm had the optimum performance.

In another study by Ozel and Pihtili [38], the thermal performances of the walls with one, two, and three insulation layer(s) under the same climate conditions using time lag and decrement factor as the performance indicators were investigated. July 15th and January 15th were chosen to represent typical summer and winter days, respectively, and according to the hourly actual climate data of for the city of Elazig, Turkey, corresponding sol-air temperatures accounted for the outdoor boundary conditions. 23°C and 20°C were assumed as the indoor air temperature conditions during the typical summer day and winter day, respectively. They concluded that the case of halving one-third of the insulation thickness at the outermost layer, another one-third in the middle of the wall, and the rest at the innermost layer performed optimally.

Carlier et al. [35] studied the impact of using Switchable Insulation Systems (SIS), the systems whose R-values can be changed by adjusting a parameter (e.g. a geometrical parameter) of the system, within the wall assemblies, as well as different wall configurations, on the energy savings potential of two case study buildings, namely a detached building and an apartment. It was observed that the SIS layer should be placed as close to exterior as possible, and the thickness, thermal mass, and thermal resistance of the layer in front of the SIS layer (closer to the outdoor conditions) should be as low as possible to maximize the SIS benefits. Also, they concluded that

it is better to place the thermally massive layer (with a low thermal resistance) as the innermost layer to be able to store free-heating/cooling thermal energy.

Using the Particle Swarm Optimization (PSO) algorithm implemented in FORTRAN, Yang et al. [39] investigated the optimum sequencing pattern for the walls according to the heating and cooling loads. They also studied the corresponding energy savings potentials. Beijing (cold), Harbin (severe cold), Shanghai (hot summer, cold winter), Guangzhou (hot summer, warm winter), and Kunming (moderate) climate conditions for January and July were taken as case study exterior boundary conditions, and the indoor air temperatures during January and July were assumed to be maintained at 18°C and 26°C, respectively. Taking C_t and R_t as the total heat capacitance and total thermal resistance of a wall assembly, respectively, Table 1 shows the optimal sequencing of layers for different cities.

Table 1. Optimal layer sequences for the 5 representative case study cities [39]

City	Optimal sequencing (from exterior to interior)
Kunming (for a large C_t)	$0.4R_t$-$0.5C_t$-$0.3R_t$-$0.5C_t$-$0.3R_t$
Kunming (for a small C_t)	$0.6R_t$-C_t-$0.4R_t$
Beijing, Harbin, Shanghai, Guangzhou	$0.5R_t$-C_t-$0.5R_t$

Another conclusion of this paper was that there is a linear relationship between the ratio of heating to cooling load and the energy savings potential, with the maximum energy savings potential being observed for the Harbin city.

Hu et al. [11] studied the thermal mass effects on the energy consumption and indoor operative temperature (as a representative of the indoor thermal comfort) for a 20-storey office building with a radiant system under two different climate conditions. Two alternatives were considered as the building's HVAC system: (a) equivalent Convective Air System (CAS) and (b) conventional hydronic system. The simulations were performed in the EnergyPlus © software. Two representative climate conditions, Beijing (cold climate) and Nanjing (hot summer and cold winter), were chosen. Indoor set-point temperature during occupied hours was 26°C. They observed that the peak cooling loads for the case of ESCS was 9-11% higher than those of the equivalent CAS case. In addition, it was found that although placing thermal mass at the outside leaded to slightly lower energy consumptions, inside thermal mass is much more beneficial in terms of the improved thermal comfort and peak energy loads.

Deng et al. [12] studied the effects of thermal mass, insulation placement within the wall assemblies, and the choice of simulation time-interval on the energy savings potential and thermal comfort level of a case study three-occupant residential building. They considered three walls with different thermal storage capacities but the same U-value of 0.83 W/m^2.K (please refer toTable 2). Also, two patterns were chosen for the HVAC systems' operation: part-time (meaning that the HVAC systems operate only when there are occupants in the building) and full-time. Three representative climate conditions, namely Chongqing, Changsha, and Shanghai, were taken into consideration. Comparing the results for the cases with two different HVAC operation schedules, it was found that although the part-time schedule resulted in an energy saving of 25.3-31.8%, the loads on the HVAC systems tend to be much steeper, and 1.4-2.1 times larger mechanical systems would be required. It was mentioned that the internal insulation led to a slightly lower energy consumption, but it increased the overheating risk.

Table 2. Three representative walls for investigating the thermal mass effect [12]

External wall type	Composition (from external to internal wall)	Mass (kg/m^2)	Thermal capacity (kJ/(m^2 K))
Heavy weight	38.7 mm EPS insulation + 15 mm cement mortar + 240 mm reinforced Concrete (RC) + 15 mm plasterboard	644.2	590.4
Medium weight	15 mm cement mortar + 196.5 mm aerated concrete block (ACB) + 15 mm plasterboard	177.1	176.8
Light weight	10 mm stainless steel plate + 47.6 mm EPS insulation + 10 mm stainless steel plate	157.9	80.8

2.1.1.2. Temperate climate

Along with those investigations presented in the previous section, there are other literature, which considered temperate climate conditions. Considering the weather conditions of Rome in Italy, Leccese et al. [36] investigated the effects of thermal mass, insulation layer placement, and the thickness distribution of insulation within the wall assemblies on the dynamic thermal behavior of concrete-based walls. Decrement factor, time lag, and thermal admittance were taken as the performance indicators. Dynamic thermal performances of 20 case studies consisting of four different concrete-based wall assemblies with the same R-value of 3.13 m^2.K/W and five material sequencing patterns were assessed (please refer to Figure 2). The indoor temperature was assumed to be free-floating and was calculated for each case at each time-step considering the thermal properties of the wall assembly and outdoor conditions. It was concluded that the best

configuration is having the thermally massive layer in the middle and two insulation layers with the same thicknesses on both sides of the concrete layer. Also, it was found that for thermally lighter walls, the thickness and distribution of the insulation layer is more important. Moreover, a lighter wall, whose surface mass is less than 230 kg/m^2, with an optimum sequence of materials can perform better compared to a heavier wall with a non-optimal sequence.

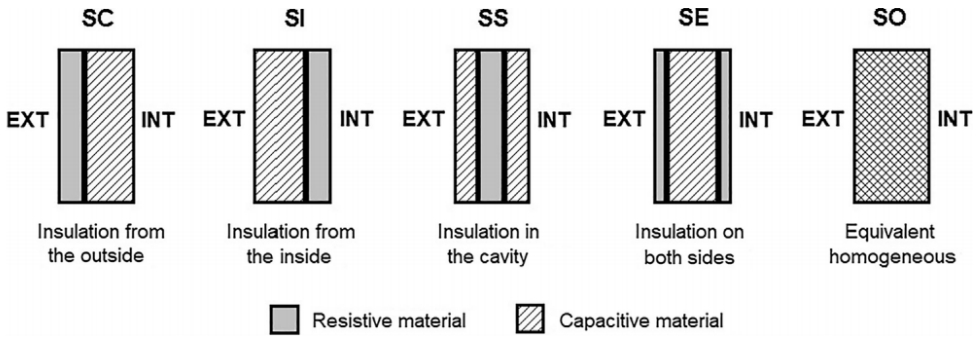

Figure 2. Schematic of different considered layer sequencing patterns

The purpose of the investigation done by Yuan et al. [40] was to determine the optimum sequence of layers according to the heating and cooling loads for a case study office building with an air conditioning system which operates intermittently (operating between 8:00 and 18:00 only). Shanghai hourly sol-air temperature conditions in the period of June 2011 to March 2014 were considered as the outside boundary conditions. It was found that except for the months of June and September, when night-time temperatures are below the set-point temperature, the energy savings potential for the wall cases with the insulation layer placed on the inside, can be at least 18% higher than that of the outside insulation walls for other months. In addition, it was said that the hotter the summers and the colder the winters are, the higher the energy savings potential of the walls with inside insulation.

Baglivo et al. investigated the optimum external wall configurations which are both thermally high-performance and eco-friendly under the climate conditions of Lecce, Italy (warm Mediterranean climate). Utilizing a Z-transfer matrix method, the heat transfer equations for each five-layer wall configuration were solved in MATLAB © software, and the corresponding dynamic thermal performances (heat fluxes and hygrothermal performances) were assessed. Also, in order to ensure the code compliance, a hygrothermal performance test (Glaser), according to EN ISO 13788 test protocol [41], was performed for wintertime (during January and February),

and the indoor surface temperature was screened to assess the condensation risk. It was found that the wall configurations which consist of a thermally massive layer at the inside, followed by a middle layer made of commonly used insulation materials and an outside layer made of eco-friendly insulation materials, can perform best according to the optimization criteria.

Under the same climate conditions and taking indoor operative temperature as a performance indicator, Congedo et al. [13] investigated the effects of the dynamic thermal performances of different wall configurations on the thermal comfort levels of low-rise residential buildings. It was assumed that there is no HVAC systems for cooling/heating. The case studies differed in terms of their component configurations (different placements of the insulation layer) and different layer thicknesses. It has been observed that double-tuff layer walls (especially the one with expanded cork panel as the insulation material) with their thermally massive layer placed at the inside, showed the optimal performance.

Considering the available options for retrofitting residential buildings in Europe, Kolaitis et al. [42] compared the potential benefits of external and internal insulation in terms of energy savings potential, water vapor condensation risk, and cost return period. Three case study walls were assumed, namely a base case with no insulation layer applied and walls with inside and outside insulation layers. To investigate the effect of climatic conditions, meteorological data of Athens, Greece (representative of warm Mediterranean climate) and Kozani, Greece (typical of moderate Oceanic climate) were considered as outside boundary conditions. Indoor air temperature was allowed to fluctuate within 20°C to 26°C range. A residential apartment with a floor area of 99.6m^2 typical of South European construction was taken into account as the case study building. It was found that adding an 80mm-thick EPS insulation either at the inside or at the outside layer can result in a 21-89% reduction in total annual HVAC energy consumption. The exteriorly-insulated case, on average, had 8% more energy savings potential compared to the case with inside insulation. The energy savings were more evident for milder climate conditions.

Carbonari and Scarpa [43] assessed different options for improving the thermal performance of a heavy masonry building located in the temperate climate of Bologna, Italy, as well as its thermal and visual comfort. It was concluded that external insulation would be more beneficial in terms of the energy performance of buildings.

2.1.1.3. Cooling-dominated climate

There are some papers which investigate the optimum wall configurations in cooling-dominated regions. Rosti et al. [44] aimed to find the optimum sequence of layers for buildings with passive air conditioning systems, specifically Earth-Air Heat Exchanger (EAHX) mechanical systems under the climate conditions of Shiraz, Iran. For the purpose of comparison, seven wall configurations with identical thermal storage capacities and R-values were assumed under two alternative HVAC systems, namely conventional, and EAHX. Using decrement factor and time lag as the performance indicators, they observed that the wall with three layers of insulation placed at the inside, middle, and outside of the wall performed best for the case of conventional air conditioning system. The cases of external insulation and internal mass had the optimum thermal performance for the EAHX system.

Al-Sanea et al. [45] studied the effect of thermally massive layer placement and surface absorptivity on the energy savings potential and critical thermally massive layer thickness for case study walls with the same overall R-value of 2.86 RSI for Riyadh, Saudi Arabia. It was concluded that for a given critical thermal mass thickness, walls containing solid concrete block (placed at the inside surface of the insulation layer) with a lower surface absorptivity, had a higher energy savings potential. Under similar climate conditions, Eben Saleh [46] investigated the effects of insulation thickness and placement within the wall assemblies on the overall thermal performance and thermal comfort of a building. Ten different wall assemblies were taken into account, which varied in terms of the insulation thickness and placement (please refer to Table 3). It was concluded that for the hot and dry climate of Riyadh, 5-10 cm insulation thickness placed at the outside of the thermal mass resulted in lower heating and cooling loads and mitigated the thermal bridging effects. Also, they found that despite resulting in lower overall energy loads, by placing the insulation at the outer side, the cooling energy loads during late nights in summers, and heating energy loads during day-time in winters, were higher.

Table 3. Case study wall assemblies

Case studies	Layers (from outside to inside)	Overall R-value (m^2.K/W)
1	20cm concrete	0.118
2	2cm cement plaster + 5cm foam insulation + 20cm concrete	1.314
3	2cm cement plaster + 7.5cm foam insulation + 20cm concrete	1.894
4	2cm cement plaster + 10cm foam insulation + 20cm concrete	2.481
5	20cm concrete + 5cm foam insulation + 2cm cement plaster	1.314
6	20cm concrete + 7.5cm foam insulation + 2cm cement plaster	1.894
7	20cm concrete + 10cm foam insulation + 2cm cement plaster	2.481
8	2cm cement plaster + 5cm foam insulation + 2cm cement plaster	1.215
9	2cm cement plaster + 7.5cm foam insulation + 2cm cement plaster	1.799
10	2cm cement plaster + 10cm foam insulation + 2cm cement plaster	2.381

Table 4 presents a summary of the papers reviewed and compares their performance indicators, weather conditions considered, and the results and findings.

Table 4. Summary of the reviewed literature

	Outdoor climate conditions	Indoor temperature conditions	Performance indicator(s)	Method(s)	Results
[38]	Elzing, Turkey	• Winter: 20°C • Summer: 23°C	• Decrement factor • Time lag	Implicit finite difference method implemented in MATLAB ©	3-layer insulation wall with one-third of the insulation layer placed at the inside, another one-third at the middle, and the rest at the outside layer of the wall had the lowest decrement factor and the highest time lag
[36]	Rome, Italy			RC model in MAPLE ©	Three-layer wall whose thermally massive layer is sandwiched between two insulation layers with identical thicknesses had the lowest decrement factor and highest time lag
[45]	Shiraz, Iran	25°C		Finite difference method (for the case of convenient HVAC system)	
[39]	• Beijing • Harbin • Shanghai • Guangzhou • Kunming	• Winter: 18°C • Summer: 26°C	Heating and cooling loads	Particle Swarm Optimization implemented in FORTRAN ©	Three-layer wall whose thermally massive layer is sandwiched between two insulation layers with identical thicknesses had the lowest heating and cooling loads
[41]	Lecce, Italy		• Steady and periodic thermal transmittance • Decrement factor • Time lag • Heat capacity • Thermal admittance • Surface mass • Thickness • Cost • ITACA score	Heat transfer simulations in MATLAB ©	Exteriorly-insulated wall performed optimally
[13]		Free-floating indoor temperature	• Indoor operative temperature • Hourly energy demand		
[43]	• Athens, Greece • Kozani, Greece	Indoor temperature thresholds: 20°C and 26°C	• Energy savings potential • Water vapor condensation risk • Cost return period	• Simulations in TRYNSYS © • HETRAN © simulations	
[44]	Bologna, Italy	• Winter: 20°C • Summer: 26°C	Energy savings potential	Energy simulations in Enter_Lux ©	
[46]	Riyadh, Saudi Arabia	Maintained at a fixed value		Finite difference method	
[47]		Free-floating indoor temperature	Heating and cooling loads	Pre-defined computer program	
[45]	Shiraz, Iran	25°C	• Decrement factor • Time lag	Finite difference method (for the case of EAHX HVAC system)	
[11]	• Beijing • Nanjing	26°C during people's presence	• Indoor operative temperature (thermal comfort) • Peak energy loads	Energy simulation in EnergyPlus ©	

			Energy consumption		Interiorly-insulated wall had lower energy demands
[40]	Shanghai, China	• Winter: 20°C • Summer: 26°C	Heating and cooling loads	Combined analytical-numerical method implemented in MATLAB ©	Interiorly-insulated walls had at least 18% higher energy savings potential
[35]	• Oostende • Brussels • St Hubert		Energy savings potential	3R2C model implemented in MATLAB ©	• 1.1%-3.7% heating energy and 53.1%-98.7% cooling energy saving potential upon utilizing SIS-integrated walls is achievable • Placing the SIS materials as close to the exterior side of the wall as possible and the thermally massive layer as close to the interior side as possible increased the energy savings potential
[12]	• Chongqing • Changsha • Shanghai	• Winter: 18°C± 1°C • Summer: 26°C± 1°C	Energy savings potential	State-space model implemented in MATLAB ©	Thermal mass did not have a considerable effect on energy demands
			Thermal comfort		Exteriorly-insulated wall case performed better
[37]	Elzing, Turkey	• 20°C during January, February, March, November, and December • 22°C during April and September, • 23°C throughout the rest of the year	Yearly transmission loads	Implicit finite difference	Insulation location did not affect the yearly transmission loads
			Decrement factor		Exteriorly-insulated wall and the wall whose insulation layer is sandwiched between two thermally massive layers had the lowest and highest decrement factors, respectively.
			Time lag		Interiorly-insulated wall and the wall whose insulation layer is sandwiched between two thermally massive layers had minimum and maximum time lags, respectively.

2.1.1.4. Other papers

Taking a sinusoidal curve with maximum and minimum values of 1°C and 0°C, as the outside boundary temperature and 0.5°C as the constant indoor temperature, Asan [47] investigated the effects of insulation thickness and the layer placement within the case study wall assemblies on the decrement factor and time lag. A wall with a total thickness of 20 cm (insulation + thermally massive material) with varying thicknesses of the insulation and thermally massive layers and four different wall configurations shown in Figure 3 were considered.

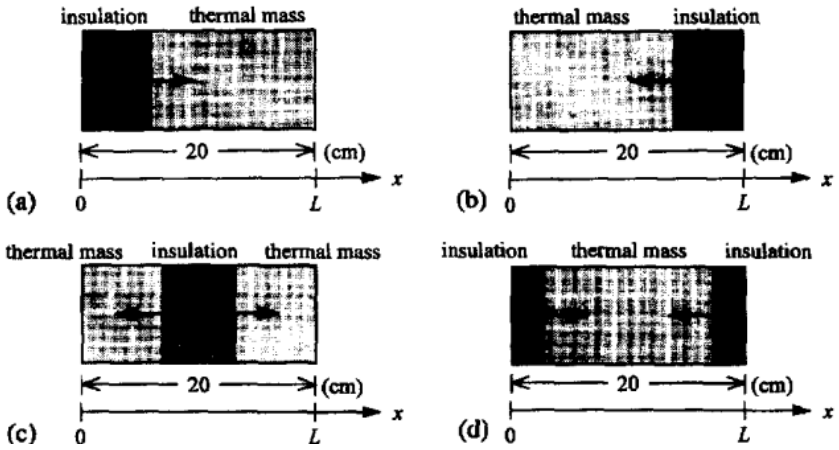

Figure 3. Wall configurations: (a) exterior insulation, (b) interior insulation, (c) lumped insulation at the middle, and (d) half of the thickness at the inside and the other half at the outside [47]

It was found that placing half of the total thickness of the insulation at the inside and the other half at the outside will lead to minimum decrement factor and maximum time lag. By defining an indicator named "coefficient of performance", Ciampi et al. [48] investigated the effects of walls' layer sequencing on the building-plant loads. It was found that for a given total thermal resistance and heat capacity, the case of having two insulation layers with the same thicknesses on both sides of a thermally massive layer will perform better, meaning that the fluctuations observed in the building's load on the plant will be lower.

Gori et al. [49] studied the effects of the number of layers and their order of placement within a wall assembly on the decrement factor and time delay assuming that the total thickness of insulation layers (L_i), as well as that of the concrete layers (L_c), are fixed. Regarding the two-layer walls, it was proven that outside insulation configuration had a lower decrement factor and a higher time lag. On the other hand, denoting the thermally massive layer by C and the insulation layer by I, they found out that the decrement factors for ICI and CIC cases with evenly distributed thicknesses are equal under the assumed conditions. Finally, they concluded that IC-configured wall performed better than the ICI-configured wall, meaning that a two-layer wall with outside insulation had a better performance compared to a three-layer wall with a sandwiched insulation layer

By defining "effective wall heat capacity" parameter, Tsilingiris [50] investigated the effects of insulation location and distribution within a wall assembly on the transient thermal performance of the walls, specifically the walls' time constant, as well as the stability of a case study building i.e. the building's capability to delay the impact of a change in outdoor temperature on the indoor air temperature and decrease the indoor temperature swings. It was concluded that the walls' length did not affect the effective heat capacity as long as the thermal resistance is evenly distributed within the wall. Also, walls whose insulation layers were placed at the inside, outside and in their middle were considered to investigate the effect of insulation location on the effective heat capacity, and it was found that exteriorly-insulated wall had the best thermal performance.

2.1.2. Thermal mass effect for improving the performance of the walls and buildings

In addition to the literature which regarded the wall configurations' effect, there are other papers which investigated the thermal mass effect on the transient thermal performance of the walls and the energy demand of the buildings. Amongst the concrete-based wall assemblies, Insulated Concrete Form (ICF) and tilt-up walls are two popular assemblies in North American construction. These durable walls have different benefits such as reduced construction time and improved thermal performance due to better airtightness [51]. The core of an ICF wall contains one layer of concrete sandwiched between two layers of insulation while a tilt-up wall is made of an insulation layer sandwiched between two concrete layers. Two rather similar investigations that considered the thermal performance of the ICF and tilt-up walls were the ones performed by Kosny et al. [52] and Doebber and Elis [53]. Considering Minneapolis/Denver (Cold), Washington DC/Atlanta (Temperate), Phoenix/Miami (Hot) as representative climate conditions, they investigated the effects of thermal mass and reduced air-infiltration rate on the total energy demand of a single-storey ranch house by simulating the energy performance of the building. An ICF and 10 wood-frame walls were the case studies for [52] while [53] compared the performances of the building taking a waffle Precast Concrete Panel (PCP), sandwich PCP, conventional wood-frame, highly-insulated wood-frame, and ICF as different case study walls. One consideration for both papers was the assumption of lower air-infiltration rates for the concrete-based walls. It was concluded that the effects of thermal mass and infiltration rate on the energy saving depended on the climate conditions, and that heating and cooling loads as a result of air leakage are very important.

Investigating the possibility of improving the thermal performance of the buildings by the means of thermal mass effect was also seen in other investigations. Li et al. [14] investigated the possibility of increasing indoor thermal comfort and decreasing energy consumption of a case study four-storey residential building with the intermittent heating system by taking advantage of a Phase Change Material (PCM) layer integrated in the walls. Considering thermally massive structures typical of Tunisian construction, Daouas [54] investigated the effects of wall orientation on yearly transmission loads and energy savings potential and found the optimum insulation thickness according to a life-cycle cost analysis. Zilberberg et al. [10] developed a new methodology to optimize the thickness of the buildings' structural elements according to the operational and embodied energy consumption taking into account heavyweight walls. Ekrami et al. [55] identified strategies and systems for improving the energy performance of the buildings with concrete-based components. Specifically, they mentioned that ICF walls with embodied pipes can have improved thermal performances. Saber et al. [52,57,58] performed both field tests and thermal performance simulations for two case study ICF walls located in Ottawa, Canada. They found that the benefits of thermal mass is more evident during summers in Ottawa. Also, thermal mass contributed to dampening the fluctuations.

2.2. Thermal bridging effect in steel stud and wood-frame walls

Amongst the different construction types, Lightweight Steel-Framed (LSF) and wood-frame structures are considered in this investigation. Some of the advantages of LSF construction are reduced number of staff required, higher construction speed, lower environmental footprint as a result of recyclability of the wastes, and reduced required budget [20,22,59-61]. The structure is made of repeating steel studs standing vertically and steel runners configuring horizontally. On the other hand, cost-effectivity, sustainability, higher thermal mass compared to the LSF construction, which brings the potential of improving thermal comfort of the occupants, and environmental-friendliness are some of the advantages of wood-frame construction [61]. Wood-frame structures consist of repeating vertical and horizontal wood studs.

Despite all the aforementioned advantages, thermal performance of the stud walls can be affected due to the so-called 'thermal bridging effect'. Thermal bridges are parts of a building envelope where the uniformity of thermal resistance is considerably affected [62]. Due to the relatively higher thermal conductivity of steel and wood compared to the insulation, thermal bridges occur due to the presence of steel and wood studs. Heat transfer is multi-dimensional at the place of studs, which results in an ununiformed distribution of temperature gradient within the wall assembly and an increased heat transfer through the envelope. This problem is more intense for LSF walls because the thermal conductivity of steel is higher than the surrounding insulation, and it reduces the effectiveness of the insulation. Thus, neglecting this effect can lead to the errors in evaluated heat fluxes through the wall, and eventually the heating and cooling demands of the buildings containing stud walls as part of their envelope systems [20,21]. Unfortunately, commonly-used whole building energy simulation software tools are not capable of taking into account the thermal bridging effect. As a result, it is necessary to find feasible ways of considering the thermal bridges, especially those created due to the presence of steel and wood studs.

In what follows, the standards and relevant papers regarding the thermal bridging effect will be presented.

2.2.1. Thermal bridges in standards

Different standards have regulated the methods and procedures for taking into account the thermal bridging effect. ISO 8990 [63] and ASTM C1363 [64] regulate the procedure for finding the

overall thermal transmittance of the stud walls by performing experimental tests, which is called Guarded Hot-Box method. ISO 9869 [65] and ASTM C1155 [66] considered the calculations of in-situ thermal transmittances by means of standardized methods. They consist of temporal measurements of interior and exterior wall surfaces' temperatures, using which the overall U-values of the assemblies can be calculated. On the other hand, ISO 10211 [62] presents a procedure for numerically calculating the overall U-values of the building envelope assemblies by means of computer simulations. The concepts of point and linear thermal bridges are also introduced in the same standard, and by performing tests, the corresponding values for a number of thermal bridges were calculated and presented in a catalogue in ISO 14683 standard [67]. Linear thermal bridges are defined as ones which have a uniform cross-section along one of the orthogonal axes while point thermal bridges are localized areas of additional heat flow which occur only at infrequent locations. An example of point thermal bridge is the penetration of a structural beam [16]. Examples of linear and point thermal bridges are shown in Figure 4.

A b

Figure 4. Examples of thermal bridges: a) a linear and b) a point thermal bridge [19]

ASHRAE Fundamentals handbook [23] presents methods for manually calculating the U-values of the stud walls. Area-weighted parallel path method assumes that there are two heat flow paths perpendicular to the wall's surface, through which heat transfer can be assumed one-dimensional. Then, the overall U-value can be calculated by means of an area-weighted average procedure. This method is proved to be proper for wood-frame walls, but due to the much higher thermal conductivity of steel compared to wood, the method is not applicable to LSF walls [68]. Isothermal plane method assumes that the temperature on either surfaces of a wall component is uniform; thus the parallel paths occur only through the stud cavity and not through the entire wall. Zone and modified zone methods, developed by Kosny and Christian [69], consider an area, which is thermally affected by the presence of studs, and calculates the overall U-value for the affected

zone using the parallel path method. Using the parallel path method, the overall U-value of the wall is then calculated considering the thermal transmittances of the zone and the rest of the wall. Modified zone method was proven to be an effective way of calculating the U-values of the steel-stud walls [23,31].

2.2.2. Assessing the effective thermal transmittance of the stud walls

In addition to standards, other investigations were also done in terms of calculating the overall U-value of the stud walls. Gorgolewski [70] proposed a modified method for calculating the U-values of LSF assemblies based on the one presented by EN ISO 6946 [71]. The analytical method originally outlined in EN ISO 6946 [71] is applicable for building elements including masonry and timber-framed construction but not for LSF construction. By assessing the U-values of 52 case studies using the newly proposed method, and comparing the results with those of the finite element computer models, it was proven that the mean prediction error was less than 3% and the maximum error was 8%. Santos et al. [24] assessed the overall U-values of three case study LSF wall assemblies following four different methods, namely experimental laboratory testing using hot and cold climatic chambers, 3D finite element method simulation using ANSYS CFX ©, 2D finite element method simulation using THERM ©, and utilizing analytical estimations by the means of the tables presented in ISO 6946 [71] standard. A maximum deviation of 2.6% was found between analytical and 2D simulation results. Also, the obtained U-values using these two methods had a better agreement for the case that had vertical studs only. In addition, compared to 3D simulation, 2D simulation proved to be a better method for calculating the overall U-values of the case study walls. Muzzi et al. [72] calculated the R-value of an LSF wall using isothermal plane and ANSYS © finite element simulation methods and found a deviation of 9% between the results.

Infrared Thermography (IRT) has also been the method of interest in the literature for assessing the U-values of the walls. In this method, the average surface temperatures of the Region Of Interest (ROI) are measured, from which the surface-to-surface U-values can be calculated. Taking into account the IRT method and indoor/outdoor air temperatures and heat fluxes, Atsonios et al. [73] proposed two methods for in-situ measurements of LSF walls' overall U-values, namely Representative Points Method (RPM) and Weighted Area Method (WAM). The results for two case study LSF walls were compared to those of the heat transfer simulations performed in COMSOL © following the theoretical procedure presented in ISO 10211 [62]. Results of RPM

were accurate but the deviations from simulation results were below 5% for WAM. Also, these methods were used for a well-known LSF wall case, and the calculated U-values were in good agreement with the theoretical one. Mahmoodzadeh et al. [68] used external IRT method for calculating the U-value of three case study wood-frame walls, and then compared the results with those obtained from the parallel path method and 3D finite element computer simulation implemented in Siemens NX ©. The magnitudes of deviations of results obtained from the thermography measurements compared to those of the computer simulations were in the range of 10-11.53%. Also, in the absence of a highly-conductive material such as steel, the thermal transmittances calculated following IRT and parallel path methods are compatible with errors less than 6%.

2.2.3. Assessing the thermal bridging effect in stud walls

There have been some studies considering the identification and assessment of the thermal bridges and their impact on the thermal performance of stud walls. Major and Kosin [74] investigated the heat loss through three case study walls: one case study wood-frame and two case study steel-stud walls. Five climate conditions in Poland, namely Gdansk, Poznan, Czestochowa, Olsztyn, and Zakopane, were chosen, and the corresponding heat losses during winters through these walls were evaluated. ANSYS © software was used to numerically simulate the heat transfer phenomena through the walls. It was concluded that the heat losses through the wood-frame wall were lower, and also "Thermo" steel-stud walls perform better than "Full" steel-stud structures. By calculating the monthly cooling and heating energy savings of a residential building, Soares et al. [75] studies the effects of utilizing drywalls made of Phase Change Materials (PCM) for improving the thermal performance of LSF walls under seven representative European climate conditions. EnergyPlus © and GenOpt © software tools were used to find the optimum solution with regard to the thermophysical properties of PCM. It was concluded that the presence of PCMs can lead to the energy savings of 10-46% under the climate conditions considered, except for the Csb-Coimbra climate, under which the energy saving potential is nearly 62%. Also, for each climate condition, an optimum solution can be found, however, the optimum thickness of the PCM-drywall is 4cm for all cases. Purdy and Beausoleil-Morrison [76] specified thermal sub-zoning of the building, thermal bridges of the envelope system, and the infiltration modelling method as the important design parameters affecting the heating and cooling demands of a typical wood-frame Canadian

house located in Ottawa, Ontario. In a similar investigation, and by comparing the heating and cooling demands of a typical light steel residential building under Csb climate conditions, Santos et al. [77] identified the essential parameters for designing the optimum building envelope system, namely the thermal insulation of the opaque parts, design parameters of the fenestrations, overhang size, and ventilation rate. Roque et al. [28] investigated the impact of steel frame on the thermal performance, as well as the performance of the sound insulation, of LSF walls using THERM © and INSUL © software tools. It was found that the type and position of steel frame has a considerable impact on the thermal performance of steel-stud walls, such that the difference between U-values of walls with and without steel frame can differ by up to 82% with regard to the type and position of steel frame. However, by applying a continuous insulation layer on the exterior side of steel frame can reduce this difference to less than 1%, implying that this could be the most suitable measure to reduce the thermal bridging effect as a result of steel frame's presence.

As mentioned earlier, currently, common whole building energy simulation software tools are not capable of taking into account different types of thermal bridges, including those that occur due to the existence of the studs. Along with what standards present, a number of papers intended to propose methods using which the thermal bridging effect can be implemented in the whole building energy simulation tools. Using transfer function method, Ascione et al. [78] proposed a method for calculating bi-dimensional heat flows. They evaluated the heat flows through two case study thermal bridges and validated the results by comparing them to those of a finite volume method. Maximum error between the results for the time step of 1h was 4.5%. Viot et al. [30] assessed the validity of the results produced by following different existing methods of accounting for the steady-state and dynamic effects of thermal bridges on the thermal performance of wood-frame walls. The heat transfer through the stud walls was simulated using COMSOL Multiphysics © software. They concluded that in the case of wood-frame walls, using the catalogue values for linear thermal bridge coefficient lead to a considerable overestimation of the additional heat losses. Also, it was noted that neglecting the dynamic effects of wood studs results in erroneous heat fluxes, and that the existing methods are not applicable for considering dynamic effects of wood studs. Similarly, Yu et al. [60] reviewed different calculation methods presented to account for the thermal bridging effect for LSF assemblies and precast sandwich walls with steel connectors, and concluded that more precise and comprehensive methods are required.

Specifically, there are three investigations, which considered the dynamic thermal performance of steel-stud and wood-frame walls and proposed methods for evaluating the thermal bridging effects. Gomez et al. [31] investigated the thermal bridging effect on the thermal performance of LSF buildings in Brazil. Two case study commercial buildings were considered, and using EnergyPlus ©, corresponding energy consumptions were calculated. They replaced the stud cavity of the wall by a homogeneous layer, such that the overall thermal performances of the real wall and the fictitious wall containing the homogenous layer instead of the cavity are identical. Modified zone method was used to calculate the equivalent thermal resistance of the fictitious layer, while an area-weighted average and a mass-weighted average approaches were taken for calculating the density and specific heat capacity of the layer, respectively. They concluded that the existence of metal studs increased the peak thermal load by nearly 10%. On the other hand, Viot et al. [30] and Purdy and Beausoleil-Morrison [76] utilized parallel path method for calculating the thermal resistance and the same methods as [31] for obtaining the equivalent density and specific heat capacity of the homogeneous layer replacing the wall cavity for case study wood-frame walls.

2.3. Summary

2.3.1. Thermal mass and thermally massive layer placement within wall assemblies

In this section, available literature on effects of thermal mass and layer sequencing of walls on transient thermal performance of walls and energy performance of buildings under different climate conditions was reviewed. Decrement factor, time lag, heating and cooling loads (energy savings potential), and thermal comfort were the main performance indicators amongst the papers. Although results and conclusions highly depend on the cases studied, either walls whose thermally massive layer(s) was (were) sandwiched between two insulation layers or exteriorly-insulated walls were proven to have minimum decrement factors and maximum time lags. On the other hand, conclusions about which wall resulted in lower energy demands were controversial. Although different papers discussed the effects of thermal mass and optimum sequence of wall layers on thermal performance of walls and energy demand of buildings, this investigation aims to answer the following questions:

- To what extent thermal performance of walls under transient conditions is dependent on layer sequencing of walls?
- Can thermal mass and wall layer sequencing affect the energy performance of buildings?

- Regarding the transient thermal performance of walls and the energy performance of buildings, is optimum sequence of wall layers different under different climate conditions? Is it dependent on other design parameters such as indoor set-point temperature?
- Is there a link between the transient thermal performance of walls and energy performance of buildings (i.e. are optimum sequences of wall layers similar)?

2.3.2. Stud thermal bridges

In addition, papers and standards which considered the effects of thermal bridges due to the presence of studs on transient thermal performance of walls were reviewed. Different methods for taking into account the effects of thermal bridges on the transient thermal performance of stud walls were presented. Next, available literature regarding the impact of thermal bridges in stud walls on the energy performance of buildings was presented. The importance of thermal bridging effect on the thermal performance of steel-stud and wood-frame walls has been identified and methods have been proposed to take it into account. However, to the best of authors' knowledge, a validated simplified method which can help the energy simulators consider the effect of thermal bridges of stud walls in a rather straightforward manner, is missing. In fact, a method is required that can present, for each stud wall assembly, an equivalent wall which has the following characteristics:

- Heat transfer phenomena over the equivalent wall should be one-dimensional because common whole building energy simulation tools only take multi-layer walls that have homogeneous layers.
- Transient thermal performance of the equivalent wall should be as similar as possible to that of the original stud wall.

CHAPTER 3: Methodology

In this section, the procedure followed to assess the thermal mass and thermal bridging effects is described. Instead of presenting the cases and specifications, this chapter considers the general process and the idea behind this investigation. In the following sections, firstly, the procedure for assessing the thermal mass effect, as well as the impact of materials' sequence within the case study wall assemblies, on transient thermal performance of walls and energy performance of a case study office building is described. Next, available methods for assessing the thermal mass effect, and specifically the method followed in this research is presented, and finally, the method for taking into account the thermal bridging effect in the stud walls is discussed.

3.1. Assessing the thermal mass effect on the thermal performance of the walls

In this section, a method for assessing the impact of thermal mass on the transient thermal performance of four case study walls are presented. This method also considers the effects of thermally massive layer placement within a wall assembly on the transient thermal performance of walls. Three case study walls were considered: an ICF wall, a tilt-up wall, and a wall made of one layer of EPS insulation. Thermal resistance of these walls were identical. Also, overall heat storage capacity of ICF and tilt-up cases were identical but that of EPS wall was much lower. Firstly, two sinusoidal outside temperature profiles representative of heating-dominated and cooling-dominated climates were considered as outside boundary conditions. Then, sol-air temperature for Montreal, Canada and Miami, U.S.A. were taken as outside boundary conditions. Indoor temperature was maintained at 20°C throughout the year. Transient thermal performance of the case study walls under these climates were assessed using COMSOL Multiphysics © simulation software. ISO 10211 [62] regulates that the results of a heat transfer simulation can be reliable if the simulation software is cable of producing certain results for four case studies. These case studies are presented in ISO 10211[62]. In order to make sure that COMSOL © is capable of performing our required heat transfer simulations, validation of results for those four case studies were done. Case studies, as well as simulation case setups and results, are presented in Appendix.

The main governing equation for evaluating the thermal performance of the case studies is the heat conduction across each of these walls. Three-dimensional form of the heat conduction equation is as follows:

$$\frac{\partial}{\partial x}\left(k\frac{\partial T}{\partial x}\right)+\frac{\partial}{\partial y}\left(k\frac{\partial T}{\partial y}\right)+\frac{\partial}{\partial z}\left(k\frac{\partial T}{\partial z}\right)+q_v=\rho c_p\frac{\partial T}{\partial t} \quad (1)$$

For the specific cases of our interest, as there is no thermal anomaly in the geometries, heat is only conducted across the walls to the direction normal to wall surfaces. As for the first step, steady-state conditions are applicable. Also, there is not any heat generation within the assemblies. Thus, the governing equation will be as follows:

$$\frac{\partial}{\partial x}\left(k\frac{\partial T}{\partial x}\right)=\rho c_p\frac{\partial T}{\partial t} \quad (2)$$

Regarding the sol-air temperature conditions of Montreal and Miami, firstly, annual sol-air temperatures for these cities should be calculated. Total solar radiation incident on a surface is as follows [79]:

$$E_s=E_{bn}\cos\theta+E_dR_d+\rho ER_r \quad (3)$$

Where:

E_s: Total solar irradiance incident on a surface $\left[\frac{\mathrm{W}}{\mathrm{m}^2}\right]$

E_{bn}: Beam normal solar irradiance $\left[\frac{\mathrm{W}}{\mathrm{m}^2}\right]$

θ: Incident angle [degrees]

E_d: Diffuse solar irradiance $\left[\frac{\mathrm{W}}{\mathrm{m}^2}\right]$

ρ: Ground reflectivity

E: Global horizontal irradiance $\left[\frac{\mathrm{W}}{\mathrm{m}^2}\right]$

In addition, R_d and R_r can be calculated using Equation 13 and Equation 14, respectively:

$$R_d=(1+\cos s)/2 \quad (4)$$

$$R_r=(1-\cos s)/2 \quad (5)$$

Where s is the tilt angle of the surface. Beam normal, diffuse, and total horizontal solar irradiances can be found in the weather file containing TMY data for each city from the EnergyPlus website [80]. Then, sol-air temperature (in °C) can be calculated using the following equation [23]:

$$T_{sol-air} = T_o + \frac{\alpha E_s}{h_o} - \frac{\varepsilon \Delta R}{h_o} \quad (6)$$

Where:

T_o: Outside temperature [°C]

α: Surface solar absorptance

h_o: Outside convection/radiation coefficient $\left[\frac{\mathrm{W}}{\mathrm{m^2.^\circ C}}\right]$

ε: Hemispherical emittance of the surface

ΔR: Difference between emitted radiation by blackbody at outside air temperature and long-wave radiation incident on the surface $\left[\frac{\mathrm{W}}{\mathrm{m^2}}\right]$

For a vertical surface, e.g. walls, equation 15 becomes:

$$T_{sol-air} = T_o + \frac{\alpha E_s}{h_o} \quad (7)$$

3.2. Effects of materials' sequencing on the thermal performance of the walls under heating-dominated, cooling-dominated, and temperate climates

Another part of this investigation was devoted to assessing the transient thermal performances of concrete walls with different placements of thermally massive layer(s) under three case study climate conditions. Three sinusoidal profiles representative of heating-dominated, temperate, and cooling-dominated climates were assumed as the outside temperature conditions. Indoor temperature was maintained at 20°C for all cases. Eleven different case study walls with different layer configurations were considered. COMSOL Multiphysics © software was utilized to simulate the heat transfer phenomena through these walls. Then, by developing a MATLAB © code, the following performance indicators were assessed for each case study wall:

Decrement factor: decreasing amplitude of the thermal wave during its propagation process from outside to inside [81]. This is an indicator of how much the fluctuations in outdoor conditions are dampened before affecting the indoor conditions.

Quasi-steady state conditions: conditions for which the values of heat fluxes are identical to those of the corresponding points in the previous cycle.

Time required to reach quasi-steady state conditions: the time (in days) that is required for stabilization of the heat flux results and hence to reach quasi-steady state conditions.

Amplitude of changes of heat flux and surface temperature of the walls' interior surface

3.3. Impacts of thermal mass and layer configuration of walls on the energy performance of an office building

The next step was to assess the energy performance of a one-story office building taking into account four case study wall assemblies. The idea was to assess the impact of thermal mass and thermally massive layer placement on the energy performance of a building. Three climate conditions, namely, Montreal, Canada (heating-dominated), Denver, U.S.A. (temperate), and Miami (cooling-dominated) were chosen as alternatives of outside boundary conditions. The purpose is to investigate whether the optimum sequence of layers differs under different outside climate conditions. As for indoor temperature conditions, two cases were considered: (i) the indoor temperature was maintained at 20°C throughout the year (Case A), and (ii) during summertime, there was a set-point of 24°C during people's presence and a setback of 35°C during the rest of the day. On the other hand, during wintertime, the set-point and setback values were 22°C and 18°C, respectively (Case B). The aim was to assess the simultaneous effects of indoor temperature conditions and thermal mass on the energy performance of buildings. It is worth mentioning that other considered design parameters were kept for comparison's sake. Energy simulations were performed in OpenStudio © and EnergyPlus © whole building energy simulation software tools. Because energy demand was our performance indicator (and not energy consumption) the "Ideal Air Load" option was enabled to account for the HVAC system. This option means that there is an ideal HVAC system with an unlimited capacity that provides enough heating/cooling to compensate for the heat loss/gain at each time step. By comparing resulting heating and cooling loads, optimum sequence of wall layers, as well as the effect of thermal mass on the energy performance of building, can be assessed.

3.4. Assessing the thermal bridging effect on the transient thermal performance of the stud walls

As mentioned earlier, the aim of this section of the study is to outline a hand calculation method for developing an equivalent stud wall, whose transient thermal behavior is as similar to that of the original stud wall as possible. In fact, the cavity of stud walls is replaced by one layer such that the thermal performance of the equivalent wall is similar to that of the original stud wall. To this end, thermal properties of the equivalent layer should be determined. Two case study walls were taken into account: a steel stud wall and a wood-frame wall. As for the wood-frame wall, thermal conductivity of the homogeneous layer is calculated using the ASHRAE Fundamental handbook's parallel path method [23]. In fact, it is assumed that the two-dimensional heat transfer phenomena through the wall, which occur due to the existence of wood studs, is estimated assuming that there are two parallel paths of one-dimensional heat flow; one through the stud section and the other through the multi-homogeneous layer section that does not have the studs. Figure 5 shows the procedure of replacing the stud cavity with a homogeneous layer. Thermal conductivity of the homogeneous layer replacing the stud cavity can then be calculated taking into account its R-value and the length of the stud cavity. Density and specific heat capacity of the equivalent homogeneous layer are calculated using an area-weighted and mass-weighted approach, respectively [30,31]:

$$\rho_{el} = \sum_{i=1}^{n} C_i \rho_i \tag{8}$$

where:

ρ_{el} = density of the equivalent layer [$\frac{kg}{m^3}$],

C_i = volumetric (areal) fraction of the ith material in the cavity, and

ρ_i = density of the ith material in the cavity [$\frac{kg}{m^3}$].

$$C_i = \frac{V_i}{V_{el}} \tag{9}$$

where:

V_i = volume of the ith material in the cavity [m^3], and

V_{el} = total volume of the cavity [m^3].

, and for specific heat capacity of the equivalent homogeneous layer:

$$\sum_{i=1}^{n} V_i c_i \rho_i = V_{el} c_{el} \rho_{el} \tag{10}$$

where:

c_i = specific heat capacity of the ith material in the cavity [$\frac{J}{kg.K}$], and

c_{el} = specific heat capacity of the equivalent layer replacing the cavity [$\frac{J}{kg.K}$].

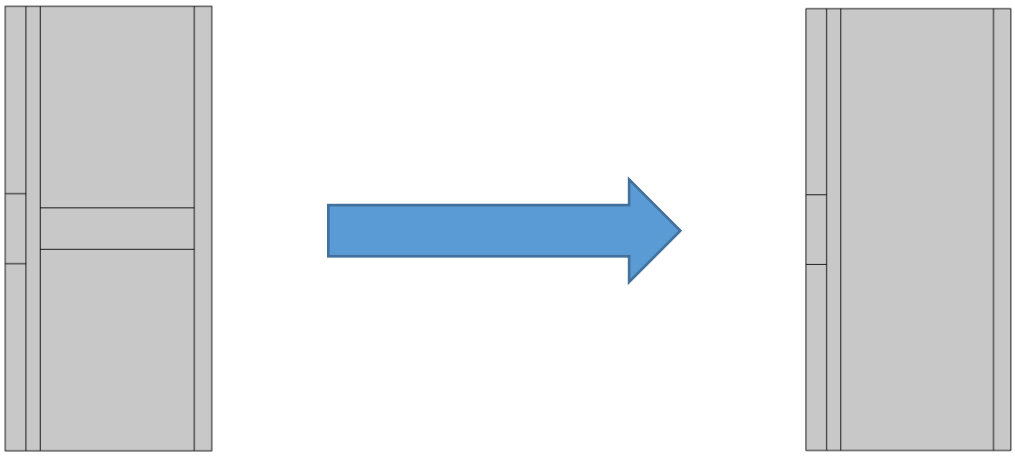

(a) (b)

Figure 5. Schematics of the model geometries implemented in COMSOL Multiphysics © for the case study wood-frame wall: (a) original wall; (b) equivalent wall

On the other hand, regarding the steel-stud wall case, thermal conductivity of the equivalent layer replacing the cavity is calculated using the modified zone method proposed by the ASHRAE Fundamentals handbook [23]. Figure 6 demonstrates a schematic of the process of calculating the overall thermal resistance of a steel-stud wall using modified zone method. Firstly, length of the zone affected by the studs should be calculated:

$$W = L + z_f \sum_{i=1}^{n} d_i \tag{11}$$

where:

W = width of the modified zone $[m]$,

L = size (width) of the stud flange $[m]$,

d_i = thickness of material layers existing between the stud and exterior wall surface $[m]$, and

z_f = zone factor.

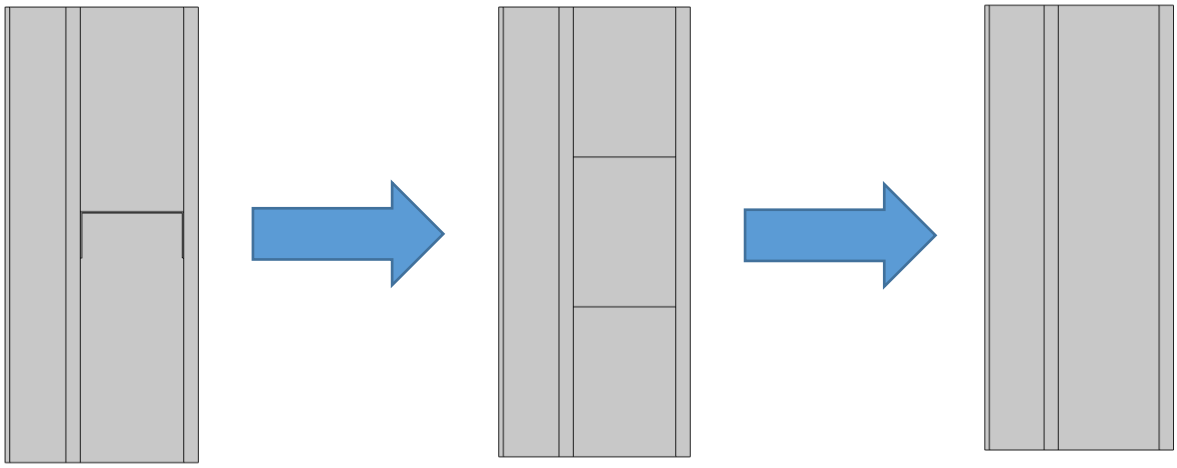

(a) (b) (c)

Figure 6. Schematics of the simulation model geometries implemented in COMSOL Multiphysics © for the steel stud wall: (a) original wall; (b) three-part wall; and (c) equivalent wall

Zone factor can be obtained from figure 6 of chapter 27, ASHRAE Fundamentals handbook [23]. Next, overall resistance of the layers between the cavity and the exterior wall surface, and overall R-value of the layers between the cavity and the interior wall surface, should be calculated. Then, thermal resistance of the equivalent layer, which replaces the zone affected by the presence of studs is calculated following parallel path method. Corresponding thermal conductivity of the layer can then be calculated from the resulting R-value. Finally, the cavity is replaced by a homogeneous layer, thermal resistance of which is obtained using parallel path method. Thermal conductivity of the homogeneous layer can then be calculated considering the equivalent thermal resistance of the

layer and the length of stud cavity. Similar to what presented for the wood-frame wall case, densities and heat capacities of the equivalent layers replacing the affected zone and the stud cavity are calculated using the area-weighted and mass-weighted approaches.

In the next chapter, firstly, case studies and their design parameters will be presented, and then, results of the analysis will be discussed.

CHAPTER 4: Case studies, results and discussion

In this chapter, considered cases and corresponding results for delivering the following purposes are discussed:

- Investigating the effects of thermal mass and layer configuration of walls on their transient thermal performance
- Studying the effects of thermal mass and layer configuration of walls on energy performance of a case study office building
- Applying the presented method on two case study walls (a steel-stud wall and a wood-frame wall) for assessing the effects of thermal bridges on the transient thermal performance of the walls

Firstly, case studies, along with their design specifications and simulation configurations, are described, and then, corresponding results are presented and discussed.

4.1. Thermal mass effect on the transient thermal performance of the concrete-based wall assemblies

4.1.1. Geometry

Three case study walls were considered for this investigation, namely an ICF wall, a tilt-up wall, and a wall made of a homogeneous Expanded Polystyrene (EPS) insulation layer. The ICF wall has a six-inch concrete layer sandwiched between two three-inch insulation layers. The tilt-up wall is comprised of a six-inch insulation layer sandwiched between two three-inch concrete layers. Two-dimensional schematics of these assemblies are illustrated in Figure 7. Although ICF walls usually have interior and exterior finishes, for the sake of consistency and equal thermal resistances, these layers were not taken into account. Also, with the aim of isolating the effects of thermal mass, another geometry made up of only one layer of EPS insulation was investigated. The thickness was adjusted such that its overall thermal resistance was equal to that of ICF and tilt-up walls. The required thickness of EPS layer was found to be 6.17 in. Also, the thermal capacitance of ICF and tilt-up walls is 311 $kJ/m^2.K$ while the thermal capacitance of EPS wall is 2.6 $kJ/m^2.K$.

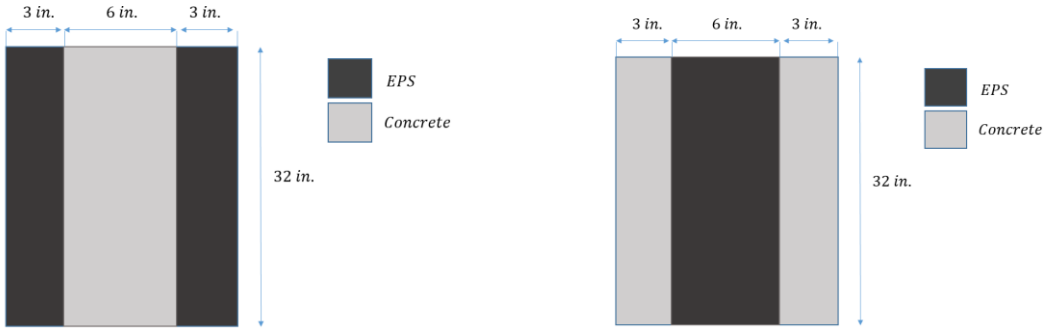

(a) (b)

Figure 7. Schematics of (a) the ICF; and (b) the tilt-up walls

4.1.2. Boundary conditions

Indoor temperature was maintained at 20°C throughout the simulation and according to the recommendation of ASHRAE Fundamentals handbook [23], indoor convection coefficient was assumed to be 8.33 W/m^2.K. This value was considered for all simulations in COMSOL Multiphysics © throughout this investigation. Initially, two different sinusoidal outside temperature cases were assumed: (a) An outside sinusoidal temperature profile fluctuating between -20°C and -8°C (heating season) and (b) An outside sinusoidal temperature profile fluctuating between 20°C and 32°C (cooling season) throughout the day. Minimum and maximum values of these profiles occurred at 3A.M. and 3P.M. respectively. Simulations started from midnight with the initial temperatures being -18.24°C and 21.76°C for the first and second cases, respectively. Figure 8 shows the sinusoidal outside climate conditions considered for this study. Number of days that each wall requires to reach quasi steady-state conditions was taken as a parameter to show the thermal mass effect on the transient thermal response of walls to a change in outdoor temperature conditions. Finally, sol-air temperature conditions of Montreal (as a case study heating-dominated city) and Miami (as a cooling-dominated region) for a Typical Metrological Year (TMY) were considered as exterior boundary conditions. Convection coefficient for all exterior boundaries were 33.33 W/m^2.K per the recommendation of ASHRAE Fundamentals handbook [23]. The initial conditions for Montreal and Miami corresponded to those of December 31st. Also, the effects of night-time cooling were ignored in the sol-air boundary condition in each location. All these walls were assumed to be south-oriented.

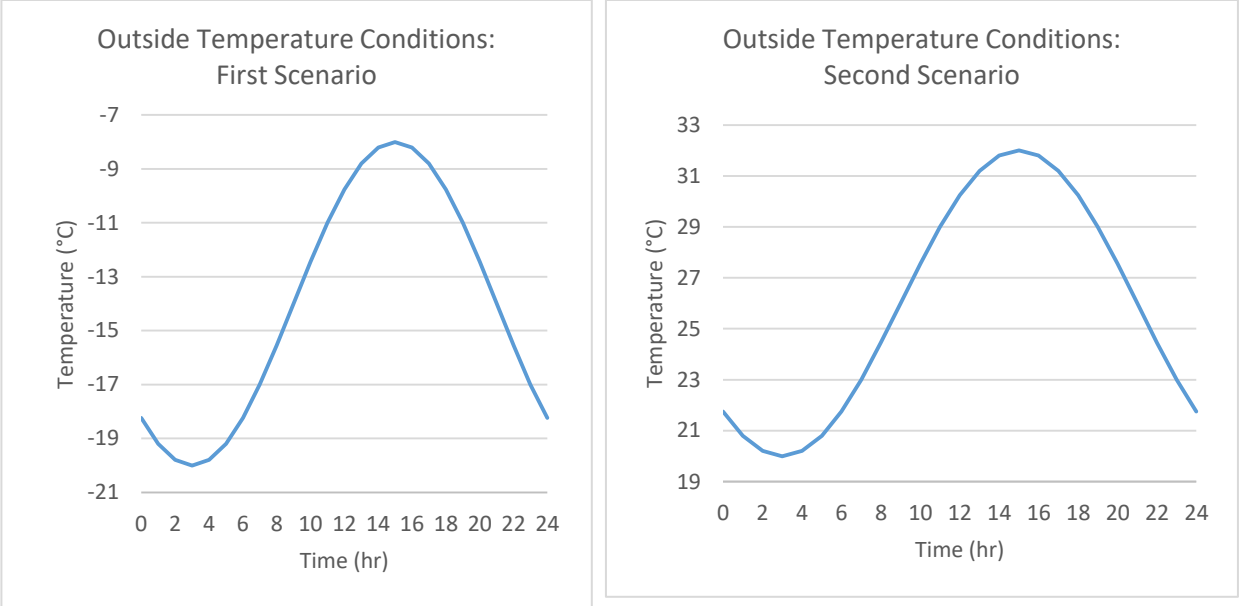

(a) (b)

Figure 8. Sinusoidal outside temperature conditions: (a) first case; (b) second case

4.1.3. Material properties

Table 5 presents the properties of materials used for this investigation. EPS was chosen as the insulation material while concrete is the thermally massive material. It should be mentioned that the material properties were temperature-independent.

Table 5. Material properties of EPS and concrete materials

Material	Thermal conductivity (W/m.K)	Density (kg/m^3)	Thermal capacity (J/kg.K)
EPS	0.05	11.5	1450
Concrete	1.8	2300	880

4.2. Results and discussion

Firstly, steady-state simulations at the initial boundary temperatures were performed, and then these results were used as initial conditions for the transient heat transfer simulations. The resultant R-value of the assemblies were 3.13 m^2.K/W. Figure 9 shows the energy flux (W/m^2) through the interior surfaces of ICF, EPS, and tilt-up walls considering the first sinusoidal outside temperature scenario (Figure 8a). Because the indoor temperature is maintained at 20°C throughout the

duration, integrated heat fluxes, i.e. the summation of instantaneous heat fluxes for a full cycle are the same for all three cases. Therefore, the effects of thermal mass are restricted to the time lag, peak demand shifting, and the time required for each wall to reach quasi-steady state conditions. The temperature profile is also illustrated in Figure 9. It took 7 days for ICF wall to reach quasi steady-state conditions while tilt-up wall required only one day to reach quasi steady-state conditions. On the other hand, considering the transient thermal response of EPS wall, the amplitude of the heat flux changes was larger. This is due to the fact that the concrete layer of ICF wall is placed between the insulation layers. As a result, any change in the temperature conditions was dampened by the insulation layer and then the layer with high thermal mass both reduced the amplitude of the heat flux changes and created a time lag between the changes in the outdoor temperature conditions and the transient thermal behavior of the wall. Whereas, the concrete layers of the tilt-up wall are directly exposed to the boundary temperature conditions; thus, the exposed exterior concrete layer responded rapidly to the temperature variations. In addition, the thermal response of tilt-up wall stabilized faster, i.e. sooner reached quasi steady-state conditions. On the contrary, because the overall thermal capacitance of EPS wall is comparatively lower, any change in boundary temperature conditions had a more direct impact on the thermal response of EPS wall. Positive values in Figure 9 refer to the case of heating energy demand, while cooling energy demands are shown by negative values. Another effect of thermal mass is peak demand shifting. It is evident from Figure 9 that there is a time lag of nearly 7 hours between the daily maximum heat flux transferred from the interior surface of ICF wall and daily minimum outside temperature. This time lag is approximately 6.5 hours for tilt-up wall while a minimal time lag between the response of EPS wall and outside temperature profile was observed. Considering the fact that the amplitude and the phase of the second exterior temperature scenario (Figure 8b) are the same compared to those of the first scenario (Figure 8a), same trends were found, with the only difference being the instantaneous values of the heat fluxes.

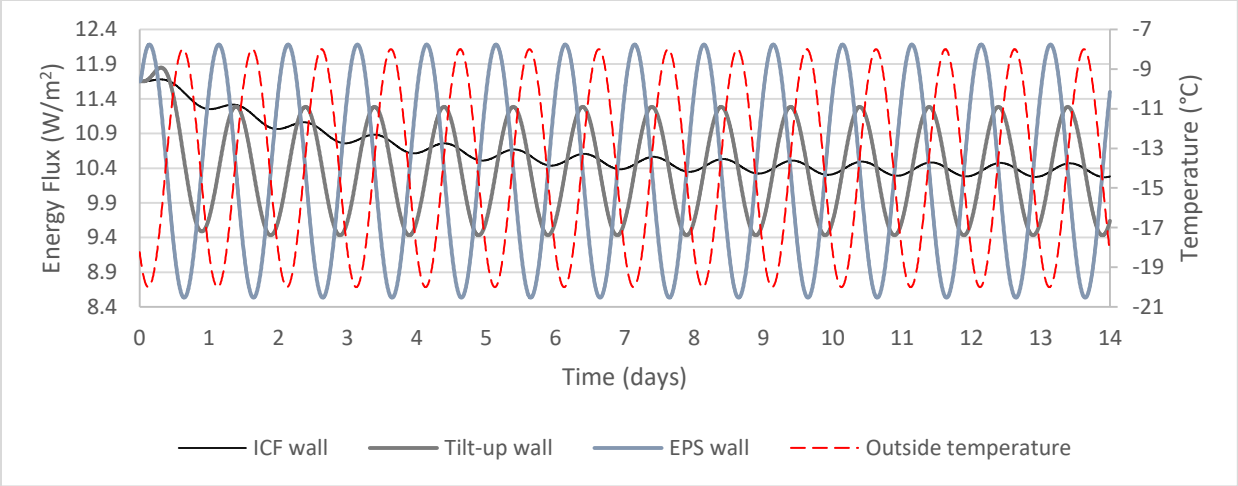

Figure 9. Heat fluxes transferred over the interior surface under the first assumed sinusoidal exterior temperature profile (heating scenario) for the ICF, tilt-up and EPS walls

Next, ICF, tilt-up, and EPS walls were simulated using the sol-air temperature conditions of Montreal and Miami as the exterior boundary conditions. Figure 10 and Figure 11 show the instantaneous heat fluxes through the interior surface of the walls, as well as the heating and cooling demands, throughout a year for Montreal (heating dominated) and Miami (cooling dominated) cases, respectively. Comparing the performances of the ICF and tilt-up assemblies, the amplitude of the heat flux changes was larger for the tilt-up case because its concrete layers are directly in contact with exterior and conditioned interior boundaries. As an example, the minimum and maximum values of instantaneous heat fluxes, as well as the amplitude of heat flux changes, for February 1st for Montreal case are presented in Table 6. The amplitudes of heat flux changes for ICF, tilt-up, and EPS wall cases under Montreal TMY sol-air temperature conditions were 0.43 W/m^2, 2.00 W/m^2, and 4.64 W/m^2, respectively. As expected, these fluctuations are wider for the heat fluxes through the interior surface of EPS wall assembly because its overall heat storage capacitance is negligible. Integrated heat fluxes (i.e. the summation of instantaneous heat fluxes) for the case study walls are shown in Table 7. As the indoor temperature is kept constant at 20°C throughout the year, for each city, the overall integrated heat fluxes were the same for all case study walls (within 0.3% difference). However, it does not necessarily mean that the heating demands or the cooling demands for all three cases are the same because the amount of heat stored in the thermally massive layer can contribute to the energy demands. As shown in Table 7, compared to the EPS wall, the ICF wall had 7.7% while the tilt-up wall had 5.4% less heating

energy demand in Montreal. The differences in cooling energy demands were significant, although cooling energy demand represents a very small portion of total energy demand (e.g. 3.3% for the ICF case) for the cold climate of Montreal. The cooling energy demands for ICF wall and tilt-up wall cases were 71.13% and 47.8% less than that of EPS wall case, respectively. Similarly for Miami, differences between the heating energy demands of the case studies were larger although heating energy demand represents a very small portion of total energy demand (e.g. 2.9% for the tilt-up wall case) for the hot and humid climate of Miami. The heating energy demands of ICF wall and tilt-up wall were 3.1%, and 46.1% of heating energy demand of EPS wall, respectively. There was a slight difference in cooling energy demands. Compared to EPS wall, ICF wall had 6.1% while tilt-up wall had 3.6% less cooling energy demand.

Table 6. Maximum and minimum values and amplitudes of the heat fluxes for February 1st for Montreal case

Walls	Minimum heat flux (W/m^2)	Maximum heat flux (W/m^2)	Amplitude (W/m^2)
ICF	8.02	8.88	0.43
Tilt-up	4.40	8.39	2.00
EPS	0.83	10.11	4.64

Table 7. Integrated heat fluxes for the ICF, tilt-up, and EPS wall assemblies under Montreal and Miami TMY sol-air temperature conditions

Wall	Montreal			Miami		
	Heating (kW/m^2)	Cooling (kW/m^2)	Integrated heat flux (kW/m^2)	Heating (kW/m^2)	Cooling (kW/m^2)	Integrated heat flux (kW/m^2)
ICF	32.06	1.10	30.96	0.04	19.46	-19.42
Tilt-up	32.86	1.99	30.87	0.59	19.98	-19.39
EPS	34.74	3.81	30.93	1.28	20.73	-19.45

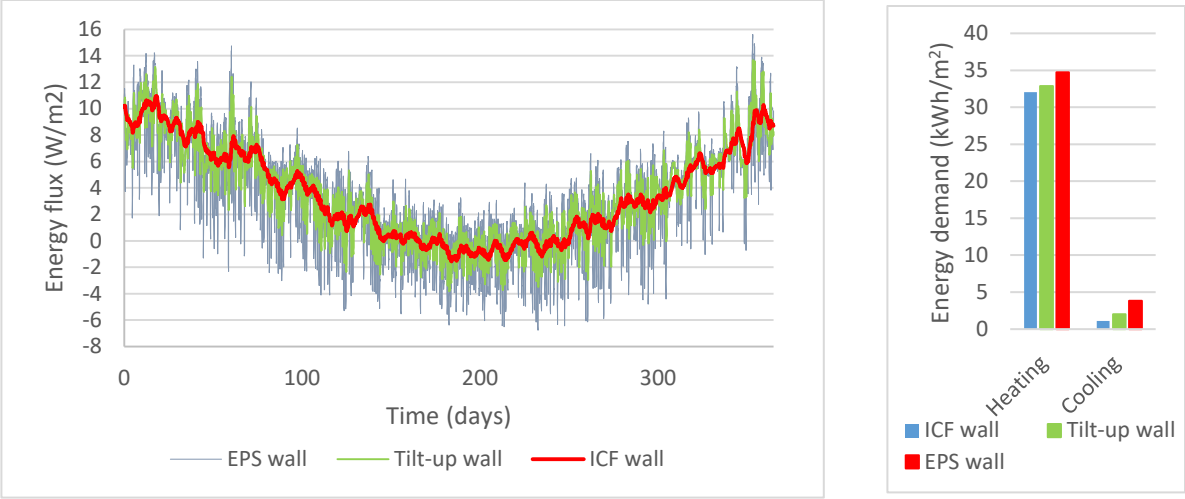

(a) (b)

Figure 10. (a) Interior surface energy fluxes and (b) heating and cooling energy demands for the ICF and tilt-up assemblies under Montreal TMY sol-air temperature conditions

As a result, it can be concluded that the benefits of the thermal mass in terms of energy savings is more evident during the secondary seasons for each city, i.e. summers in Montreal and winters in Miami.

In order to better understand the effect of the concrete layer placement within the thermally massive walls, energy demands of ICF and tilt-up walls were compared. ICF wall in Montreal needed 2.5% less heating energy than the tilt-up wall. Also the ICF wall demanded 2.6% less cooling energy compared to the tilt-up wall in Miami. Thus, based on the cases studied, the thermally massive layers can benefit the buildings in terms of the energy savings if they are not directly exposed to the exterior conditions. Finally, minimum indoor surface temperatures for each wall assembly were also calculated for each location. In Montreal, minimum interior surface temperatures were 18.7°C, 18.4°C and 18.1°C for ICF, Tilt-up wall and EPS respectively. It means that the risk of condensation is higher for the EPS wall compared to ICF and tilt-up walls. In addition, ICF wall had a lower risk of condensation compared to the tilt-up wall case. In Miami, maximum indoor surface temperatures were 20.4°C, 20.6°C and 21.0°C for ICF, tilt-up and EPS walls, respectively. Although interior surface temperature is not a reasonable performance indicator for thermal comfort, this finding gives a hint that ICF and EPS walls can lead to the highest and lowest level of thermal comfort, respectively. Indoor operative temperature would be a better performance indicator for the level of thermal comfort.

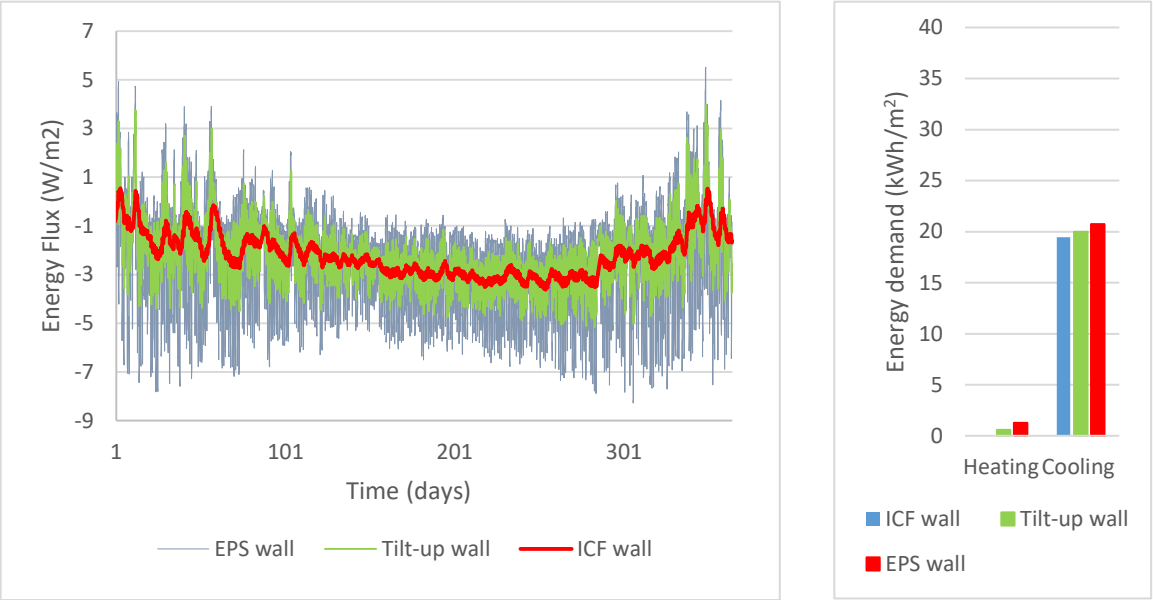

(a) (b)

Figure 11. (a) Interior surface energy fluxes and (b) heating and cooling energy demands for the ICF and tilt-up assemblies under Miami TMY sol-air temperature conditions

4.2. Effects of layer sequencing on the transient thermal performance of the concrete walls

4.2.1. Case studies

Another part of this investigation was devoted to assessing the transient thermal performances of concrete walls with different placements of thermally massive layer(s) under three case study climate conditions. Three sinusoidal profiles representative of heating-dominated, temperate, and cooling-dominated climates were assumed as the outside temperature conditions. As can be seen in Figure 12, minimum and maximum values for all temperature profiles occurred at 3 A.M. and 3 P.M., respectively. Indoor temperature was maintained at 20°C for all cases. Three sets of case studies with different purposes were considered: (a) three three-layer walls with one layer of insulation and two thermally massive layers (the purpose is to investigate the effects of insulation placement within a wall assembly) (Figure 13); (b) three three-layer walls with one thermally massive layer and two layers of insulation (the aim is to study the impact of thermally massive layer placement within a wall assembly) (Figure 14); and (c) two two-layer walls (Figure 15), ICF wall, tilt-up wall, and a wall made of one homogeneous layer (Figure 16). As for the three-layer walls, each layer's thickness is 3in, while for the two-layer walls each layer is 6in thick. ICF wall

contains 6in of concrete sandwiched between two 3in insulation layers while tilt-up wall has a 6in-thick insulation layer sandwiched between two 3in-concrete layers. The wall with one homogeneous layer wall is made of a 12in thick homogeneous layer, whose thermal properties were modified such that its overall thermal resistance and thermal storage capacitance are equal to those of the ICF and tilt-up walls. Concrete and EPS accounted for the thermally massive and insulation materials, respectively. COMSOL Multiphysics © software was utilized to simulate the heat transfer phenomena through these walls.

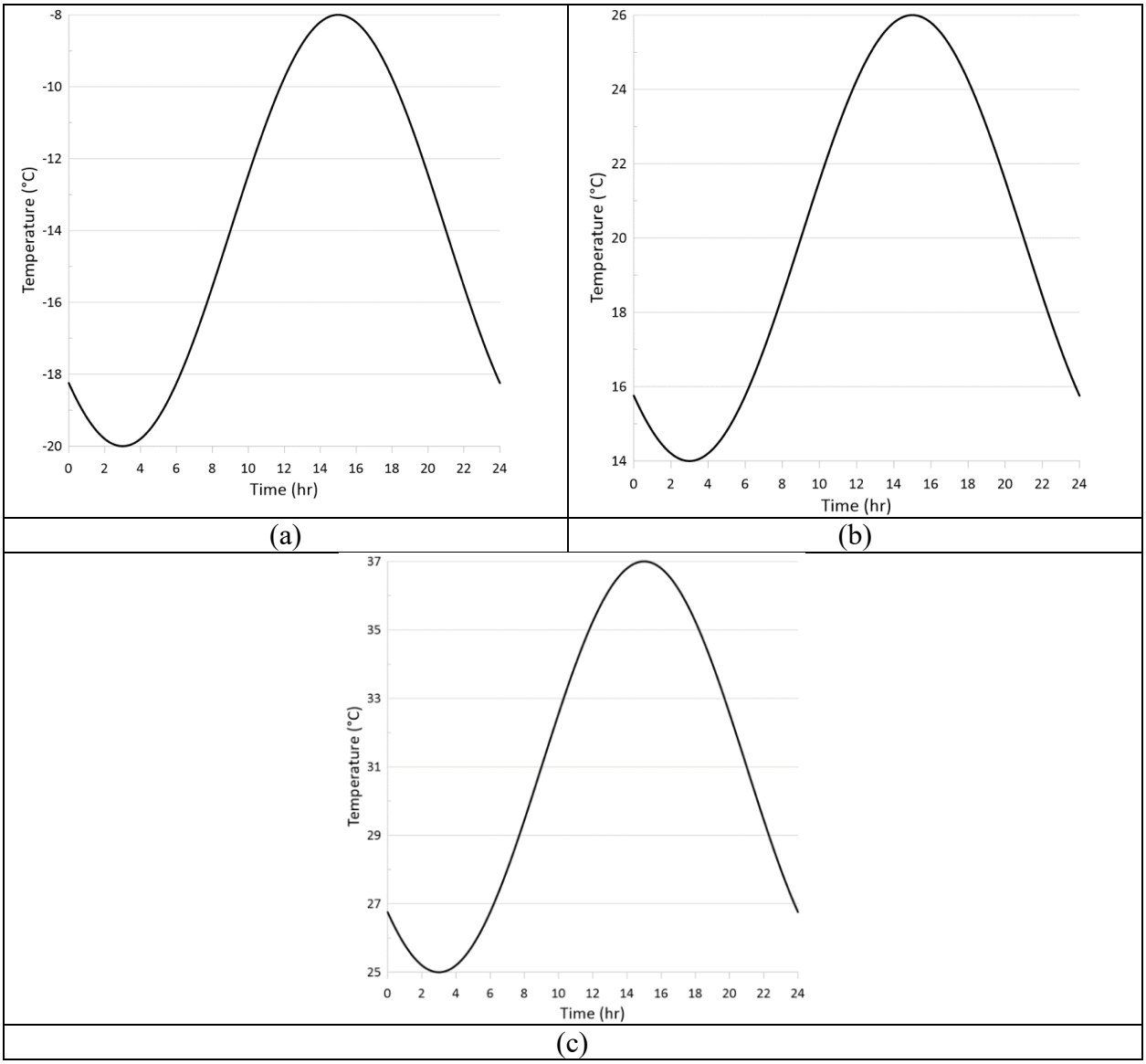

Figure 12. Outside boundary temperatures for one cycle (one day) for: (a) heating-dominated, (b) temperate, and (c) cooling-dominated climate conditions

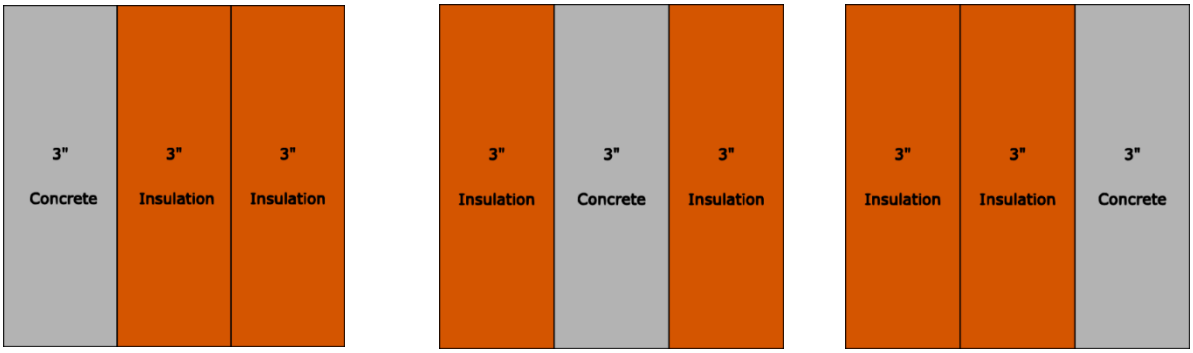

Figure 13. Three-layer walls with one concrete layer and two insulation layers

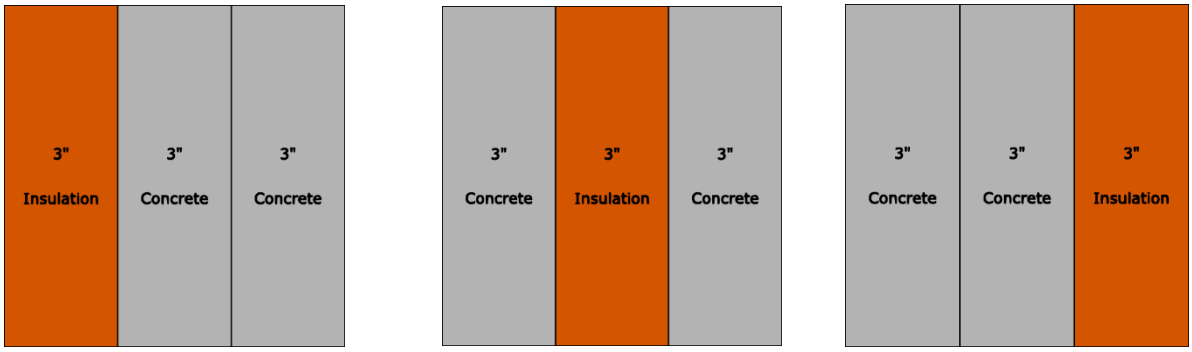

Figure 14. Three-layer walls with one insulation layer and two concrete layers

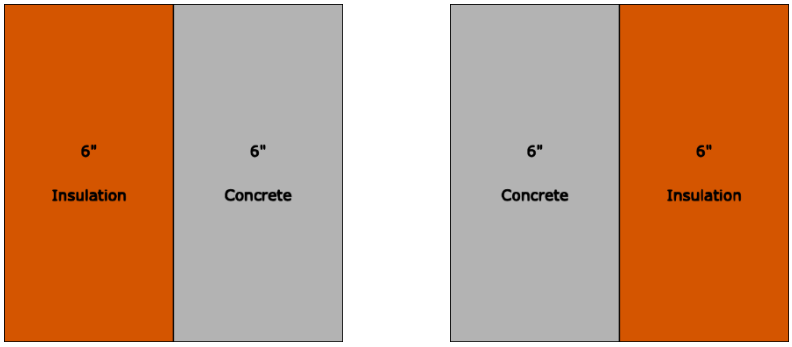

Figure 15. Two-layer walls

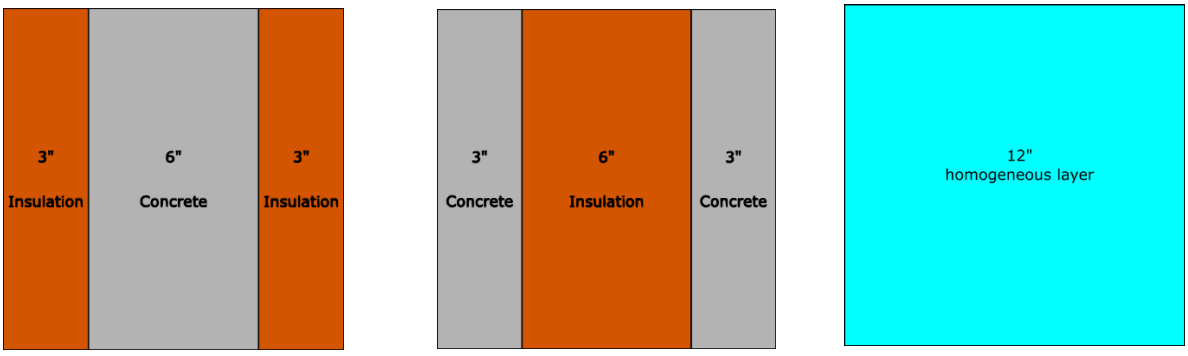

Figure 16. ICF, tilt-up, and homogeneous walls with modified concrete layers

4.2.2. Results and discussion

4.2.2.1. Three-layer walls with one layer of concrete

Firstly, with the aim of investigating the effects of placing the thermally massive layer within a wall assembly, the results for three-layer wall cases with one layer of concrete and two layers of insulation will be discussed. Figure 17 shows the heat flux results for these simulation cases under heating-dominated, cooling-dominated, and temperate climates. Also, Table 8 gives, for each case study wall, the decrement factor, heat flux and temperature amplitudes, and the time required to reach quasi-steady state conditions under the heating-dominated climate. As the amplitudes of the sinusoidal outdoor temperature profiles are identical, identical values for these parameters were found under all case study climates. It can be observed that the wall whose concrete layer is sandwiched between two insulation layers had the lowest decrement factor and heat flux and indoor surface temperature amplitudes and the longest required time to reach quasi-steady state conditions. On the other hand, having the thermally massive layer exposed to the outside conditions resulted in the largest decrement factors, amplitudes of heat fluxes and indoor surface temperatures, and the shortest time required to reach quasi steady-state conditions.

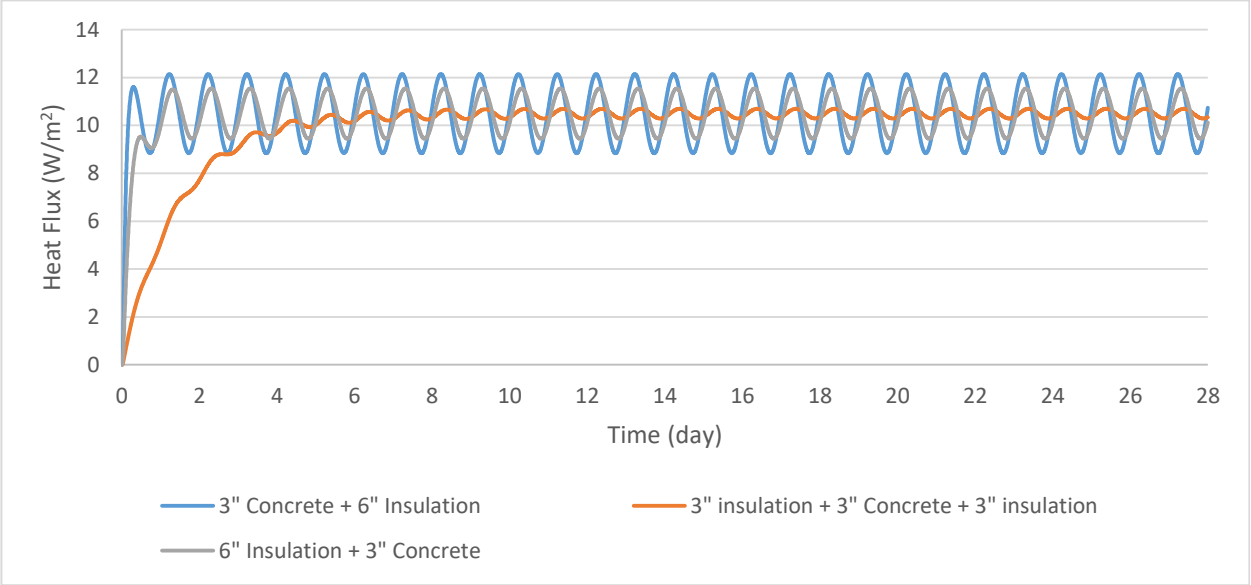

(a)

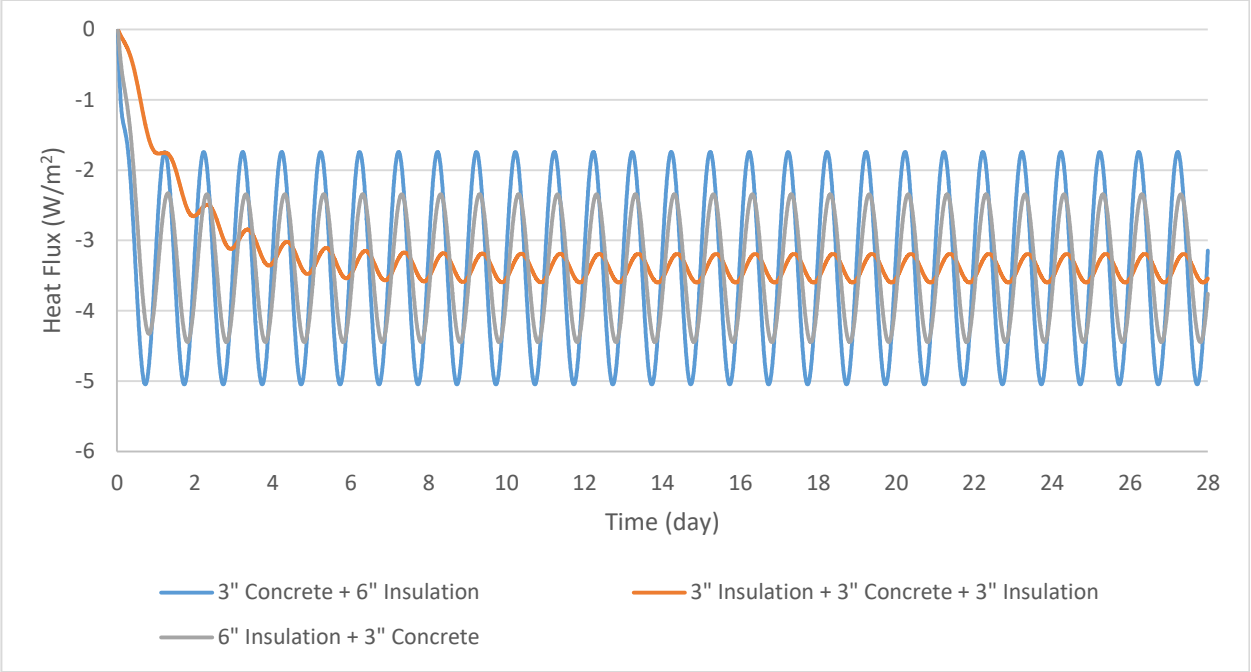

(b)

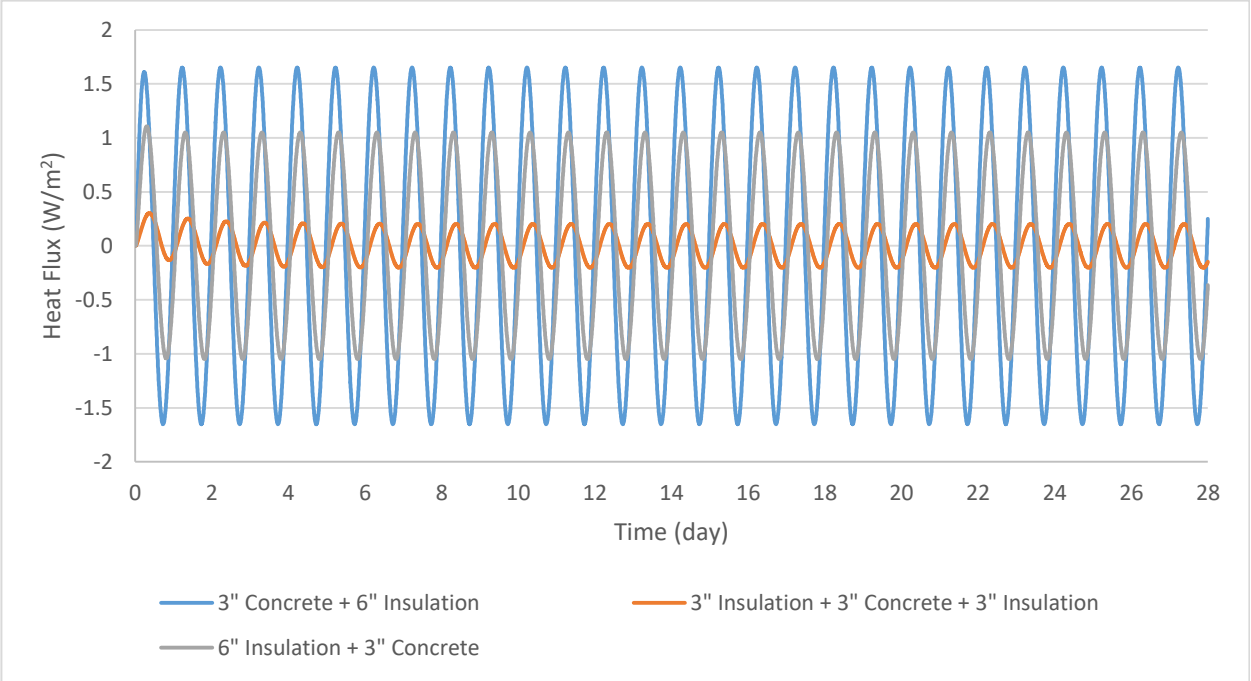

(c)

Figure 17. Transmitted heat flux from the interior side of three-layer wall cases with one layer of concrete under: (a) heating-dominated; (b) cooling-dominated, and (c) temperate climates

Table 8. Thermal performance indicators for three-layer walls with one layer of concrete under heating-dominated outdoor temperature conditions

Wall	Composition	R-value (m^2.K/W)	Decrement factor	Indoor surface temperature amplitude (°C)	Heat flux amplitude (W/m^2)	Time required to reach quasi-steady state conditions (days)
Wall 1	3" C + 6" I	3.09	0.0330	0.1981	1.6512	2
Wall 2	3" I + 3" C + 3" I	3.09	0.0041	0.0244	0.2030	14
Wall 3	6" I + 3" C	3.09	0.0210	0.1259	1.0494	3

4.2.2.2. Three-layer walls with one layer of EPS insulation

Next, the effects of placing insulation layer within a wall assembly on the transient thermal performance of the walls will be investigated by assessing the simulation results for three-layer walls with one layer of EPS insulation. Heat flux results for these cases are demonstrated in Figure 18. In addition, Table 9 presents the values of thermal performance indicators for these cases under heating-dominated outdoor temperature conditions. Identical values were found under the other two climate conditions for these parameters. It can be seen that having the insulation as the outermost layer of the wall led to the smallest heat flux and indoor surface temperature amplitudes and the decrement factor, as well as the largest time required to reach quasi steady-state conditions. On the other hand, the wall with its insulation layer being placed at the inside had the largest heat flux and indoor surface temperature amplitudes, the largest decrement factor, and the lowest time required to reach quasi steady-state conditions. Comparing wall 3 and wall 4, although the R-value of wall 3 is almost twice as high as that of wall 4, it performs almost the same regarding the decrement factor and amplitudes while it reacts quicker to a change in outdoor conditions.

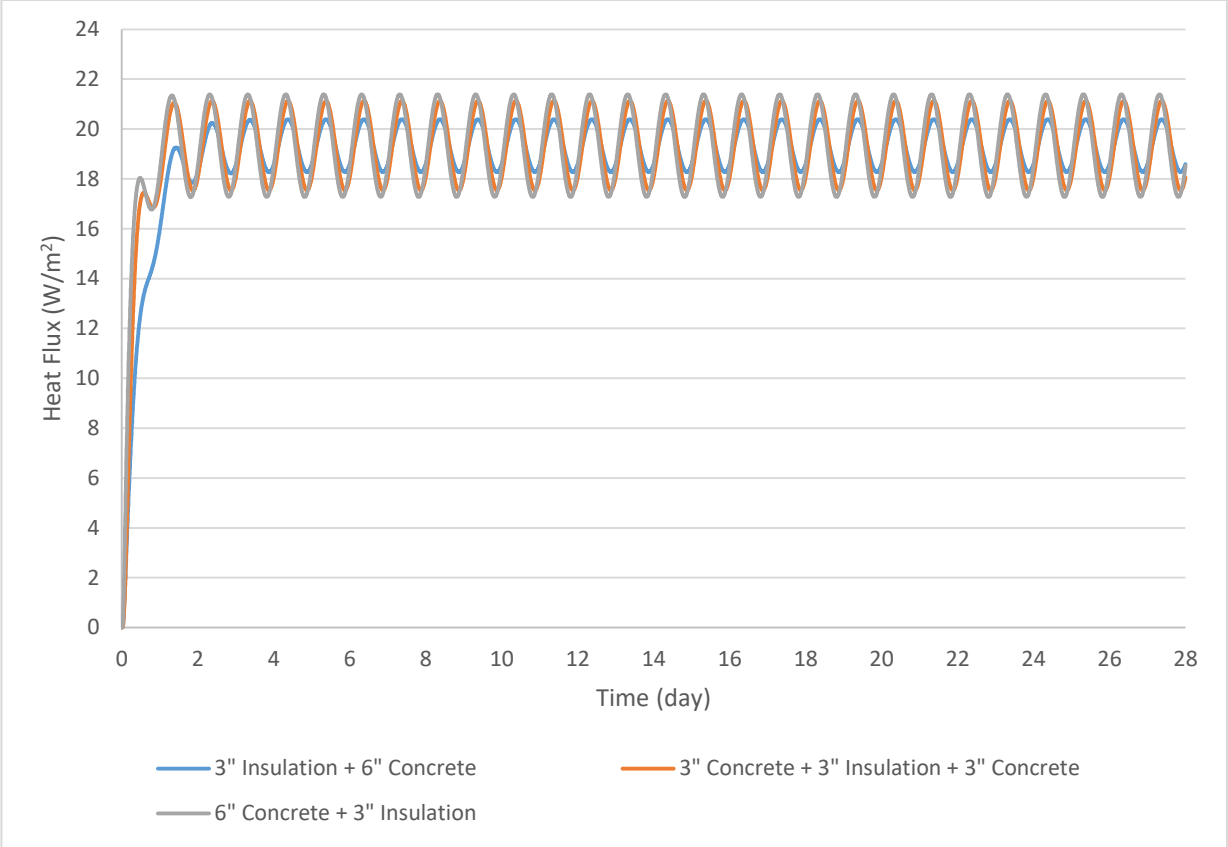
Heat Flux (W/m²)
Time (day)
3" Insulation + 6" Concrete
3" Concrete + 3" Insulation + 3" Concrete
6" Concrete + 3" Insulation

(a)

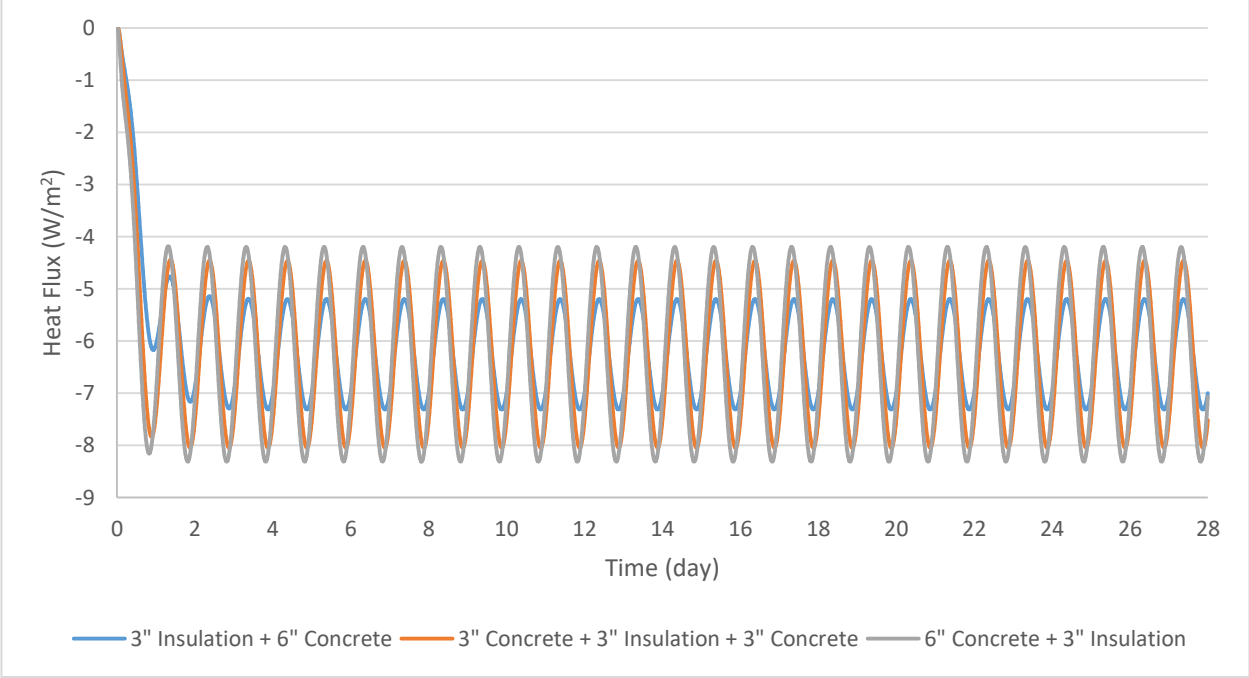
Heat Flux (W/m²)
Time (day)
3" Insulation + 6" Concrete
3" Concrete + 3" Insulation + 3" Concrete
6" Concrete + 3" Insulation

(b)

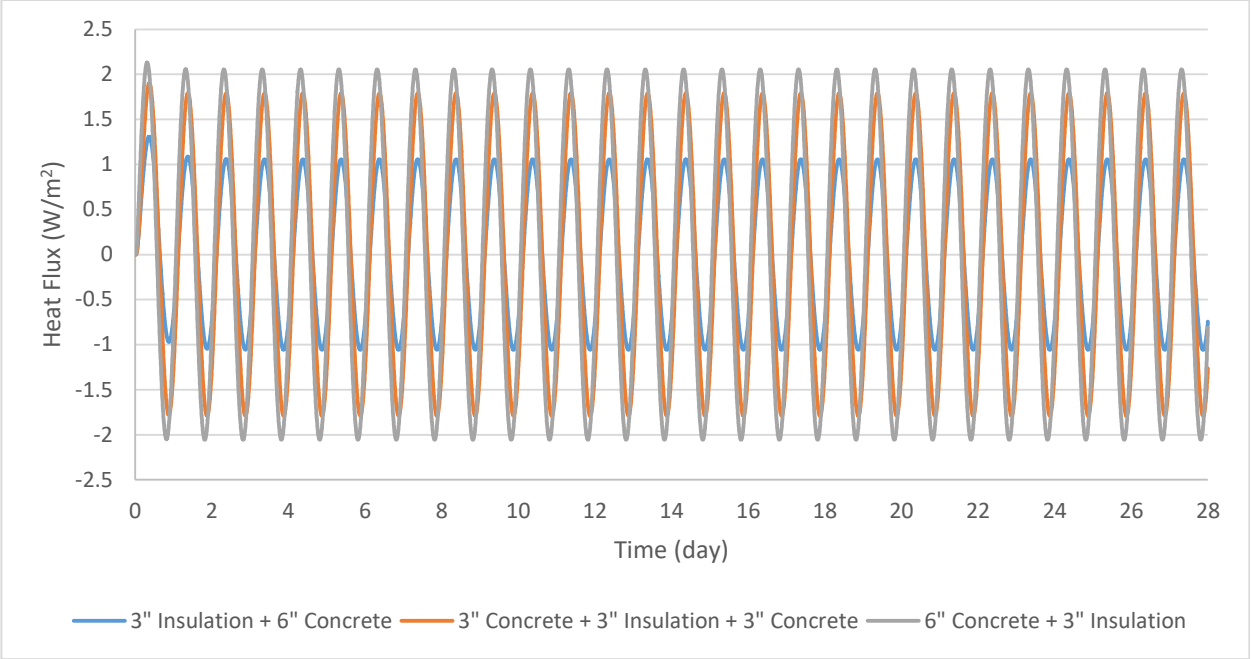

(c)

Figure 18. Heat fluxes transferred through the interior sides of three-layer walls with one insulation layer under: (a) heating-dominated; (b) cooling dominated, and (c) temperate outside temperature conditions

Table 9. Performance indicator for three-layer wall cases with one insulation layer under heating-dominated conditions

Wall	Composition	R-value (m^2.K/W)	Decrement factor	Indoor surface temperature amplitude (°C)	Heat flux amplitude (W/m^2)	Time required to reach quasi-steady state conditions (days)
Wall 4	3" I + 6" C	1.61	0.0212	0.1270	1.0580	6
Wall 5	3" C + 3" I + 3" C	1.61	0.0358	0.2148	1.7900	3
Wall 6	6" C + 3" I	1.61	0.0411	0.2468	2.0563	3

4.2.2.3. Two-layer, ICF, tilt-up, and homogeneous walls

Finally, the results of five cases with the same R-values are discussed, namely two-layer walls (interiorly and exteriorly insulated), ICF, tilt-up, and homogeneous walls. Figure 19 and Table 10 show the surface heat fluxes through the inside surface of the walls and the values of thermal

performance indicators for these assemblies under heating-dominated, cooling-dominated, and temperate outside temperature conditions, respectively. As can be seen, the wall made of one homogeneous layer had the lowest decrement factor, heat flux and indoor surface temperature amplitudes, while the ICF wall had the longest time required to reach quasi steady-state conditions. On the other hand, placing the concrete layer at the innermost side of the wall resulted in the largest decrement factor and the biggest amplitudes of heat fluxes and indoor surface temperatures, as well as the shortest time required to reach quasi steady-state conditions.

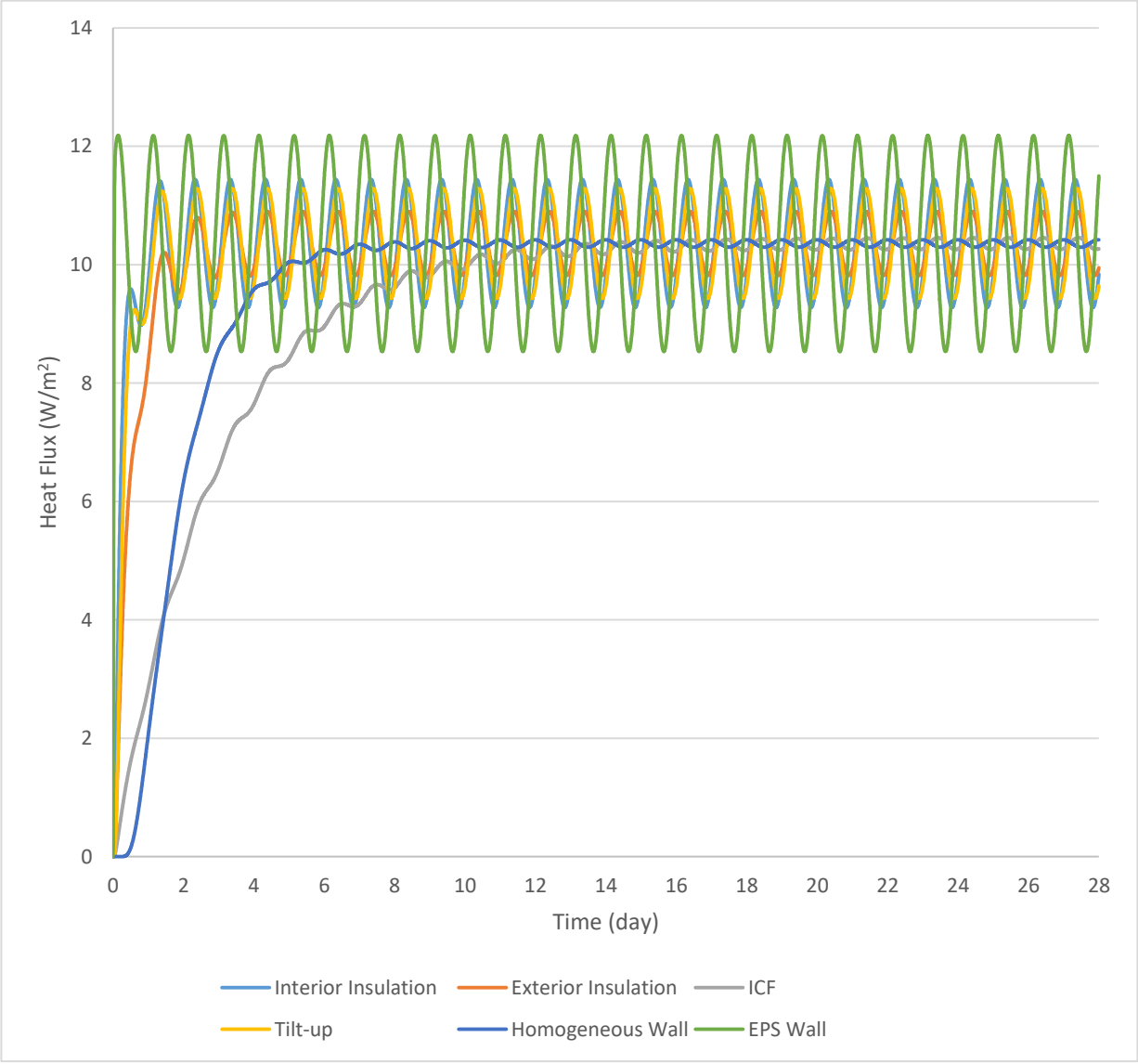

(a)

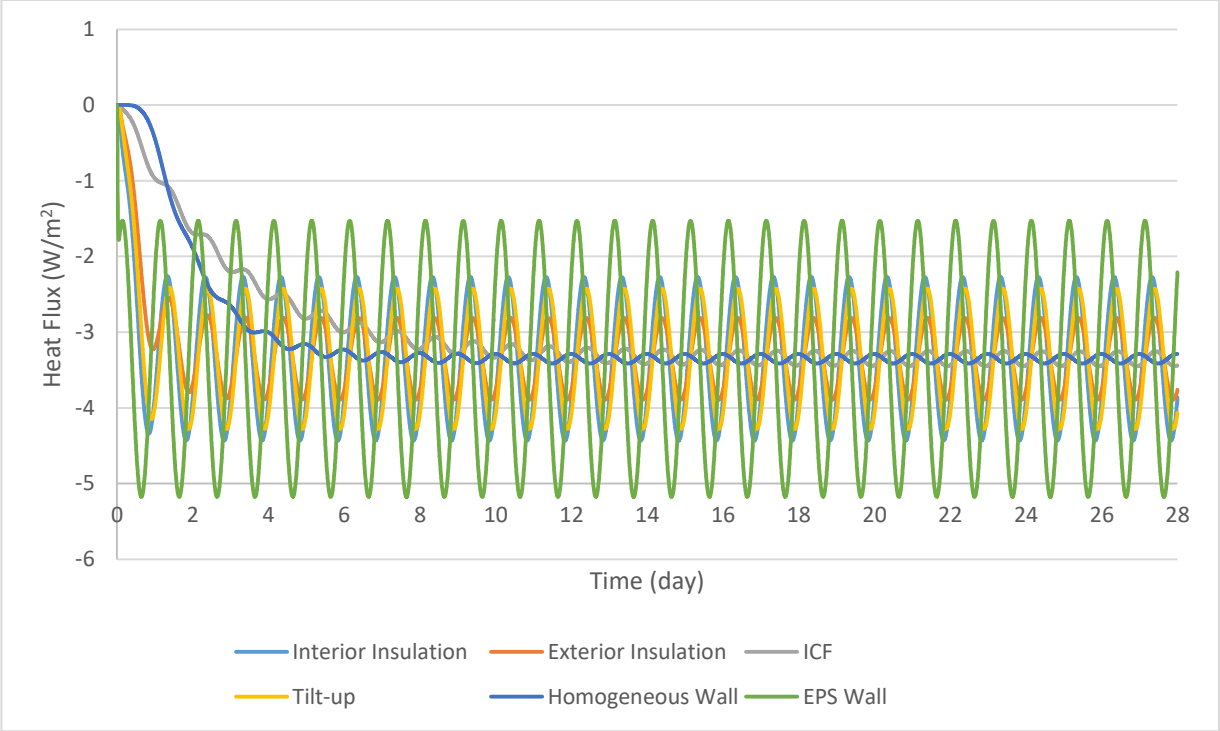

(b)

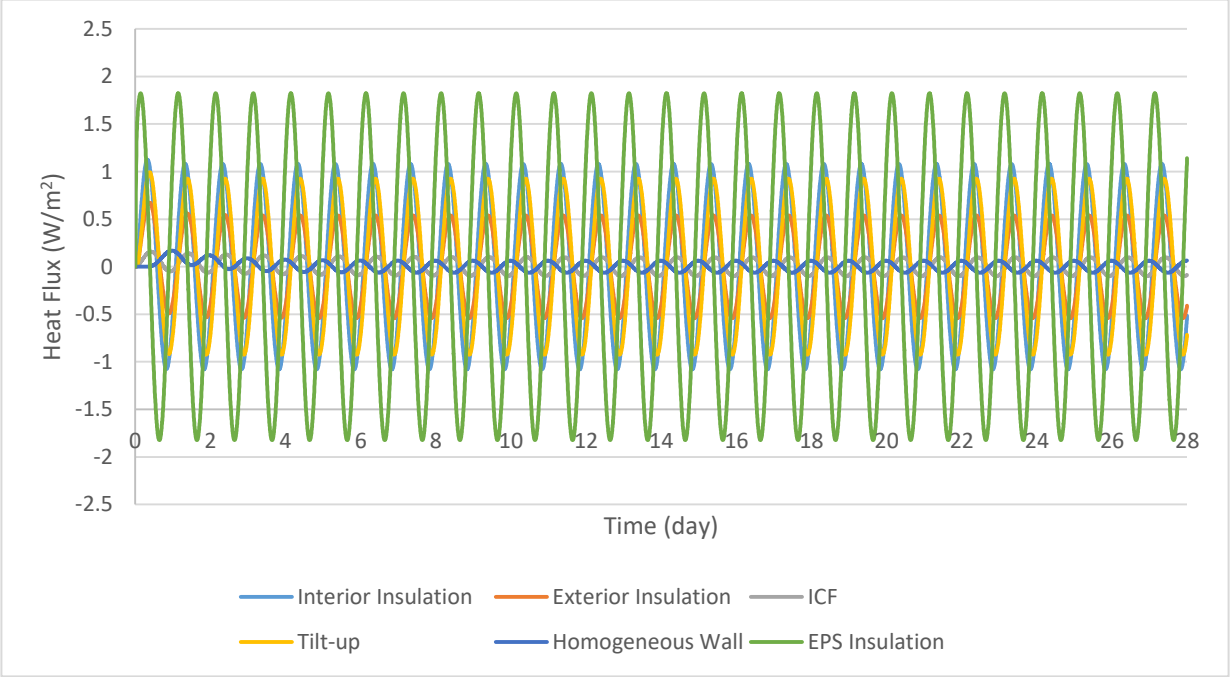

(c)

Figure 19. Heat flux through the interior surfaces of four case study walls: inside insulation, outside insulation, ICF, and tilt-up under: (a) heating-dominated; (b) cooling-dominated, and (c) temperate conditions

Table 10. Thermal performance indicators for four case study walls: inside insulation, outside insulation, ICF, and tilt-up under heating-dominated temperature conditions

Wall	Composition	R-value (m^2.K/W)	Decrement factor	Indoor surface temperature amplitude (°C)	Heat flux amplitude (W/m^2)	Time required to reach quasi-steady state conditions (days)
Wall 7	6" C + 6" I	3.13	0.0216	0.1296	1.0800	3
Wall 8	6" I + 6" C	3.13	0.0108	0.0647	0.5392	6
Wall 9 (ICF)	3" I + 6" C + 3" I	3.13	0.0020	0.0118	0.0987	26
Wall 10 (Tilt-up)	3" C + 6" I + 3" C	3.13	0.0185	0.1110	0.9252	3
Wall 11 (Homogeneous wall)	12" Homogeneous layer	3.13	0.0013	0.0076	0.0634	13

Based on the case studies evaluated, it can be observed that the thermally massive component of the walls should be as protected from indoor and outdoor conditions as possible in order to have the lowest decrement factor, the smallest heat flux and indoor surface temperature amplitudes, and the longest time required to reach quasi-steady state conditions. Specifically, because the variations of the outdoor temperature is usually more intense, the thermally massive layer should not be directly exposed to the outside conditions.

4.3. Impact of materials sequencing of the walls on the energy performance of an office building

4.3.1. Case study

The next step was to assess the energy performance of a one-story office building, schematic of which can be seen in Figure 20. The building is chosen based on the U.S. DOE reference building archetypes for a small office building [82]. The case study building had a total floor area of 511.16 m^2. The building had six zones, namely four perimeter zones, one core zone, and an attic. The same assemblies were assumed as the case study exterior walls: (a) ICF; (b) tilt-up; (c) a wall made of one homogeneous layer with identical thermal resistance and overall thermal storage capacity compared to ICF and tilt-up walls; and (d) EPS walls. Window to wall ratio for this building was 37.3%. Three climate conditions were considered: Montreal, Miami, and Denver, which represented the heating-dominated, cooling-dominated, and temperate climates, respectively. Two cases for the indoor temperature conditions were taken into account: (i) the indoor temperature was maintained at 20°C throughout the year (Case A), and (ii) during summertime, there was a

set-point of 24°C during people's presence and a setback of 35°C during the rest of the day. On the other hand, during wintertime, the set-point and setback values were 22°C and 18°C, respectively (Case B). Total number of people was assumed to be 25. Internal load as a result of people's activity during their presence was assumed to be 130 W/m^2, per the recommendation of ASHRAE Fundamentals handbook for people with low activity levels in a small office building [23]. The lights and equipment generated 10 W/m^2 and 7.5 W/m^2 of the floor area, respectively. Air Change per Hour (ACH) of ventilation was 0.498 ACH for all zones. Infiltration rates are shown in Table 11. Schedules for people's presence, operation of lights and equipment, and hot water used were set according to the Canadian National Energy Code for Building (NECB)'s [83] recommendation for small office buildings in Montreal. Table 12 presents the thermal transmittances of the other building envelope components. In addition, for the sake of comparison, these design parameters were not changed for the building under other climate conditions. OpenStudio © and EnergyPlus © whole building energy simulation software tools were used to perform the energy evaluations. As for the HVAC system, the "Ideal Air Load" option was enabled, meaning that there is an ideal HVAC system with an unlimited capacity that provides enough heating/cooling to compensate for the heat loss/gain. This makes the indoor air temperature reach the set-point values while operating. In fact, at each time step, the load on the HVAC system is equal to the heating/cooling demand.

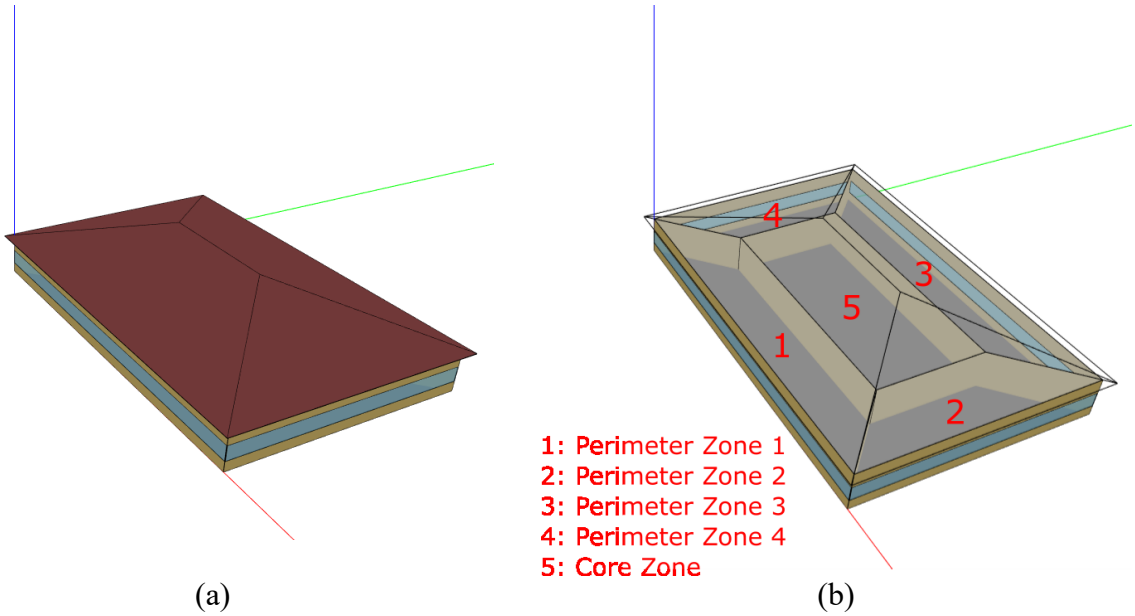

(a) (b)

Figure 20. Schematics of the case study building: (a) outside view; (b) representations of the zones

Table 11. Zone infiltration

Zone	Infiltration ACH
Attic	0.748
Perimeter Zone 1	0.220
Perimeter Zone 2	0.247
Perimeter Zone 3	0.220
Perimeter Zone 4	0.247

Table 12. Thermal transmittance values of the building components

Component	U-value ($W/m^2.K$)
Fixed windows	1.9
Floor	0.18
Roof	0.15
Doors	1.9

4.3.2. Results and discussion

4.3.2.1. Case A

Figure 21 presents the heating and cooling energy demands for the entire building maintaining the indoor temperature at 20°C. It is evident that the heating and cooling energy demands were lower for the building that has tilt-up walls under all three considered climate conditions. However, the differences in energy consumptions were not considerable. For example, the case with tilt-up walls demanded almost the same cooling energy compared to ICF case under Miami climate conditions. Although the differences in percentage were higher when comparing heating demands in Miami and cooling demands in Montreal, it should be noted that these loads do not account for a large portion of the total energy demands.

Montreal

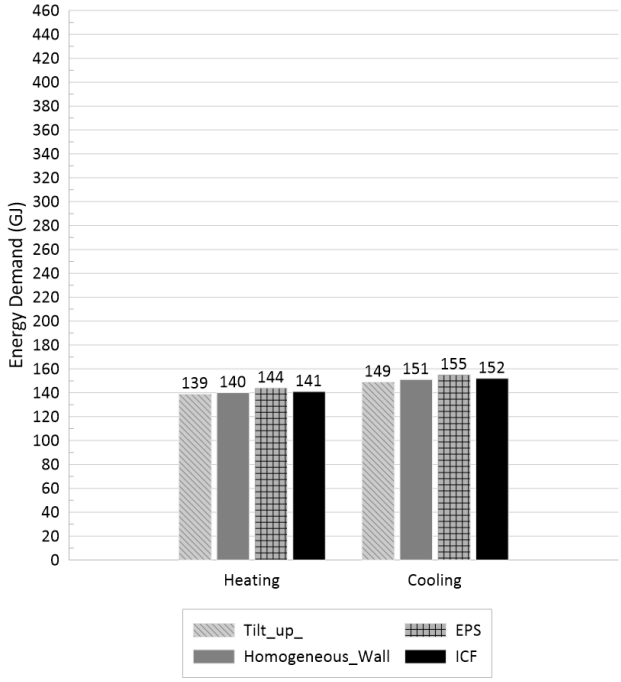

(a)

Miami

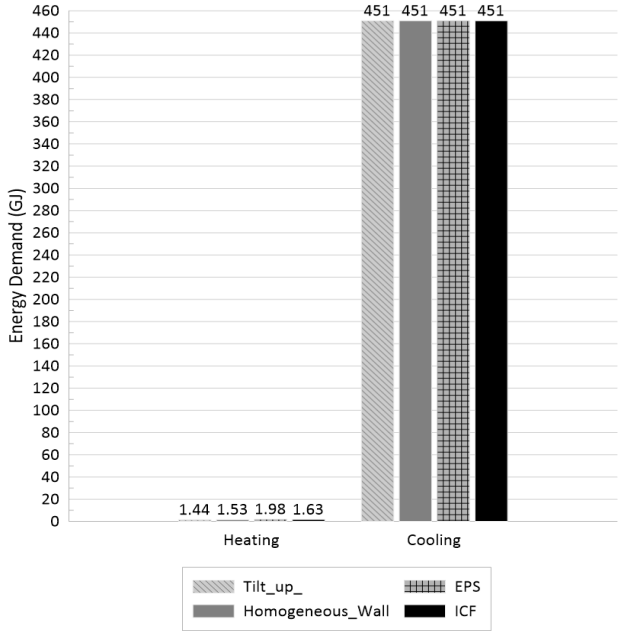

(b)

Denver

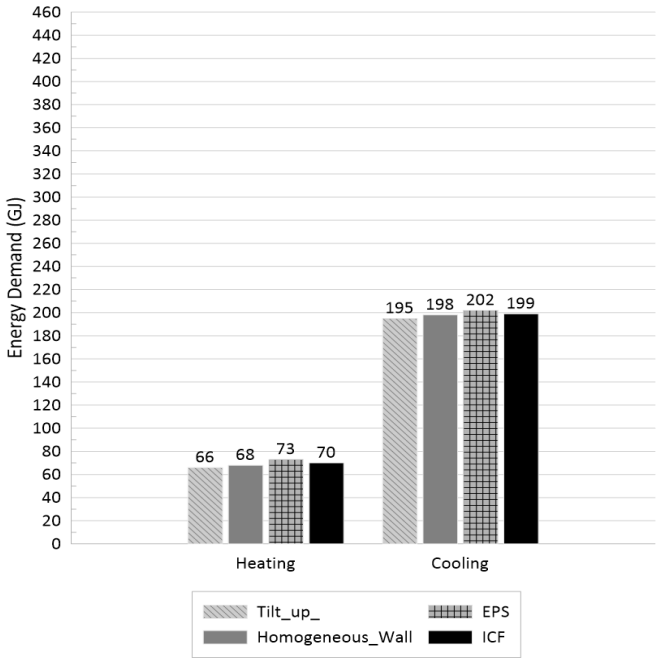

(c)

Figure 21. Heating and cooling energy demands under: (a) Montreal; (b) Miami, and (c) Denver climate conditions

4.3.2.2. Case B

Next, the case studies were simulated assuming the aforementioned schedule for the indoor temperature set-point. Figure 22 shows the energy demands for the entire building, from which it can be observed that tilt-up case had the lowest energy demands amongst the case studies considered. For example, the case with tilt-up walls demanded 4.1% less cooling energy compared to ICF case under Denver climate conditions. It can be seen that the differences in energy demands were more tangible under Denver climate conditions, which is a temperate climate. Comparing the results for this scenario and those of the previous one, the energy demands were decreased because in Case A, the thermal zone should be also conditioned during the unoccupied hours, which resulted in a higher energy demand. For example, the ICF case demanded 12.8% less heating energy in Montreal under Case B compared to Case A.

Montreal

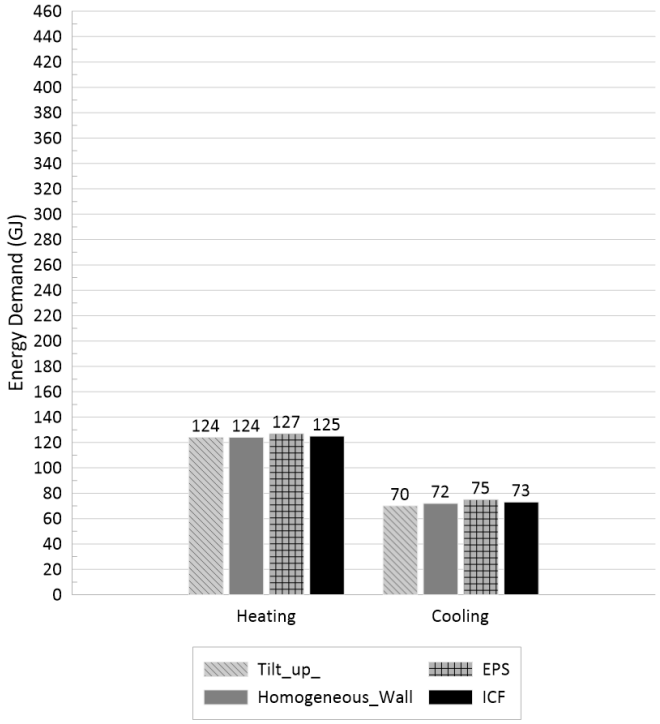

(a)

Miami

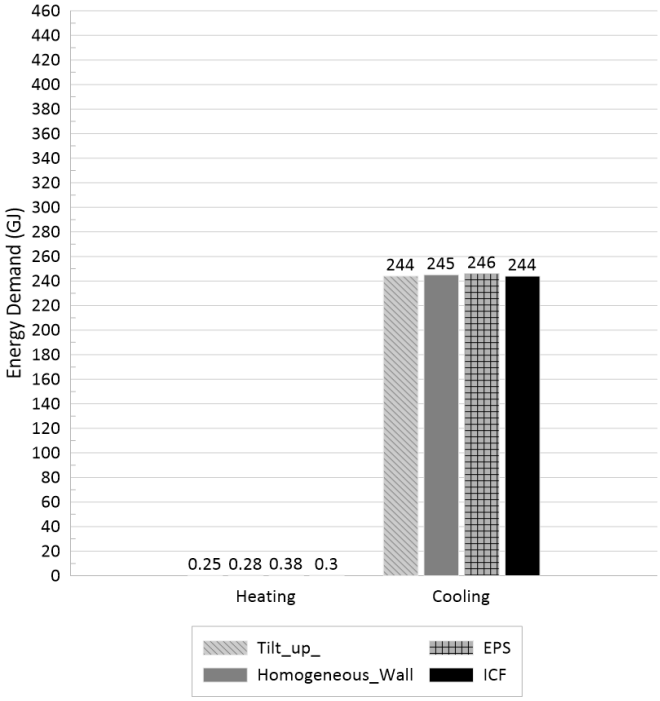

(b)

Denver

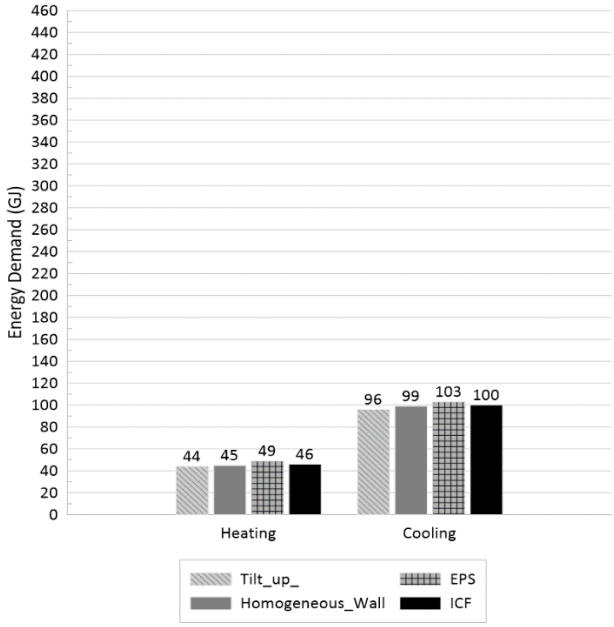

(c)

Figure 22. Energy demands for the ICF, tilt-up, and homogeneous wall cases under: (a) Montreal; (b) Miami, and (c) Denver climate conditions

4.3.2.3. Effects of the performance of ICF and tilt-up walls on the energy demands

In this section, by identifying the components that contribute to the overall heating and cooling loads, results for the specific cases of the office building located in Montreal with ICF and tilt-up walls, as alternatives of exterior wall assemblies, will be discussed.

To better analyze the sensible heating and cooling demands, firstly, the components that contributed to the hourly heating and cooling loads were identified, which are as follows:

- Internal convective heat gain (the heat transfer mode between indoor air and internal heat gain sources (i.e. people, lights, and electric equipment) is purely convective)
- Convection between indoor air and indoor surfaces of the walls, roof/ceiling, floor, and windows
- Heat gain/loss as a result of air transfer (mechanical ventilation and infiltration)

The heating and cooling loads of the perimeter zone 1 (please refer to Figure 23) for ICF and tilt-up wall cases were chosen as the example cases for the sake of comparison and explanation. Table

13 and Table 14 show the heating energy demand and cooling energy demand breakdown of the perimeter zone 1 for ICF and tilt-up cases under the weather conditions of Montreal. As expected, the annual heat gain/loss as a result of air transfer and internal gains were identical for both cases, and the differences were due to discrepancies in the convective heat transfer between indoor air and internal surfaces. Heat balance equation for the internal surface of the wall is [84]:

$$q"_{LWX} + q"_{SW} + q"_{LWS} + q"_{ki} + q"_{sol} + q"_{conv} = 0 \quad (20)$$

Where:

$q"_{LWX}$: Net longwave radiant exchange flux between zone surfaces $[\frac{W}{m^2}]$,

$q"_{SW}$: Net shortwave radiation flux to surface from lights $[\frac{W}{m^2}]$,

$q"_{LWS}$: Longwave radiation flux from equipment in zone $[\frac{W}{m^2}]$,

$q"_{ki}$: Conduction flux through the wall $[\frac{W}{m^2}]$,

$q"_{sol}$: Transmitted solar radiation flux absorbed at surface $[\frac{W}{m^2}]$, and

$q"_{conv}$: Convective heat flux to zone air $[\frac{W}{m^2}]$.

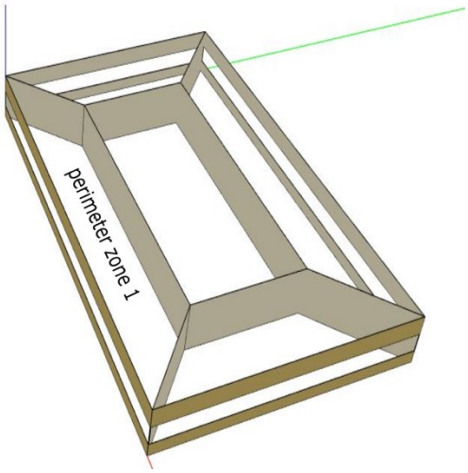

Figure 23. Schematic of the perimeter zone 1

Table 13. Heating load breakdown for ICF and tilt-up walls under Montreal weather conditions

	ICF		Tilt-up	
	Heating ($\times 10^{10}$)	Contribution to total heating	Heating ($\times 10^{10}$)	Contribution to total heating
Internal Heat Gain	0.373	-12.62%	0.377	-13.32%
Opaque Surface Convection	-0.443	14.97%	-0.330	11.67%
Windows Convection	-0.560	18.96%	-0.550	19.44%
Air Transfer	-2.326	78.69%	-2.325	82.21%
Total	-2.956	100%	-2.829	100%

Table 14. Cooling load breakdown for ICF and tilt-up walls under Montreal weather conditions

	ICF		Tilt-up	
	Cooling ($\times 10^{10}$)	Contribution to total cooling	Cooling ($\times 10^{10}$)	Contribution to total cooling
Internal Heat Gain	0.897	22.28%	0.894	23.13%
Opaque Surface Convection	3.523	87.50%	3.374	87.30%
Windows Convection	0.298	7.39%	0.289	7.49%
Air Transfer	-0.691	-17.17%	-0.692	17.92%
Total	4.027	100%	3.865	100%

For the case of the office building with ICF walls, the validity of the above equation was evaluated. Maximum discrepancy magnitude was 0.5 W. As a result, the elements of heat transfer for the internal surface can be summarized as follows:

- Conduction through the wall assembly,
- Convection between the wall's indoor surface and the indoor air, and
- Radiation heat gain/loss

Next, the conduction through ICF and tilt-up walls were assessed. Figure 24 shows the conduction heat transfer rate per surface area throughout the year. Positive values correspond to when heat flowed from the internal surface of the wall towards the core of the wall while negative values mean that the heat reached the internal surface from the core of the wall. It can be seen that the conduction values fluctuated more widely for tilt-up wall compared to ICF wall. In addition, as shown in Figure 25, the heat transferred from/to the internal surface were lower in both directions for ICF wall compared to tilt-up wall.

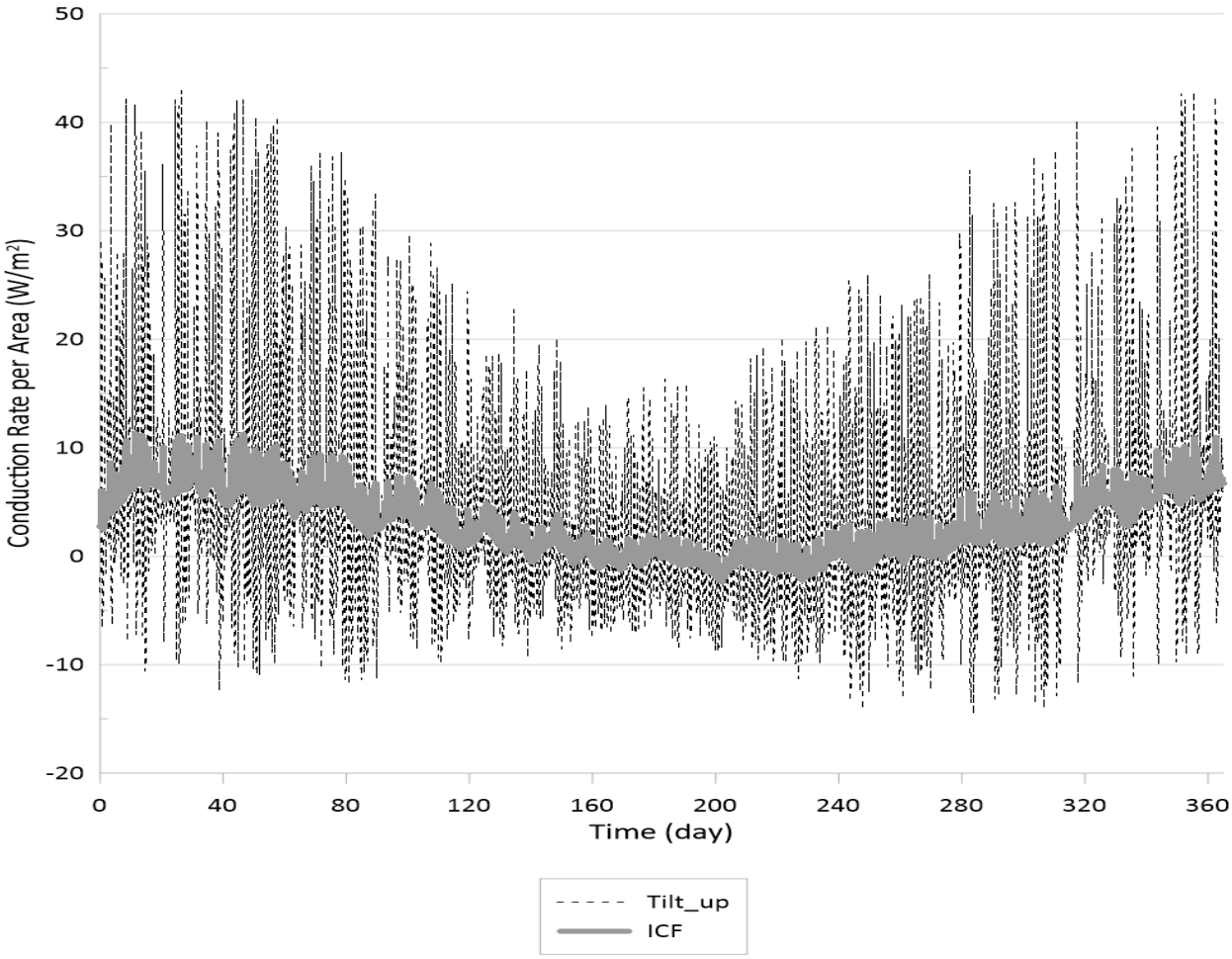

Figure 24. Conduction heat transfer rate per surface area of the wall for ICF and tilt-up assemblies

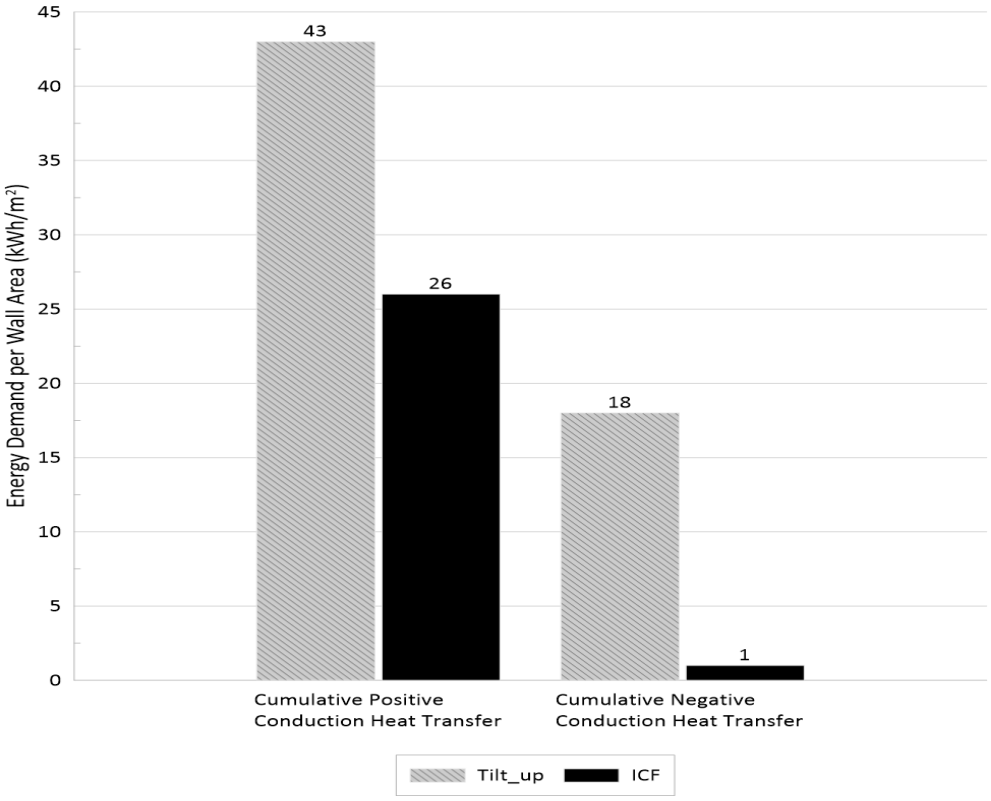

Figure 25. Cumulative positive and negative conduction heat transfer for the ICF and tilt-up walls

However, the element that determines the heating/cooling loads as a result of heat gain/loss through opaque walls is the convection heat transfer between internal surface of the wall and the indoor air. Figure 26 shows the convection heat transfer rate per wall's surface area throughout the year. Same as the conduction, positive and negative values correspond to the heating and cooling loads, respectively. As can be seen, the amplitude of changes of the convection heat fluxes was larger for ICF wall case compared to tilt-up case. Figure 27 shows the resulting heating and cooling energy demands for ICF and tilt-up assemblies, which were both lower for tilt-up wall case.

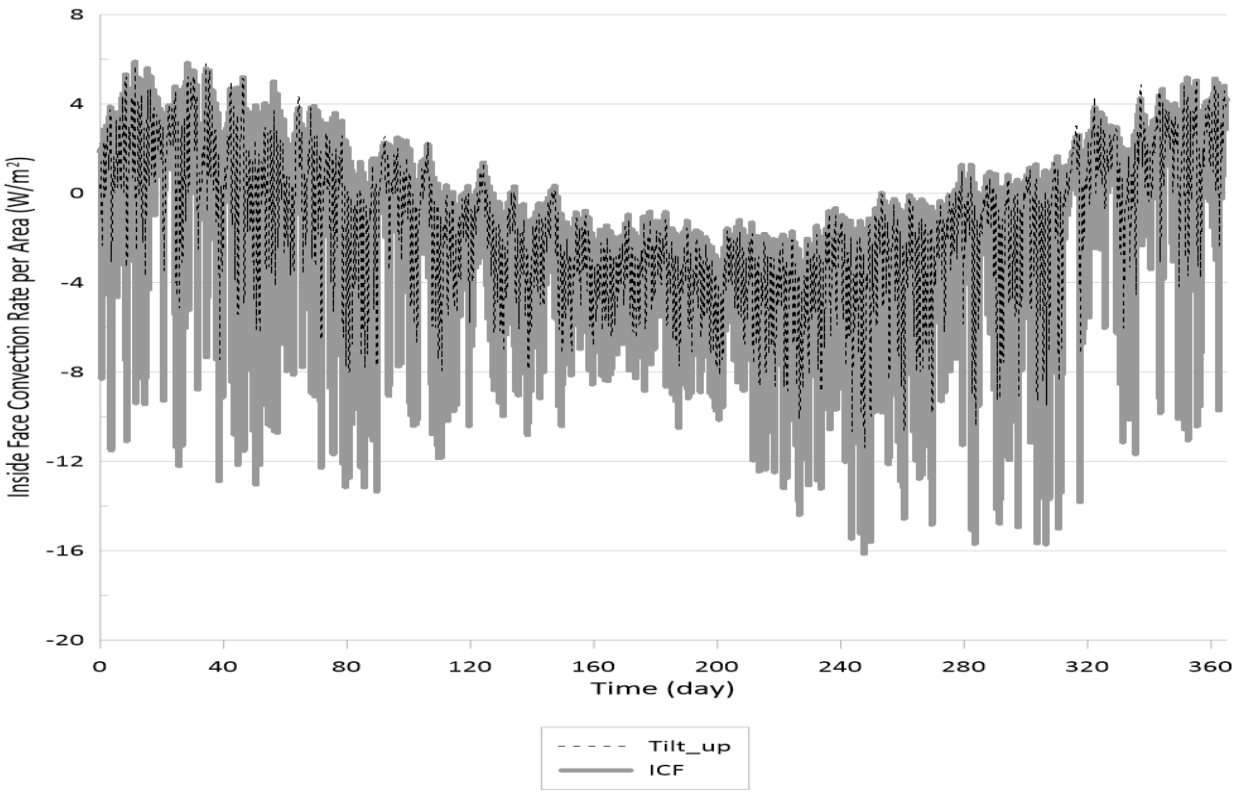

Figure 26. Convection heat transfer rate per wall's surface area for ICF and tilt-up walls

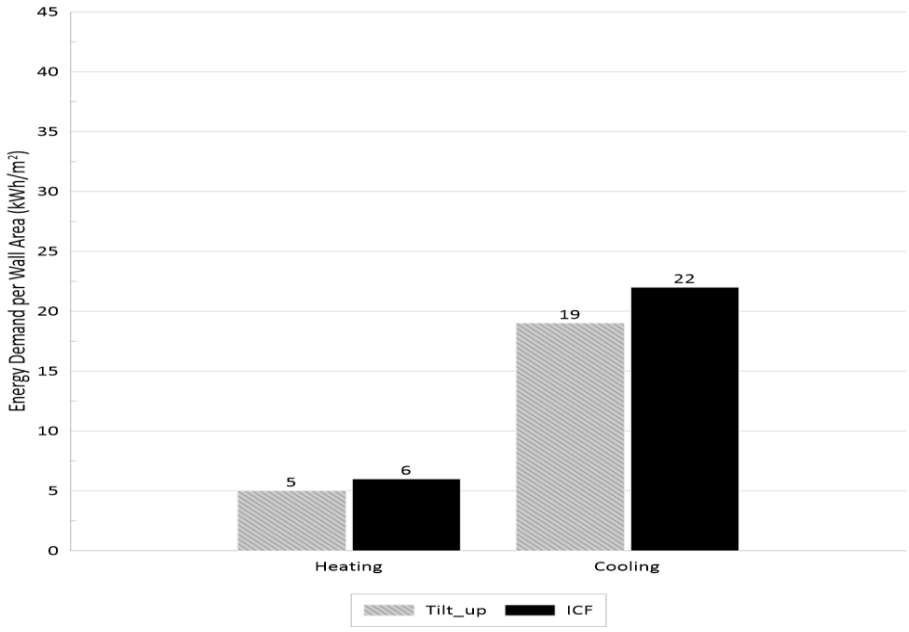

Figure 27. Heating and cooling loads as a result of convection heat transfer between internal surface of ICF and tilt-up walls and the indoor air

To better understand the reasoning behind the results, the internal surface temperature should be monitored more closely. Figure 28 represents the annual indoor surface temperatures for ICF and tilt-up walls. It can be seen that the amplitude of changes in the internal surface temperature of tilt-up wall was smaller, which resulted in lower heating/cooling loads. On the other hand, Figure 29 presents the heat convection, conduction, and indoor surface temperature for January 1st and January 2nd for ICF and tilt-up wall cases. There was a negligible time lag between the heat conduction from the internal surface of ICF wall and the indoor surface temperature, while there is a time lag between the profiles of these parameters for tilt-up wall.

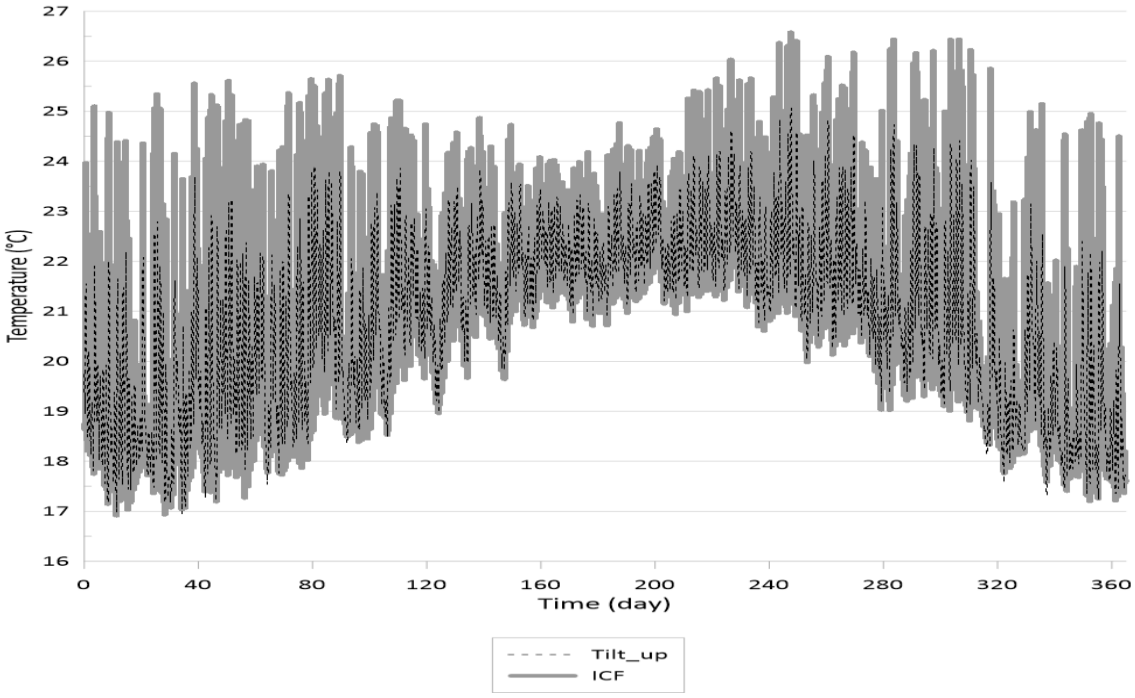

Figure 28. Internal surface temperature for ICF and tilt-up walls

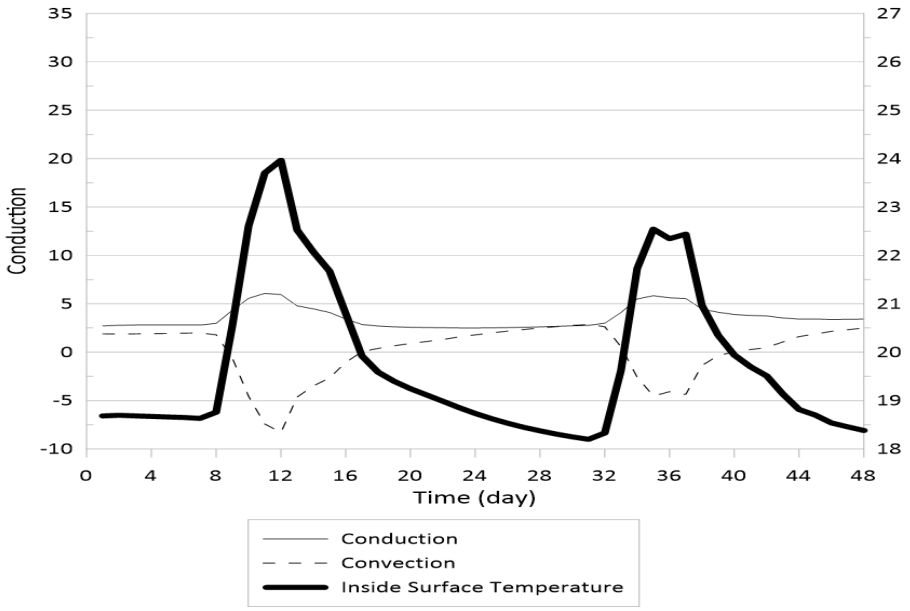

(a) ICF wall

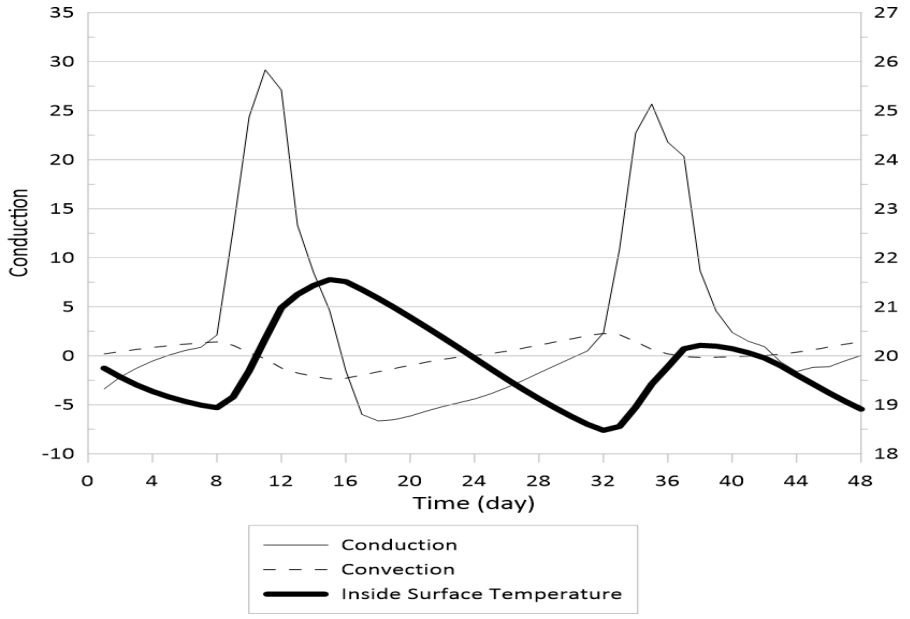

(b) Tilt-up wall

Figure 29. Heat conduction, convection, and internal surface temperature for: (a) ICF wall; and (b) tilt-up wall

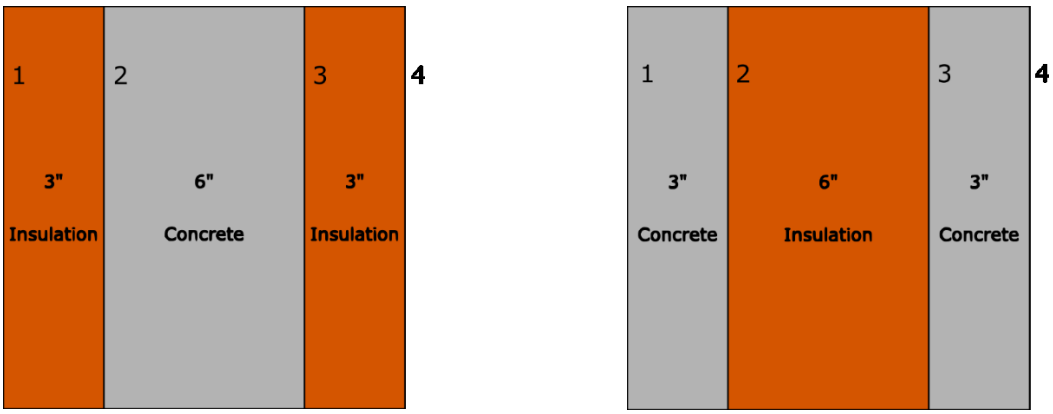

(a) (b)

Figure 30. ICF and tilt-up walls with numbered surfaces: (a) ICF; and (b) tilt-up walls

Although the amplitude of changes in the conduction from the internal surface of ICF wall was smaller compared to that of tilt-up wall, wider fluctuations were observed in the convection heat fluxes to the internal surface of ICF wall compared to those of tilt-up wall. Figure 30 shows the surfaces of ICF and tilt-up walls. Firstly, it should be noted that for ICF wall, 51% of the total R-value of the wall is between surface 2 and surface 4, while for tilt-up wall, 98.6% of the total R-value of the wall is between surface 2 and surface 4. The diffusivity of EPS insulation material is higher than that of the concrete layer because of its low thermal conductivity, density, and heat storage capacity compared to the concrete material whose thermal conductivity is higher but its product of density and specific heat capacity is much higher (please refer to Table 5). Although the resistivity of the concrete layer in tilt-up wall is lower than that of ICF wall, it can store more energy due its higher thermal capacity, and hence, can flatten the temperature fluctuations on the inner layer surface. From 8 am until 5 pm, the thermal radiation incident on the internal surface of the wall increases (as a result of people's presence, lights', and equipment's heat generation, and solar radiation). This incident heat can be transferred towards the outer surface of the wall, be stored inside the innermost layer, or increase the temperature of the layer. As for ICF case, given that the R-value of the innermost layer is rather higher, the heat cannot easily flow towards the outer layers. On the other hand, the thermal storage capacitance of EPS layer is negligible. As a result, the temperature of the internal surface of the wall increases, and the heat is conducted from the inner surface towards the thermally massive layer, which is located at the middle of the wall. Also, because the temperature of the internal surface of the wall is higher than the indoor air temperature for most of this period, the heat is dissipated back to the indoor air. The heat dissipation from the internal surface, as well as the decrease of the outdoor temperature, decreases

the surface temperature, and as a result, the convection from the indoor air increases during nighttime. In conclusion, the negligible thermal storage capacitance of the innermost layer and its high thermal resistance contributed to the wide changes in the surface temperature of the wall, and as a result, the wide changes in the convection heat transfer.

As for tilt-up wall, on the other hand, the innermost layer has a high heat storage capacitance and a rather low thermal resistance. As a result, the incident heat radiation can be stored in the concrete layer, and the surface temperature does not change rapidly within the period of 8am to 5pm. On the other hand, the surface temperature is higher during nights, and whenever the surface temperature is decreasing, the stored heat is conducted back towards the inner surface to compensate the heat loss (or lack of heat radiation for maintaining the temperature). Hence, the internal surface temperature of the wall is maintained within a more stable range compared to that of ICF wall. As a result, the heat convection between the wall and indoor air decreases. In conclusion, given the high amount of thermal mass and rather low R-value of the innermost layer for the tilt-up wall case, the heat can easily flow and be stored, and the changes in the inner surface temperature was smaller, which in turn leads to a lower convection heat transfer rate.

4.3.2.4. Peak energy demands

In this section, peak heating and cooling energy demands of the archetype office building considering three case study walls, namely ICF, tilt-up, and homogeneous walls, were compared. Montreal weather conditions were taken into account, and case B of the indoor air temperature was considered. Figure 31 shows the peak heating and cooling demands of these cases for each month. Overall peak heating demand for the case with ICF, tilt-up, and homogeneous walls were 42.25 kW, 42.82 kW, and 42.27 kW, respectively. On the other hand, peak cooling energy demands for the cases with ICF, tilt-up, and homogeneous walls were 51.96 kW, 51.90 kW, and 51.16 kW, respectively. It can be observed that the case that had ICF walls as part of its building envelope system had the lowest peak heating demand while the case with homogeneous walls had the lowest peak cooling demand. On the other hand, the case with tilt-up walls had the highest peak heating demand while the building with ICF walls had the highest peak cooling demand.

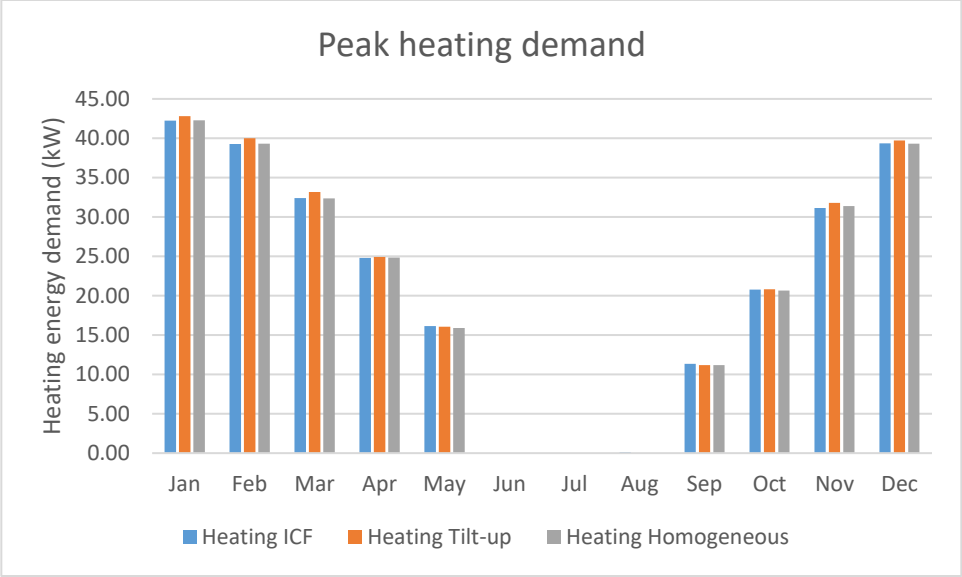

(a)

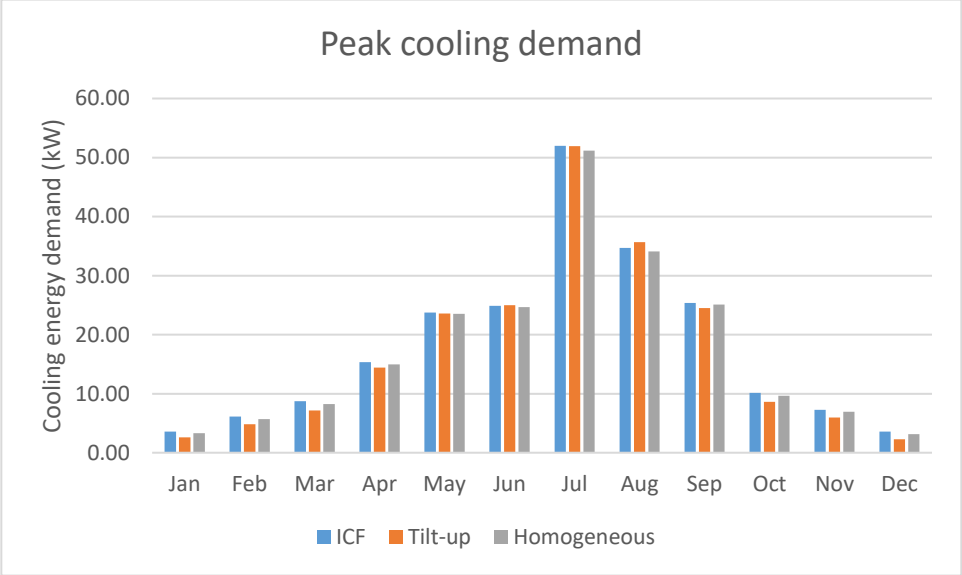

(b)

Figure 31. Monthly peak energy demands for the cases with ICF, tilit-up, and homogeneous walls: (a) heating; (b) cooling

4.3.2.4. Comparing COMSOL and EnergyPlus results

The final step is to compare the results of heat conduction from the inner surface of a south-facing ICF wall under the weather conditions of Montreal while the indoor temperature is maintained at 20°C. TMY weather data of Montreal was downloaded from the EnergyPlus website [80], and the calculations of the sol-air temperature for a south-facing wall were performed. The resulting sol-

air temperature values were then the outside boundary conditions for the COMSOL simulations. Initially, the inside and outside surface film coefficients were assumed to be 8.33 W/(m^2.K) and 33.33 W/(m^2.K), respectively. Figure 31 shows the conduction heat fluxes from the inner surface of the ICF wall according to COMSOL © and EnergyPlus © results. It can be observed that although the general trends were similar, COMSOL results cannot properly follow the fluctuations of the heat fluxes compared to EnergyPlus © results. Comparing these two sets of results, the discrepancy has been observed, which can be due to the fact that in COMSOL simulation model, constant film coefficients were assumed, whereas, EnergyPlus © calculated the film coefficients for each time step.

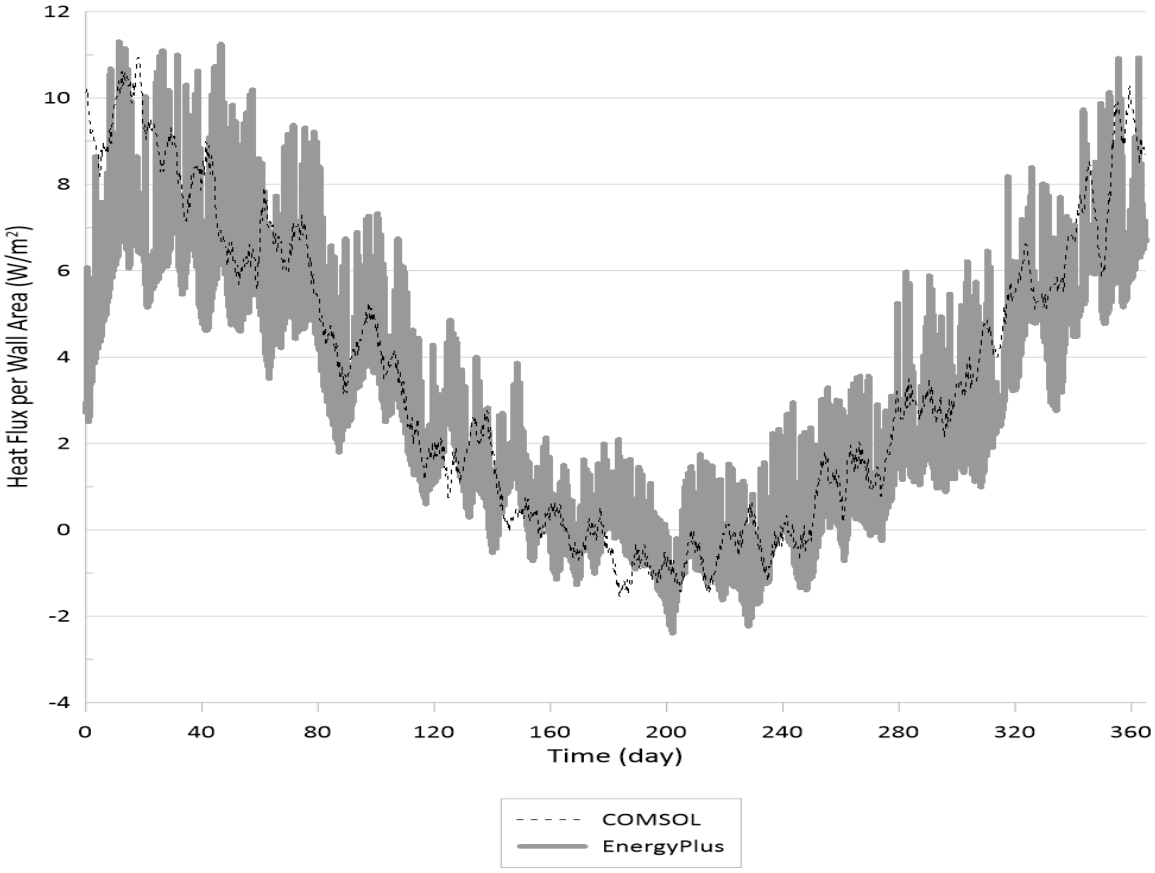

Figure 31. Conduction heat fluxes for ICF wall under Montreal weather conditions based on COMSOL and EnergyPlus simulation results assuming constant surface film coefficients

One important note is that EnergyPlus © does not assume a constant value for the surface film coefficients. As a result, the values calculated by EnrgyPlus © were imported into COMSOL ©. Figure 32 represents the results of this analysis. As can be observed, the amplitude of changes in

the heat fluxes calculated by COMSOL © model was larger compared to the previous investigation, yet there are some discrepancies. Another source of discrepancy can be the fact that sol-air temperatures were assumed as outdoor weather conditions in COMSOL © analysis while EnergyPlus © treats temperature and solar radiation separately.

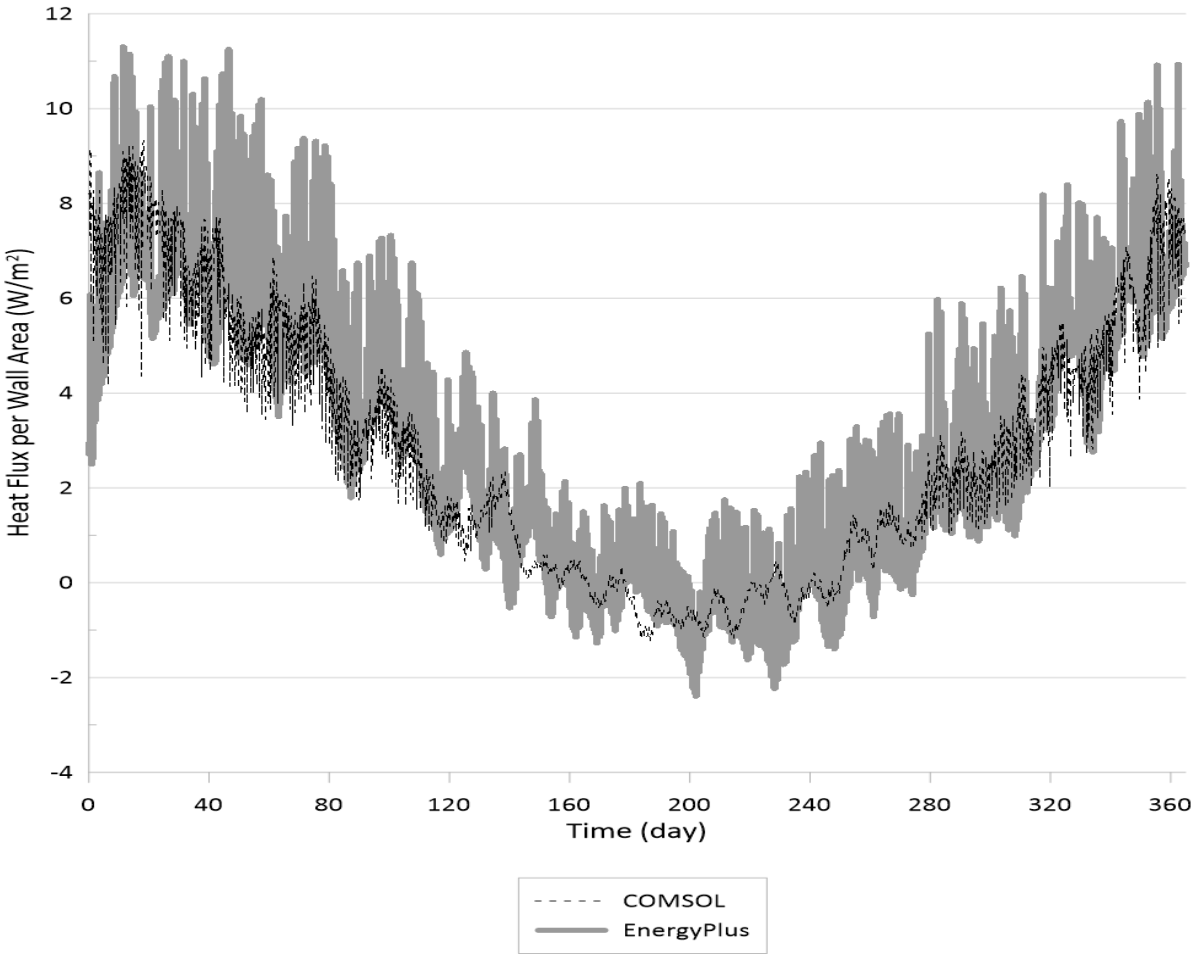

Figure 32. Conduction heat fluxes for ICF wall under Montreal weather conditions based on COMSOL and EnergyPlus simulation results using the surface film coefficients calculated by EnergyPlus

4.4. Thermal bridging effect on the transient thermal performance of steel stud and wood-frame walls

4.4.1. Case studies

Two case study walls were considered for this analysis: (i) a steel-stud wall and (ii) a wood-frame wall. A catalogue called “the Building Envelope Thermal Bridging Guide (BETB)” [19] has been

published, which considers the effective thermal performance of the building envelope components including walls. The envelope components that this catalogue takes into consideration are common to the Canadian construction. Figure 33 depicts the schematics of these walls, which correspond to wall 5.1.2 (steel-stud wall) and 7.1.1 (wood-frame wall) of BETB catalogue [19]. Table 15 and Table 16 present the thermophysical properties of the materials of the steel-stud wall while Table 17 and Table 18 give the thermophyiscal properties of the wood-frame assembly's materials. Three case study sinusoidal daily weather conditions were considered: (a) a sinusoidal curve changing between -20°C and -8°C representative of a heating-dominated climate; (b) a sinusoidal curve fluctuating between 14°C and 26°C representative of a temperate climate, and (c) a sinusoidal curve whose minimum and maximum values were 25°C and 37°C, respectively, representative of cooling-dominated climate. Minimum and maximum temperatures occurred at 3 A.M. and 3 P.M., respectively, for all three scenarios. Figure 34 shows the schematics of these profiles.

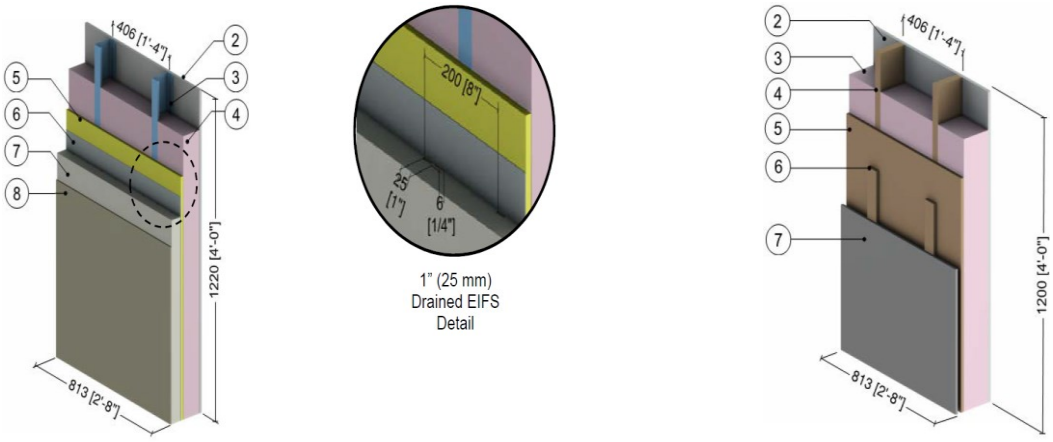

(i) (ii)

Figure 33. Schematics of the case study walls: (i) steel-stud wall; and (ii) wood-frame wall

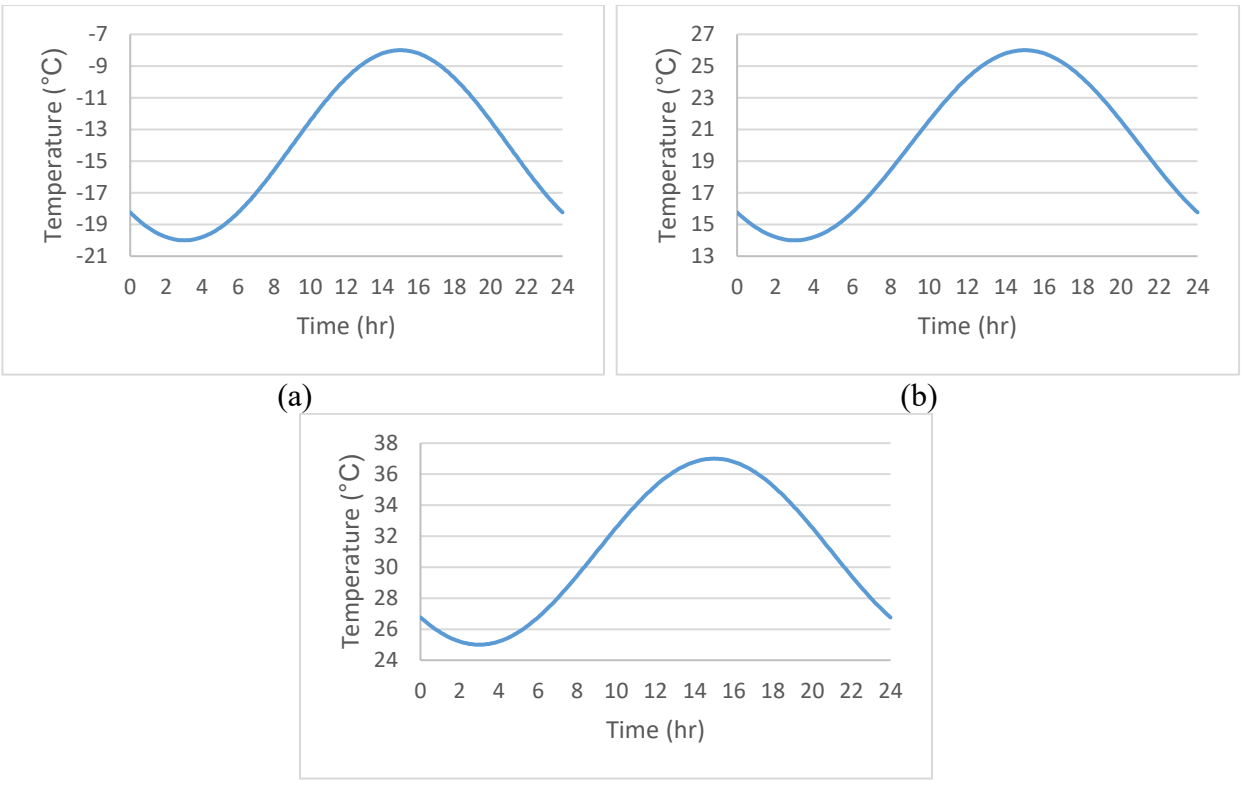

Figure 34. Outside daily temperature variations: (a) heating-dominated; (b) temperate; and (c) cooling-dominated climates

Table 15. Material properties of the steel-stud wall

ID	Assembly Component (Excluding the Studs)	Thickness (mm)	Conductivity (W/m.K)	Resistance (m^2.K/W)	Density (kg/m^3)	Specific Heat (J/kg.K)
9	Exterior Air Film	-	-	0.03	-	-
8	Lamina	4.00	0.9	0.0044	1922	850
7	Exterior Insulation Board (XPS)	50.00	0.038	4	16	1470
6	OSB	-	-	-	-	-
5	Exterior Sheathing	13.00	0.16	0.081	800	1090
4	Fiberglass Batt Insulation	92.00	0.044	2.09	14	710
2	Gypsum Board	13.00	0.16	0.081	800	1090
1	Interior Air Film	-	-	0.12	-	-

Table 16. Properties of the steel stud

Parameter	Value	Parameter	Value
Flange width	1 5/8 in.	Studs centric distance	16 in.
Flange depth	3 5/8 in.	Steel conductivity	62 W/m.K
Flange specification	18 gauge	Steel density	7830 kg/m^3
Flange thickness	0.0478 in.	Steel specific heat capacity	500 J/kg.K

Table 17. Properties of the wood stud

Parameter	Value	Parameter	Value
Stud width	16 in.	Studs centric distance	16 in.
Stud depth	140 mm.	Steel conductivity	0.1 W/m.K
Steel density	500 kg/m^3	Steel specific heat capacity	1880 J/kg.K

Table 18. Material properties of the wood-frame wall

ID	Assembly Components	Thickness (mm)	Conductivity (W/m.K)	Resistance (m^2.K/W)	Density (kg/m^3)	Specific Heat (J/kg.K)
8	**Exterior air film**	-	-	0.12	-	-
5	**Exterior Wood Sheathing**	13.00	0.1	0.13	500	1880
3	**Fiberglass Batt Insulation**	140.00	0.042	3.33	14	710
2	**Gypsum Board**	16.00	0.16	0.1	800	1090
1	**Interior Air Film**	-	-	0.12	-	-

Table 19 presents the resulting R-value, thermal conductivity, density and specific heat capacity of the layer replacing the stud cavity of the case study wood-frame wall.

Table 19. Resulting thermophysical properties of the layer replacing the cavity of the wood-frame wall

Thermal resistance	Thermal conductivity	Density	Specific heat capacity
2.97 RSI	0.0471 W/m.K	59.49 kg/m^3	1630.42 J/kg.K

Table 20 presents the results of R-values, thermal conductivities, densities, and specific heat capacities of the middle layer existing in the cavity for the three-part cavity wall (Figure 5b). Table 21 gives the corresponding values for the equivalent layer replacing the entire cavity (Figure 5c), respectively.

Table 20. Resulting thermophysical properties of the middle layer of the three-part cavity wall (Figure 5b) for the steel-stud wall case

Thermal resistance	Thermal conductivity	Density	Specific heat capacity
0.15 RSI	0.62 W/m.K	145.37 kg/m^3	519.88 J/kg.K

Table 21. Resulting thermophysical properties of the equivalent cavity layer (Figure 5c) for the steel-stud wall case

Thermal resistance	Thermal conductivity	Density	Specific heat capacity
1.1 RSI	0.085 W/m.K	57.71 kg/m^3	550.66 J/kg.K

Next, the simulation cases, along with the corresponding boundary conditions and material properties, were implemented in COMSOL Multiphysics © 5.6 software. Regarding the wood-frame wall, the original stud wall, as well as the resulting multi-homogeneous layer wall, was modeled. On the other hand, the thermal performance of three case study wall assemblies were assessed for the steel-stud wall case: (1) the original stud wall; (2) the wall whose cavity has one equivalent layer replacing the affected zone and two layers of insulation (Figure 5b), and (3) a multi-homogeneous layer equivalent wall (Figure 5c). On the other hand, two cases were considered for the wood-frame wall: (a) original wall; (b) equivalent wall. Firstly, the walls were simulated under steady-state conditions to compare the resulting R-values. Then, transient conditions were assumed such that the indoor temperature is maintained at 20°C throughout the simulation while the outside temperature conditions is time-dependent. The simulations were performed for 8 days, and it was assumed that the daily outside temperature changes follow the patterns presented in Figure 33. The reason for considering 8 days for the simulations is to ensure that the quasi-steady state conditions i.e. the conditions for which the values of heat fluxes are

identical to those of the corresponding points in the previous cycle [81] are reached. Instantaneous heat fluxes were compared.

4.4.2. Results and discussion

The first step was to simulate the case study walls under the steady-state conditions for calculating the R-values. Table 22 shows the resulting thermal resistances of the walls. As it can be seen, there is a 4% deviation between the R-values of the original and equivalent walls for the steel-stud case, while the R-value of the original wood-frame wall was estimated with a discrepancy of nearly 0.3% using the parallel path method. Next, the resulting heat fluxes will be compared.

Table 22. Thermal resistances of the case study walls

Wall	R-value from COMSOL © simulation (m^2.K/W)	Hand-calculated R-value (m^2.K/W)
Original steel stud wall	2.85	N/A
3-part wall (steel stud case)	2.45	N/A
Equivalent wall (steel stud case)	2.72	2.73
Original wood-frame wall	3.47	N/A
Equivalent wall (wood-frame case)	3.46	3.47

4.4.2.1. Steel stud wall

Calculated width of the modified zone (W) for the steel-stud wall considered was 135.08 mm. Figure 35 shows the instantaneous heat fluxes through the interior surface of the case study wall assemblies of the steel stud case under heating-dominated, cooling dominated, and temperate exterior temperature conditions. As it can be seen from the graphs, the heat flux trends were similar in all cases. However, comparing the results of the three-part wall and original wall, the maximum deviations between the instantaneous heat fluxes were 18.24% and 22.27% for the heating-dominated and cooling-dominated climate conditions, respectively, which shows that the three-part wall cannot accurately estimate the thermal behavior of a steel-stud wall under transient conditions. It should be noted that because there were values of instantaneous heat fluxes near zero, comparing the deviations of the heat fluxes for the temperate climate may lead to misleading conclusions. In fact, percentage differences were high, while the heat fluxes were small values, and such comparison is not valid. On the other hand, the maximum deviations between the

instantaneous heat fluxes of the original stud wall and the equivalent wall were 5.19% and 5.52% under heating-dominated and cooling-dominated conditions, respectively. 4% difference between the R-values of these walls were identified.

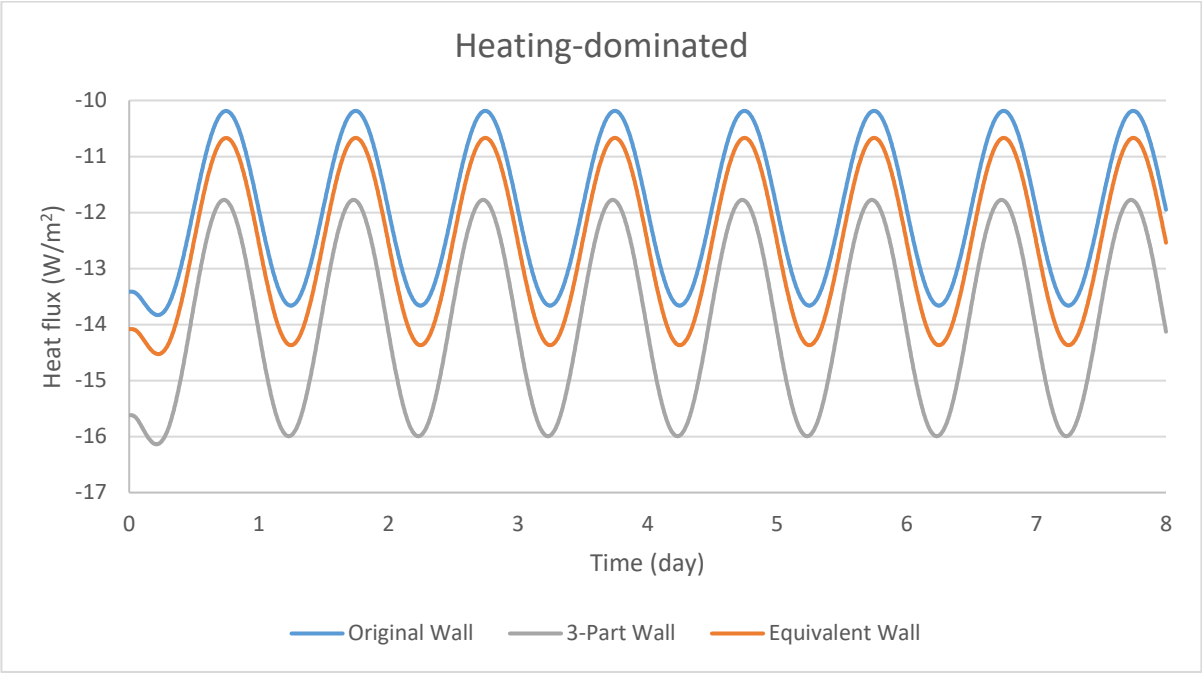

(a)

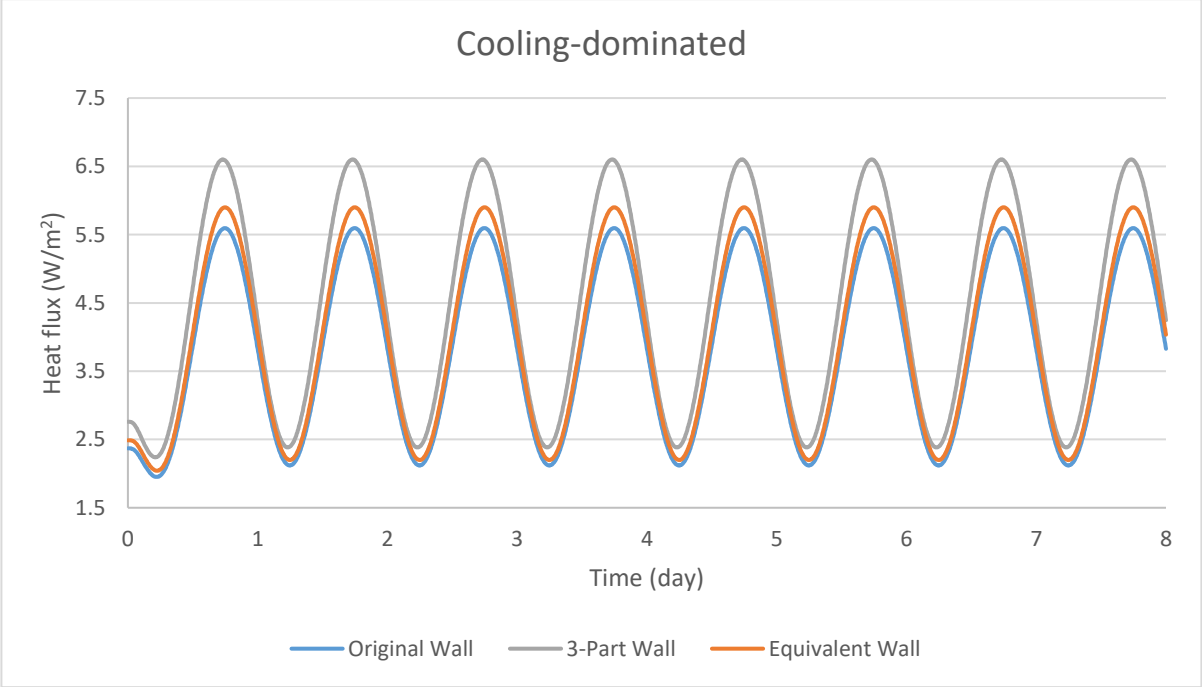

(b)

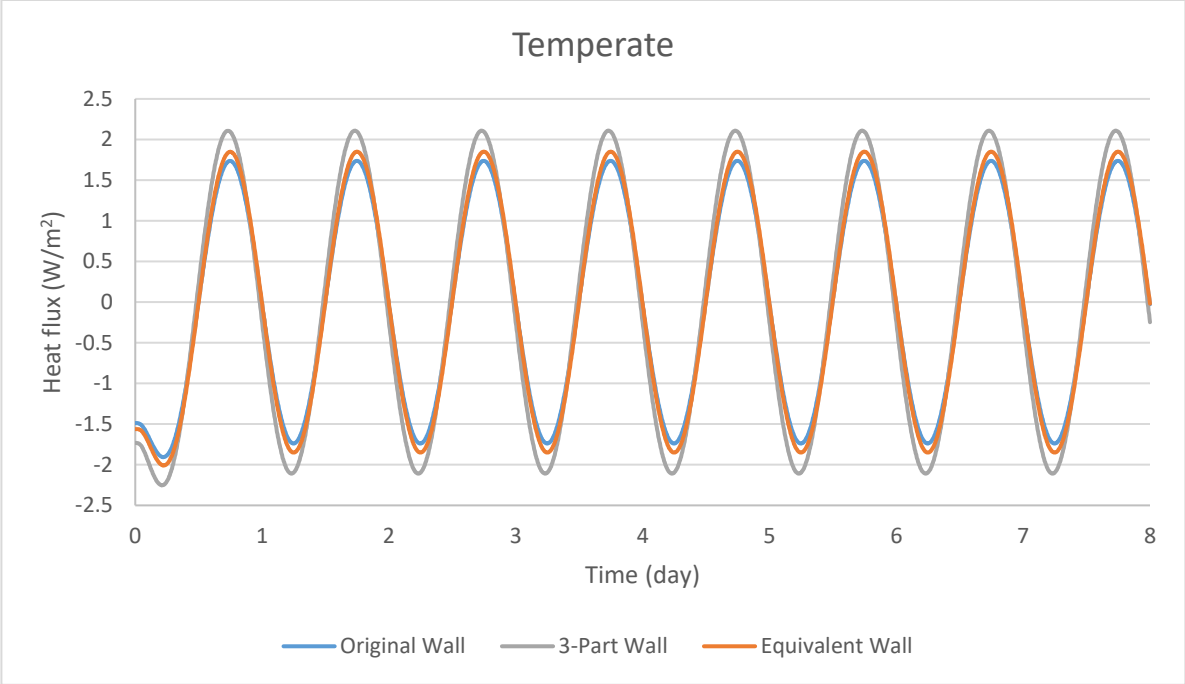

(c)

Figure 35. Resulting heat fluxes for the steel stud wall cases under: (a) heating-dominated; (b) cooling dominated; and (c) temperate temperature conditions

4.4.2.2. Wood-frame wall

The heat fluxes from the interior surface of both the original wood-frame wall and its corresponding equivalent wall are illustrated in Figure 36. Same as what has been seen in the steel stud wall case, the heat flux trends of the original and equivalent wood-frame assemblies were similar. Maximum deviations between the heat flux results of the original and equivalent walls were 4.30% and 18.4% for the heating-dominated and cooling-dominated climates. This implies that the equivalent wall can better predicate the thermal behavior of the real wood-frame wall under the case study heating-dominated climate. It should be noted that the thermal mass of the wood-frame wall is higher than the steel-stud wall, and that might be a reason why the equivalent wall method was not found to be as productive for the wood-frame wall case. Finding the maximum deviations between the heat fluxes of the walls were avoided for the temperate climate conditions due to the potential misleading conclusions.

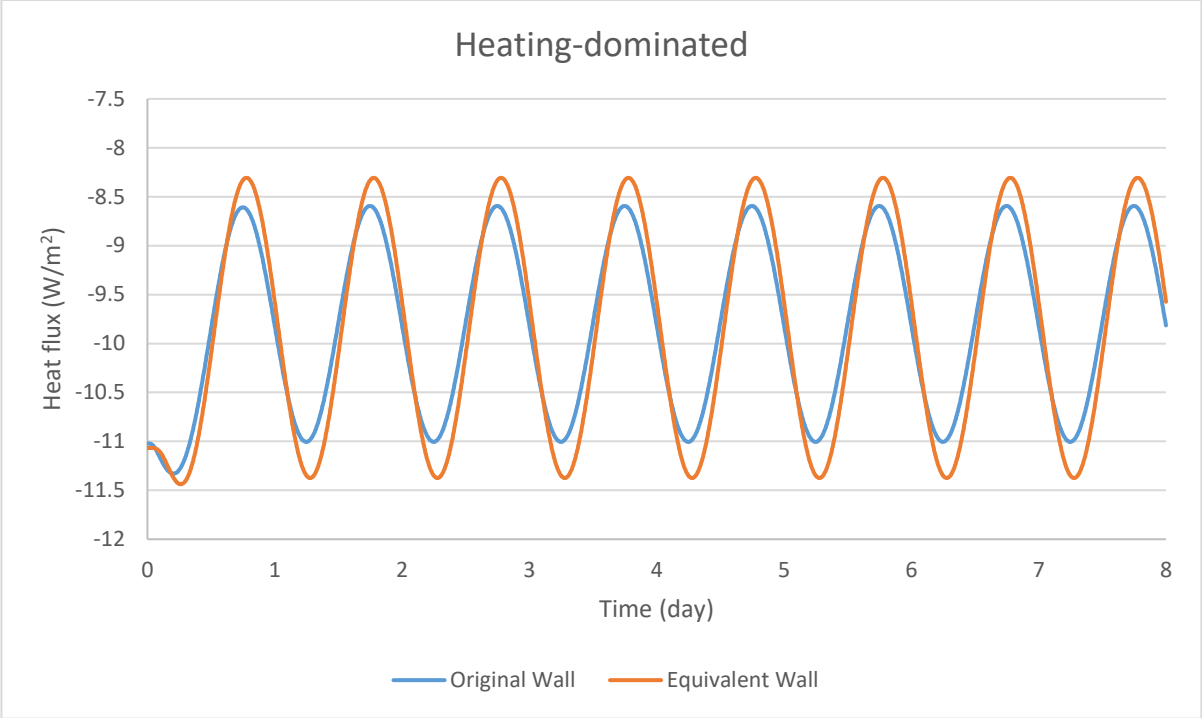
Heating-dominated
-7.5
-8
-8.5
-9
-9.5
-10
-10.5
-11
-11.5
-12
Heat flux (W/m²)
0
1
2
3
4
5
6
7
8
Time (day)
Original Wall
Equivalent Wall

(a)

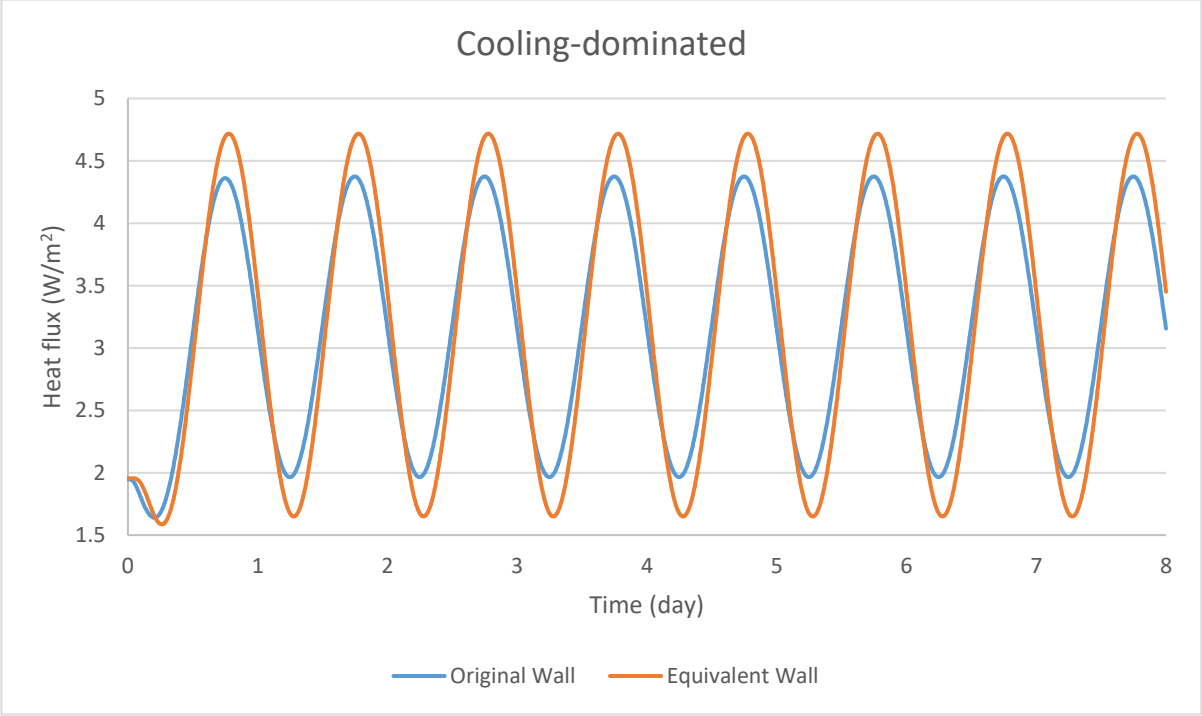
Cooling-dominated
5
4.5
4
3.5
3
2.5
2
1.5
Heat flux (W/m²)
0
1
2
3
4
5
6
7
8
Time (day)
Original Wall
Equivalent Wall

(b)

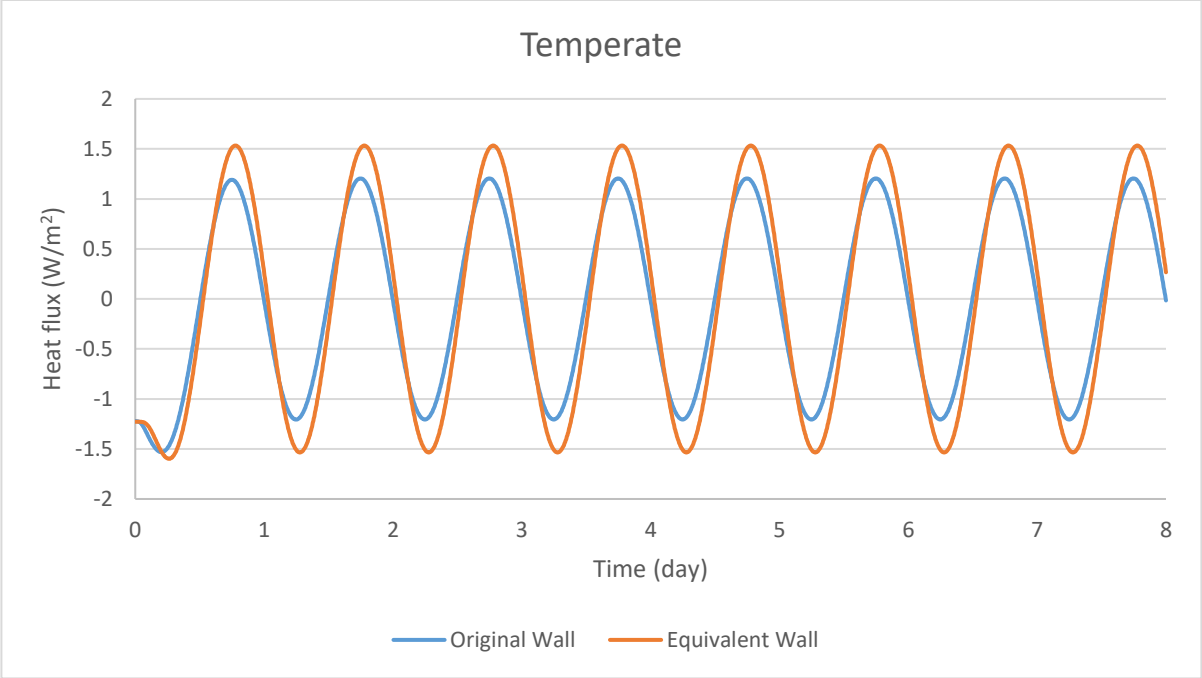

(c)

Figure 36. Resulting interior heat fluxes for the original and equivalent wood-frame walls under: (a) heating-dominated; (b) cooling-dominated; and (c) temperate climates

CHAPTER 5: Conclusion and future work

This chapter aims to provide the main findings of this investigation and suggest potential future work. Three main topics were considered, namely the effects of thermal mass on transient thermal performance of walls, effects of thermally massive layer placement on transient thermal performance of walls and energy performance of buildings, and thermal bridging effect in stud walls.

5.1. Conclusion

As for the effects of thermal mass on transient thermal performance of walls, three case stud wall assemblies were considered: an ICF wall, a tilt-up wall, and a wall made of one EPS layer. The main findings and conclusion are as what follows:

- Under sinusoidal temperature conditions, the time lag between outside temperature profile and the thermal responses of the ICF and tilt-up assemblies were 7 hours and 6.5 hours, respectively.
- EPS wall was found to have minimal peak-demand shifting due to its rather low thermal storage capacitance.
- Heat fluxes from the interior side of the ICF wall had a smaller amplitude of changes as compared to those of the tilt-up and EPS walls.
- Under Montreal TMY weather conditions, maximum heat losses for ICF, tilt-up and EPS walls were 10.95 W/m^2, 13.67 W/m^2, and 15.61 W/m^2, respectively. Also, maximum heat gains under TMY Miami weather conditions were 3.63 W/m^2, 5.15 W/m^2, and 8.27 W/m^2 for these walls, respectively.
- Heat fluxes of the ICF wall tended to fluctuate less compared to the tilt-up and EPS walls.
- Based on the heating and cooling loads for Miami and Montreal, it was concluded that the thermal mass effect was more evident during the secondary season for both locations i.e. summers in Montreal and winters in Miami.
- ICF wall required 2.5% and 2.6% less energy in comparison with EPS wall for compensating for heat losses/gains through the opaque wall during the primary seasons in Montreal and Miami, respectively.
- Regarding the indoor surface temperatures, it was observed that the fluctuations in interior surface temperatures are less for the ICF wall.

- In conclusion, based on the case studies of our interest, ICF wall can shift and dampen the peak loads and reduce the energy usage in buildings better than tilt-up wall.

Second part of this investigation was devoted to assessing the effects of layer sequencing patterns of wall assemblies on transient thermal performance of walls and energy performance of a case study office building. In fact, effect of different placements of thermally massive and insulation layers were studied. Three climate conditions were taken into account for our energy simulation cases: Montreal, Miami, and Denver. The main findings are as follows:

- Under the case study sinusoidal climate conditions, the wall made of one homogeneous layer had the lowest decrement factor and the smallest heat flux and indoor surface temperature fluctuation amplitudes. On the other hand, ICF wall had the highest amount of time required to reach quasi-steady state conditions i.e. a change in outdoor temperature conditions affected the indoor conditions with more delay.
- In order to have the minimum decrement factor, the minimum indoor heat flux and surface temperature, and the maximum time required to reach quasi steady-state conditions, thermally massive layer of the wall should not be directly exposed to the fluctuations of the temperature conditions, especially the outdoor temperature conditions whose fluctuations are more intense.
- Under Montreal, Miami, and Denver climate conditions and for both indoor air temperature scenarios, the case containing tilt-up walls demanded less heating and cooling energy compared to others. On the other hand, the case with EPS walls had the highest heating and cooling demands, which showed the importance of thermal mass as a mean to reduce the energy demands of the case study office building.
- Comparing the energy performances of the ICF and tilt-up cases, under the first indoor air temperature scenario, maximum energy savings was for heating in Denver, for which the tilt-up case demanded 6% less heating energy. Under the second indoor air temperature scenario, tilt-up case, compared to the ICF case, demanded 4.5% and 4.2% less heating and cooling energies in Denver, respectively. In addition, the fluctuations in the indoor surface temperature were lower for the tilt-up wall case.

- Homogeneous wall case demanded more energy compared to the tilt-up case but less energy compared to the other cases under the three climate conditions and for both indoor air temperature scenarios.
- In conclusion, based on the cases studied, placing the thermally massive layer at the interior side of the wall can reduce the energy demand of the case study office building. However, the energy savings are not significant.

The final step of this investigation was to present a model in order to account for the effects of thermal bridges on transient thermal performance of selected stud wall assemblies. These are the main results and conclusion for this section of our investigation:

- There was 4% difference between the R-values of the original steel stud wall and its corresponding equivalent wall while thermal resistance of the 3-part wall was 14% lower than that of the original steel stud wall. On the other hand, R-value of the equivalent wall deviated from that of the original wood-frame wall by 0.3%.
- Comparing the instantaneous heat fluxes from the interior surfaces of the original steel-stud wall and those of the 3-part wall, 18.24% and 22.27% were the maximum deviations under heating-dominated and cooling-dominated climates, respectively.
- Maximum deviations between the instantaneous heat fluxes of the original steel-stud wall and its equivalent wall were 5.19% and 5.52% under heating-dominated and cooling-dominated temperature conditions, respectively.
- Instantaneous heat fluxes from the interior surface of the original wood-frame wall and its equivalent wall deviated by 4.3% and 18.4% under heating-dominated and cooling-dominated climate conditions, respectively.
- Conclusion: The presented equivalent wall method can predict the transient thermal behavior of the case study steel-stud wall with a maximum error of 5.52%. It should be noted that a 4% difference was observed between the R-values of the original wall and its thermally equivalent wall. However, the precision of this method for the wood-frame wall depended on the climate conditions, and the method can more precisely predict the thermal behavior of the case study wood-frame wall under heating-dominated climate conditions.

5.2. Future work

It should also be mentioned that because the thermal properties of the concrete are moisture-dependent, performing hygrothermal simulations can provide a better insight into the problem. However, it is out of the scope of the current study. The authors also acknowledge that for taking the decision of where to place the thermally massive layer, hygrothermal performance of the building envelope should be taken into account, and the current study is the first step towards taking this decision.

Also, given that the case study building was a small office building, a potential future work would be to consider other buildings with different design specifications e.g. building application. Also, the HVAC system considered in this study was an imaginary one which provides enough heating/cooling to compensate for the heat loss/gain at each time step. This HVAC system does not exist in the real world. Thus, another potential future work is to take into account real HVAC systems with regard to design specifications and perform the investigation. Finally, the case study walls do not cover all potential alternatives, thus, other walls should also be considered to have a better understanding of the thermal mass and thermally massive layer placement on the thermal performance of the walls and the energy performance of case study buildings.

Considering the thermal bridging effect in stud walls, as the primary aim was to provide energy simulation specialists with a simple method to account for thermal bridging effect, a possible future work is to compare the energy demands of a case study building considering stud walls and their corresponding thermally equivalent wall. Also, one steel stud wall and one wood-frame wall were the case studies of our interest. Given that the transient thermal performances of the walls depend on various design parameters such as the thickness of the cavity, it is recommended to implement this method on other stud walls and assess the differences between thermal performances of original walls and their equivalent walls.

References

[1] R. D. Torrie, C. Stone, and D. B. Layzell, "Understanding energy systems change in Canada: 1. Decomposition of total energy intensity," *Energy Econ.*, vol. 56, pp. 101–106, 2016.

[2] Y. Wang, M. Sun, R. Xie, and X. Chen, "Multiplicative Structural Decomposition Analysis of Spatial Differences in Energy Intensity among G20 Countries," *Appl. Sci.*, vol. 10, no. 8, p. 2832, 2020.

[3] Statistics Canada, "Electric power selling price index, monthly - Table: 18-10-0204-01." 2020. [Online]. Available: https://doi.org/10.25318/1810020401-eng

[4] Statistics Canada, "Raw materials price index, monthly - Table: 18-10-0034-01." 2020. [Online]. Available: doi: https://doi.org/10.25318/1810003401-eng

[5] Environment and Climate Change Canada, "Pan-Canadian framework on clean growth and climate change : Canada's plan to address climate change and grow the economy (Ser. Deslibris)." 2016.

[6] T. G. Theodosiou and A. M. Papadopoulos, "The impact of thermal bridges on the energy demand of buildings with double brick wall constructions," *Energy Build.*, vol. 40, no. 11, pp. 2083–2089, 2008.

[7] National Resources Canada's Office of Energy Efficiency, "Survey of Commercial and Institutional Energy Use (SCIEU) - Buildings 2014 – Data Tables." 2014. [Online]. Available: https://oee.nrcan.gc.ca/corporate/statistics/neud/dpa/menus/scieu/2014/tables.cfm

[8] H. Yoshino, T. Hong, and N. Nord, "IEA EBC annex 53: Total energy use in buildings—Analysis and evaluation methods," *Energy Build.*, vol. 152, pp. 124–136, 2017.

[9] A. Reilly and O. Kinnane, "The impact of thermal mass on building energy consumption," *Appl. Energy*, vol. 198, pp. 108–121, 2017.

[10] E. Zilberberg, P. Trapper, I. A. Meir, and S. Isaac, "The impact of thermal mass and insulation of building structure on energy efficiency," *Energy Build.*, vol. 241, p. 110954, 2021.

[11] R. Hu, G. Liu, and J. Niu, "The Impacts of a Building's Thermal Mass on the Cooling Load of a Radiant System under Various Typical Climates," *Energies*, vol. 13, no. 6, p. 1356, 2020.

[12] J. Deng, R. Yao, W. Yu, Q. Zhang, and B. Li, "Effectiveness of the thermal mass of external walls on residential buildings for part-time part-space heating and cooling using the state-space method," *Energy Build.*, vol. 190, pp. 155–171, 2019.

[13] P. M. Congedo, C. Baglivo, and G. Centonze, "Walls comparative evaluation for the thermal performance improvement of low-rise residential buildings in warm Mediterranean climate," *J. Build. Eng.*, vol. 28, p. 101059, 2020.

[14] Y. Li, E. Long, L. Zhang, X. Dong, and S. Wang, "Energy-saving potential of intermittent heating system: Influence of composite phase change wall and optimization strategy," *Energy Explor. Exploit.*, vol. 39, no. 1, pp. 426–443, 2021.

[15] H. Ge and F. Baba, "Effect of dynamic modeling of thermal bridges on the energy performance of residential buildings with high thermal mass for cold climates," *Sustain. Cities Soc.*, vol. 34, pp. 250–263, 2017.

[16] A. Fang, Y. Chen, and L. Wu, "Transient simulation of coupled heat and moisture transfer through multi-layer walls exposed to future climate in the hot and humid southern China area," *Sustain. Cities Soc.*, vol. 52, p. 101812, 2020.

[17] M. Ibrahim, H. Sayegh, L. Bianco, and E. Wurtz, “Hygrothermal performance of novel internal and external super-insulating systems: In-situ experimental study and 1D/2D numerical modeling,” *Appl. Therm. Eng.*, vol. 150, pp. 1306–1327, 2019.
[18] H. Ge and F. Baba, “Dynamic effect of thermal bridges on the energy performance of a low-rise residential building,” *Energy Build.*, vol. 105, pp. 106–118, 2015.
[19] M. Hershfield, “Building Envelope Thermal Bridging Guide,” *Vanc. BC*, 2014.
[20] E. De Angelis and E. Serra, “Light steel-frame walls: thermal insulation performances and thermal bridges,” *Energy Procedia*, vol. 45, pp. 362–371, 2014.
[21] D. A. Kontogeorgos, I. A. Atsonios, I. D. Mandilaras, and M. A. Founti, “Numerical investigation of the effect of vacuum insulation panels on the thermal bridges of a lightweight drywall envelope,” *J. Facade Des. Eng.*, vol. 4, no. 1–2, pp. 3–18, 2016.
[22] N. Soares, P. Santos, H. Gervásio, J. J. Costa, and L. S. Da Silva, “Energy efficiency and thermal performance of lightweight steel-framed (LSF) construction: A review,” *Renew. Sustain. Energy Rev.*, vol. 78, pp. 194–209, 2017.
[23] A. Handbook, “Fundamentals, ASHRAE–American Society of Heating,” *Vent. Air-Cond. Eng.*, 2017.
[24] P. Santos, M. Gonçalves, C. Martins, N. Soares, and J. J. Costa, “Thermal transmittance of lightweight steel framed walls: Experimental versus numerical and analytical approaches,” *J. Build. Eng.*, vol. 25, p. 100776, 2019.
[25] S. G. Maxineasa, D. N. Isopescu, I. R. Baciu, M. L. Lupu, and T. C. Dragan, “Thermal analysis of a structure made by using cold formed steel sections,” in *IOP Conference Series: Materials Science and Engineering*, 2020, vol. 789, no. 1, p. 012039.
[26] T. V. Moore, C. A. Cruickshank, I. Beausoleil-Morrison, and M. Lacasse, “Thermal evaluation of a highly insulated steel stud wall with vacuum insulation panels using a guarded hot box apparatus,” *J. Build. Phys.*, vol. 45, no. 3, pp. 303–322, 2021.
[27] P. Santos and K. Poologanathan, “The importance of stud flanges size and shape on the thermal performance of lightweight steel framed walls,” *Sustainability*, vol. 13, no. 7, p. 3970, 2021.
[28] E. Roque, P. Santos, and A. C. Pereira, “Thermal and sound insulation of lightweight steel-framed façade walls,” *Sci. Technol. Built Environ.*, vol. 25, no. 2, pp. 156–176, 2019.
[29] M. B. A. Medhi Ghobadi PhD and T. V. M. MASc, “The Thermal Bridging Effects in Steel Stud Wall Assemblies,” in *ASHRAE Topical Conference Proceedings*, 2019, pp. 242–250.
[30] H. Viot, A. Sempey, M. Pauly, and L. Mora, “Comparison of different methods for calculating thermal bridges: Application to wood-frame buildings,” *Build. Environ.*, vol. 93, pp. 339–348, 2015.
[31] A. P. Gomes, H. A. de Souza, and A. Tribess, “Impact of thermal bridging on the performance of buildings using Light Steel Framing in Brazil,” *Appl. Therm. Eng.*, vol. 52, no. 1, pp. 84–89, 2013.
[32] T. Kalema, G. Jóhannesson, P. Pylsy, and P. Hagengran, “Accuracy of energy analysis of buildings: a comparison of a monthly energy balance method and simulation methods in calculating the energy consumption and the effect of thermal mass,” *J. Build. Phys.*, vol. 32, no. 2, pp. 101–130, 2008.
[33] R. Lindberg, A. Binamu, and M. Teikari, “Five-year data of measured weather, energy consumption, and time-dependent temperature variations within different exterior wall structures,” *Energy Build.*, vol. 36, no. 6, pp. 495–501, 2004.

[34] L. A. Bellamy and D. W. Mackenzie, *Thermal performance of buildings with heavy walls*. BRANZ, 2002.
[35] R. Carlier, M. Dabbagh, and M. Krarti, "Impact of wall constructions on energy performance of switchable insulation systems," *Energies*, vol. 13, no. 22, p. 6068, 2020.
[36] F. Leccese, G. Salvadori, F. Asdrubali, and P. Gori, "Passive thermal behaviour of buildings: Performance of external multi-layered walls and influence of internal walls," *Appl. Energy*, vol. 225, pp. 1078–1089, 2018.
[37] M. Ozel, "Effect of insulation location on dynamic heat-transfer characteristics of building external walls and optimization of insulation thickness," *Energy Build.*, vol. 72, pp. 288–295, 2014.
[38] M. Ozel and K. Pihtili, "Optimum location and distribution of insulation layers on building walls with various orientations," *Build. Environ.*, vol. 42, no. 8, pp. 3051–3059, 2007.
[39] J. Yang, H. Wu, X. Xu, G. Huang, J. Cen, and Y. Liang, "Regional climate effects on the optimal thermal resistance and capacitance of residential building walls," *Energy Build.*, vol. 244, p. 111030, 2021.
[40] L. Yuan, Y. Kang, S. Wang, and K. Zhong, "Effects of thermal insulation characteristics on energy consumption of buildings with intermittently operated air-conditioning systems under real time varying climate conditions," *Energy Build.*, vol. 155, pp. 559–570, 2017.
[41] E. Iso, "Hygrothermal performance of building components and building elements. Internal surface temperature to avoid critical surface humidity and interstitial condensation. Calculation methods," *EN ISO*, vol. 13788, p. 2012, 2012.
[42] D. I. Kolaitis, E. Malliotakis, D. A. Kontogeorgos, I. Mandilaras, D. I. Katsourinis, and M. A. Founti, "Comparative assessment of internal and external thermal insulation systems for energy efficient retrofitting of residential buildings," *Energy Build.*, vol. 64, pp. 123–131, 2013.
[43] A. Carbonari and M. Scarpaa, "Optimisation of insulation and solar control strategies as function of building's intended use in the retrofit of massive buildings," 2020.
[44] B. Rosti, A. Omidvar, and N. Monghasemi, "Optimum position and distribution of insulation layers for exterior walls of a building conditioned by earth-air heat exchanger," *Appl. Therm. Eng.*, vol. 163, p. 114362, 2019.
[45] S. A. Al-Sanea, M. F. Zedan, and S. N. Al-Hussain, "Effect of masonry material and surface absorptivity on critical thermal mass in insulated building walls," *Appl. Energy*, vol. 102, pp. 1063–1070, 2013.
[46] M. E. Saleh, "Impact of thermal insulation location on buildings in hot dry climates," *Sol. Wind Technol.*, vol. 7, no. 4, pp. 393–406, 1990.
[47] H. Asan, "Effects of wall's insulation thickness and position on time lag and decrement factor," *Energy Build.*, vol. 28, no. 3, pp. 299–305, 1998.
[48] M. Ciampi, F. Leccese, and G. Tuoni, "Building-plant interaction: a parameter to optimize the distribution of thermal resistance and heat capacity in external walls of buildings," in *2nd International Building Phisycs Conference, Leuven, Belgium*, 2003, pp. 335–342.
[49] P. Gori, C. Guattari, L. Evangelisti, and F. Asdrubali, "Design criteria for improving insulation effectiveness of multilayer walls," *Int. J. Heat Mass Transf.*, vol. 103, pp. 349–359, 2016.

[50] P. T. Tsilingiris, “Parametric space distribution effects of wall heat capacity and thermal resistance on the dynamic thermal behavior of walls and structures,” *Energy Build.*, vol. 38, no. 10, pp. 1200–1211, 2006, doi: 10.1016/j.enbuild.2006.02.007.
[51] H. H. Saber, W. Maref, M. M. Armstrong, M. C. Swinton, M. Z. Rousseau, and G. Gnanamurugan, “Numerical simulations to predict the thermal response of insulating concrete form (ICF) wall in cold climate,” 2011.
[52] J. Kosny, J. E. Christian, A. O. Desjarlais, E. Kossecka, and L. Berrenberg, “The performance check between whole building thermal performance criteria and exterior wall measured clear wall R-value, thermal bridging, thermal mass, and airtightness,” Oak Ridge National Lab., Buildings Technology Center, TN (United States), 1998.
[53] I. Doebber and M. W. Ellis, “Thermal Performance Benefits of Precast Concrete Panel and Integrated Concrete Form Technologies for Residential Construction.,” *ASHRAE Trans.*, vol. 111, no. 2, 2005.
[54] N. Daouas, “A study on optimum insulation thickness in walls and energy savings in Tunisian buildings based on analytical calculation of cooling and heating transmission loads,” *Appl. Energy*, vol. 88, no. 1, pp. 156–164, 2011.
[55] N. Ekrami, R. S. Kamel, A. Garat, A. Amirirad, and A. S. Fung, “Applications of active hollow core slabs and insulated concrete foam walls as thermal storage in cold climate residential buildings,” *Energy Procedia*, vol. 78, pp. 459–464, 2015.
[56] H. H. Saber, W. Maref, M. Armstrong, M. C. Swinton, M. Z. Rousseau, and G. Gnanamurugan, “Benchmarking 3D thermal model against field measurement on the thermal response of an insulating concrete form (ICF) wall in cold climate,” 2010.
[57] M. M. Armstrong, W. Maref, H. H. Saber, M. C. Swinton, G. Ganapathy, and M. Z. Rousseau, “The impact of the thermal mass on field energy performance of insulating concrete form (ICF) wall in cold climate,” 2011.
[58] P. Santos and L. S. da Silva, “Energy efficiency of lightweight steel-framed buildings,” *Energy Effic Build*, vol. 35, pp. 180–191, 2017.
[59] S. Naji, O. C. Çelik, U. J. Alengaram, M. Z. Jumaat, and S. Shamshirband, “Structure, energy and cost efficiency evaluation of three different lightweight construction systems used in low-rise residential buildings,” *Energy Build.*, vol. 84, pp. 727–739, 2014.
[60] S. Yu, Y. Liu, D. Wang, A. S. Bahaj, Y. Wu, and J. Liu, “Review of thermal and environmental performance of prefabricated buildings: Implications to emission reductions in China,” *Renew. Sustain. Energy Rev.*, vol. 137, p. 110472, 2021.
[61] J. Kwan, “An investigation of the new opportunities of wood in mid-rise construction in British Columbia,” 2013.
[62] E. ISO 10211, *Thermal Bridges in Building Construction–Heat Flows and Surface Temperatures–Detailed Calculations*. CEN Brussels, 2007.
[63] ISO 8990, *Thermal insulation-Determination of steady-state thermal transmission properties-Calibrated and guarded*. International Organization for Standardization, 1994.
[64] A. S. for T. and M. C. D. on T. Insulation, *Standard test method for thermal performance of building materials and envelope assemblies by means of a hot box apparatus*. ASTM International, 2011.
[65] ISO 9869-1: 2014, *Thermal Insulation—Building Elements—In Situ Measurement of Thermal Resistance and Thermal Transmittance—Part 1: Heat Flow Meter Method*. ISO Geneva, Switzerland, 2014.

[66] A. S. for T. and Materials, *Standard Practice for Determining Thermal Resistance of Building Envelope Components from the In-Situ Data*. ASTM International, 2013.
[67] I. O. for Standardization, *Thermal Bridges in Building Construction: Linear Thermal Transmittance: Simplified Methods and Default Values*. ISO, 2007.
[68] M. Mahmoodzadeh, V. Gretka, K. Hay, C. Steele, and P. Mukhopadhyaya, "Determining overall heat transfer coefficient (U-Value) of wood-framed wall assemblies in Canada using external infrared thermography," *Build. Environ.*, vol. 199, p. 107897, 2021.
[69] J. Kosny and J. E. Christian, "Thermal evaluation of several configurations of insulation and structural materials for some metal stud walls," *Energy Build.*, vol. 22, no. 2, pp. 157–163, 1995.
[70] M. Gorgolewski, "Developing a simplified method of calculating U-values in light steel framing," *Build. Environ.*, vol. 42, no. 1, pp. 230–236, 2007.
[71] E. Iso, *Building components and building elements–thermal resistance and thermal transmittance–calculation method*. CEN Brussels, 2007.
[72] T. A. Muzzi, H. A. Souza, and A. P. Gomes, "Heat transfer analysis of the vertical closing system in light steel framing using the isothermal planes method and finite element method," *REM-Int. Eng. J.*, vol. 74, pp. 425–431, 2021.
[73] I. A. Atsonios, I. D. Mandilaras, D. A. Kontogeorgos, and M. A. Founti, "Two new methods for the in-situ measurement of the overall thermal transmittance of cold frame lightweight steel-framed walls," *Energy Build.*, vol. 170, pp. 183–194, 2018.
[74] M. Major and M. Kosin, "Evaluation of energy efficiency of external stud partitions with use of numerical analysis," in *IOP Conference Series: Earth and Environmental Science*, 2019, vol. 214, no. 1, p. 012005.
[75] N. Soares, A. R. Gaspar, P. Santos, and J. J. Costa, "Multi-dimensional optimization of the incorporation of PCM-drywalls in lightweight steel-framed residential buildings in different climates," *Energy Build.*, vol. 70, pp. 411–421, 2014.
[76] J. Purdy and I. Beausoleil-Morrison, "The significant factors in modelling residential buildings," 2001.
[77] P. Santos, L. Simões da Silva, H. Gervásio, and A. Gameiro Lopes, "Parametric analysis of the thermal performance of light steel residential buildings in Csb climatic regions," *J. Build. Phys.*, vol. 35, no. 1, pp. 7–53, 2011.
[78] F. Ascione, N. Bianco, R. F. De Masi, F. de'Rossi, and G. P. Vanoli, "Simplified state space representation for evaluating thermal bridges in building: Modelling, application and validation of a methodology," *Appl. Therm. Eng.*, vol. 61, no. 2, pp. 344–354, 2013.
[79] C. A. Gueymard, "Direct and indirect uncertainties in the prediction of tilted irradiance for solar engineering applications," *Sol. Energy*, vol. 83, no. 3, pp. 432–444, 2009.
[80] "Weather Data by Location," Sep. 28, 2020. https://energyplus.net/weather
[81] K. J. Kontoleon and D. K. Bikas, "Thermal mass vs. thermal response factors: determining optimal geometrical properties and envelope assemblies of building materials," 2005.
[82] U.S. Department of Energy, "New Construction — Commercial Reference Buildings," Sep. 12, 2021. https://www.energy.gov/eere/buildings/new-construction-commercial-reference-buildings
[83] N. R. C. Canada, *National Energy Code of Canada for Buildings 2017*. National Research Council of Canada, 2017.

[84] US Department of Energy, “Engineering Reference - EnergyPlus 9.0.” https://bigladdersoftware.com/epx/docs/9-0/engineering-reference/

Appendix: Assessing the validity of COMSOL Multiphysics' © results

ISO 10211 regulates that the output results of a numerical simulation tool can be considered valid if the tool is capable of producing satisfying results when simulating four case studies mentioned in the standard. In this section, these four case studies, along with the simulation results and their validation, are presented to assess the capability of COMSOL Multiphysics © software to simulate thermal bridges.

A.1. First case study

The geometry of this case is as what shown in Figure A.1, which represents a half-square column. The temperatures of 28 equidistant points were calculated analytically, and the results are used as the validation reference for numerical results in ISO 10211 standard. It should be noted that the maximum allowable deviation from the analytical results is 0.1°C. Due to the similarity, the length of the square will not influence the results, however, a value of 0.8 m has been assigned to the side of the square (BC in Figure A.1).

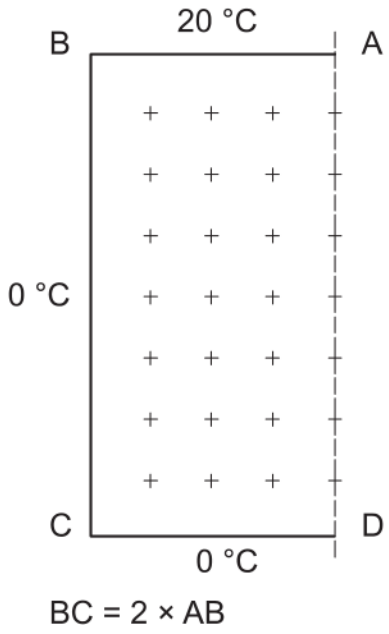

Figure A.1. Schematic of the geometry for the first case study [62]

In addition, Table A.1 presents the thermophysical properties of the material used for this simulation. Given that heat transfer is steady-state and that the field is made of a material with homogeneous thermal conductivity, thermophysical properties of the material does not affect the

results, however, COMSOL Multiphysics © software is not capable of simulating the heat transfer unless the material properties are identified.

Table A.1. Thermophysical properties of the material for the first case study

Property	Value
Thermal conductivity	1 W/m.K
Density	1 kg/m^3
Specific heat capacity	1 J/kg.K

As for the boundary conditions, constant temperature with a value of 20°C was assigned to the upper side of the square while the left side and the bottom of the square were kept at 0°C. Finally, a symmetry boundary condition was applied to the right side of the geometry.

A 7 × 4 matrix of nodes was considered, and the steady-state temperatures were calculated for each of these nodes. Analytical results, as well as the values calculated using numerical simulation, are presented in Table A.2. As can be observed, the differences between analytical and numerical findings are within the allowable range for all nodes. In addition, Figure A.2 and Figure A.3 illustrate the temperature distribution within the solid and isothermal contours, respectively.

Table A.2. Analytical and numerical results for the first case study

X index	Y index	Analytical result (°C)	Numerical result (°C)	Deviation (°C)
1	1	0.3	0.342	**0.042**
2	1	0.6	0.630	**0.030**
3	1	0.8	0.820	**0.020**
4	1	0.9	0.886	**0.014**
1	2	0.7	0.740	**0.040**
2	2	1.4	1.360	**0.040**
3	2	1.8	1.767	**0.033**
4	2	1.9	1.908	**0.008**
1	3	1.3	1.263	**0.037**
2	3	2.3	2.309	**0.009**
3	3	3.0	2.986	**0.014**
4	3	3.2	3.219	**0.019**
1	4	2.0	2.015	**0.015**
2	4	3.6	3.641	**0.041**
3	4	4.7	4.658	**0.042**
4	4	5.0	5.000	**0.000**
1	5	3.2	3.189	**0.011**

2	5	5.6	5.609	**0.009**
3	5	7.0	7.014	**0.014**
4	5	7.5	7.465	**0.035**
1	6	5.3	5.251	**0.049**
2	6	8.6	8.639	**0.039**
3	6	10.3	10.316	**0.016**
4	6	10.8	10.811	**0.011**
1	7	9.7	9.655	**0.045**
2	7	13.4	13.379	**0.021**
3	7	14.7	14.730	**0.030**
4	7	15.1	15.086	**0.014**

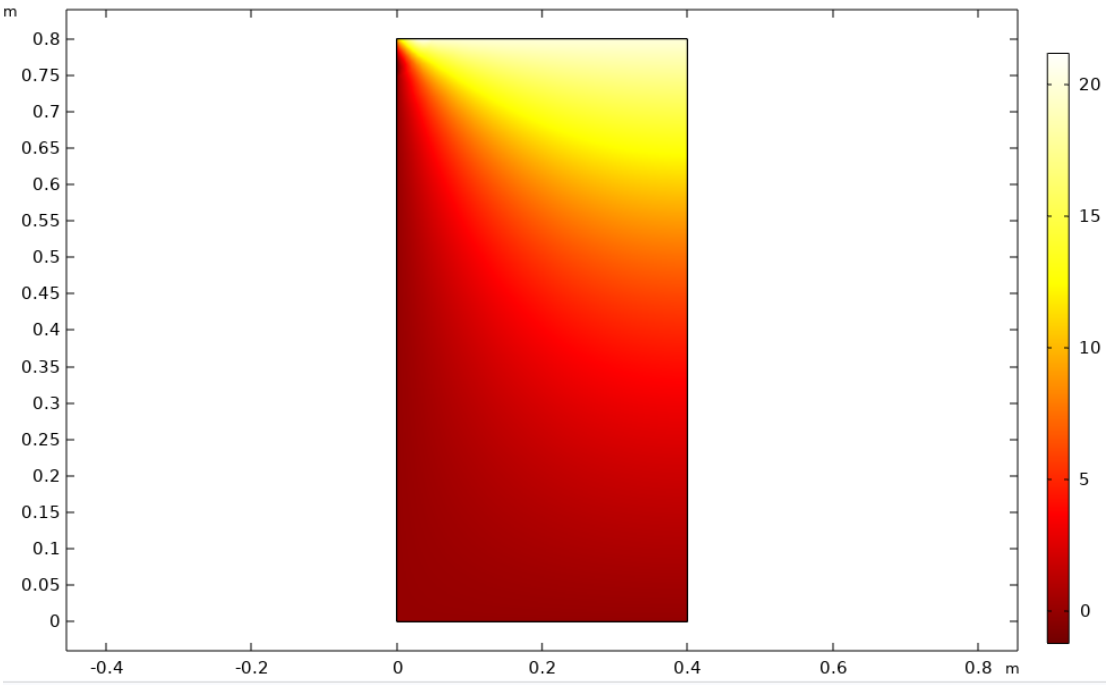

Figure A.2. Temperature distribution: first case study

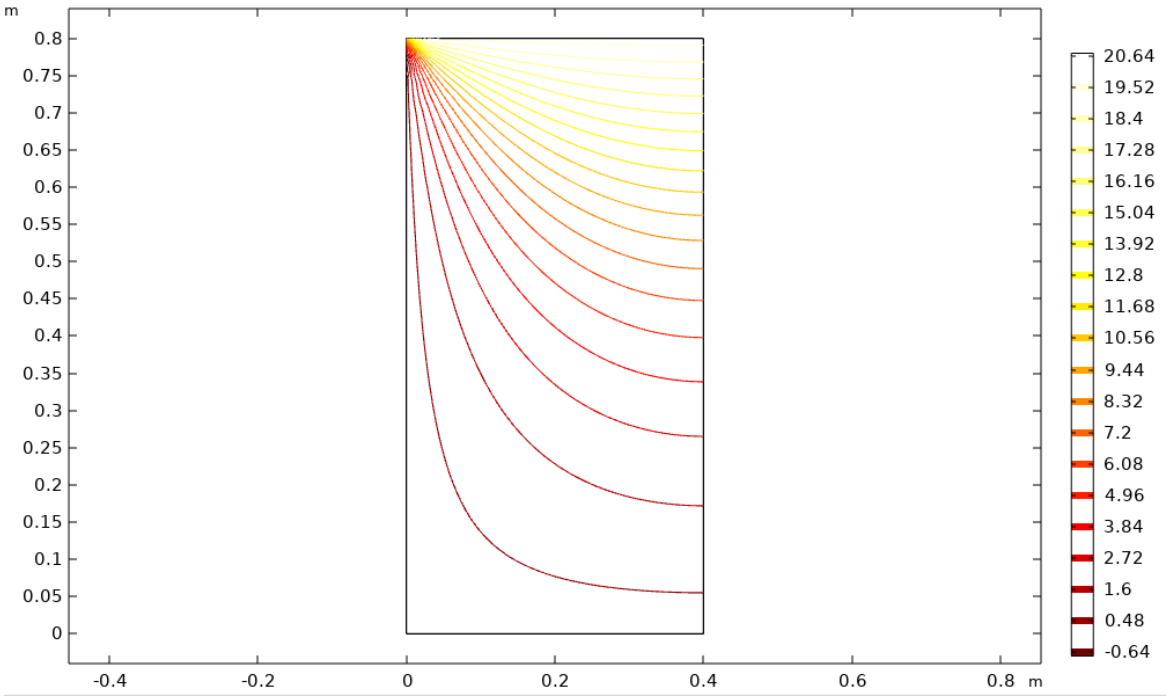

Figure A.3. Isothermal contours: first case study

A.2. Second case study

This case represents the two-dimensional heat transfer in a composite wall with four different materials [62]. A concrete layer on the top side, an aluminum layer on the left and bottom sides, an insulation material layer occupying the largest space in the structure, and a wooden batten between the aluminum and concrete layers account for the different parts of this wall. Figure A.4 provides more information regarding the geometry of the second case study. Also, Table A.3 indicates the dimensions that must be considered for this case.

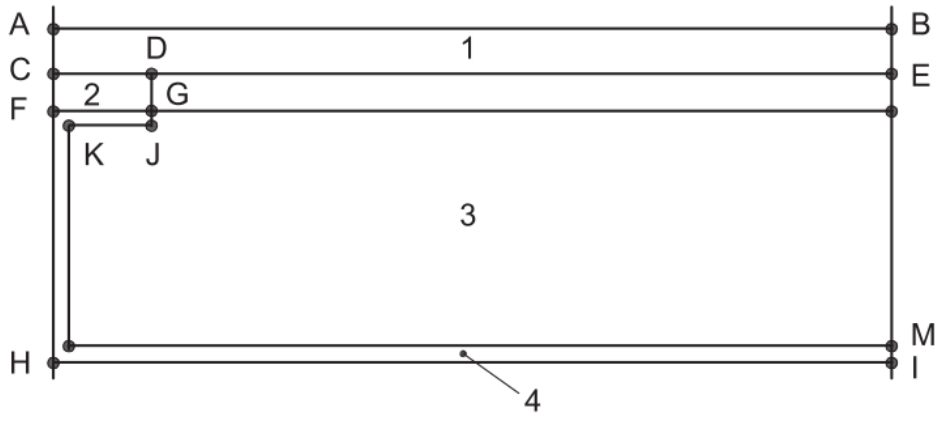

Key

1 concrete
2 wood
3 insulation
4 aluminium

Figure A.4. Geometry: second case study [62]

Table A.3. Geometry dimensions: second case study

Side	Length (mm)
AB	500
AC	6
CD	15
CF	5
EM	40
GJ	1.5
IM	1.5
FG-KJ	1.5

Table A.4 summarizes the thermal properties of the materials for the second case study. All materials have homogeneous thermal conductivities, which are temperature-independent.

Table A.4. Thermophysical properties of the materials in the second case study

	Thermal conductivity (W/m.K)	Density (kg/m^3)	Specific heat capacity (J/kg.K)
Concrete	1.15	2300	880
Wood	0.12	500	2500
Insulation	0.029	150	1000
Aluminum	230	2700	900

Considering the boundary conditions, left and right sides of the geometry were considered to be isolated while the top side represented the so called "cold side", which was kept at 0°C and had a convective heat transfer resistance of 0.06 m^2.K/W. Bottom side showed the so called "warm side" of the wall, which was maintained at 20°C and had a convective heat transfer resistance of 0.11 m^2.K/W.

Temperature distribution within the wall and the heat flux through it are the two parameters that are intended for the validation of results for this case study. Figure A.5 and Figure A.6 illustrate the temperature distribution and isotherm contours within the wall. Also, the total heat transfer through the wall was 9.49 W/m that had a difference of 0.08% with the expected analytical result for the case, which is within the acceptable range (0.1 W/m).

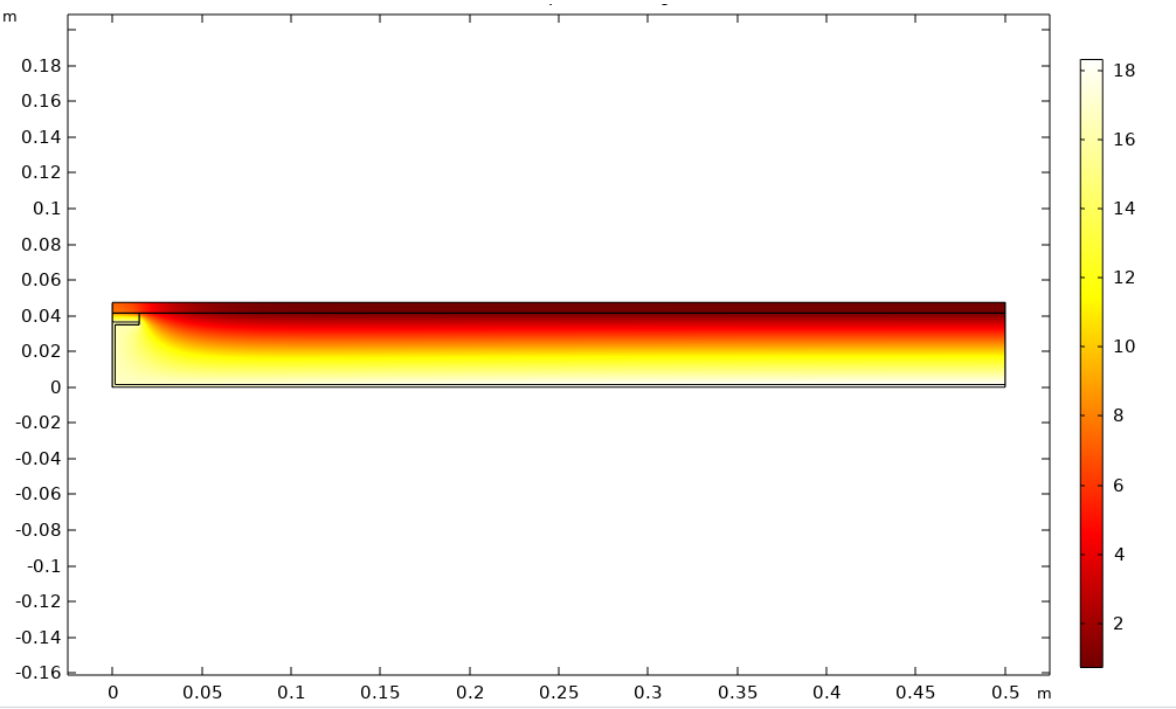

Figure A.5. Temperature distribution within the wall: second case study

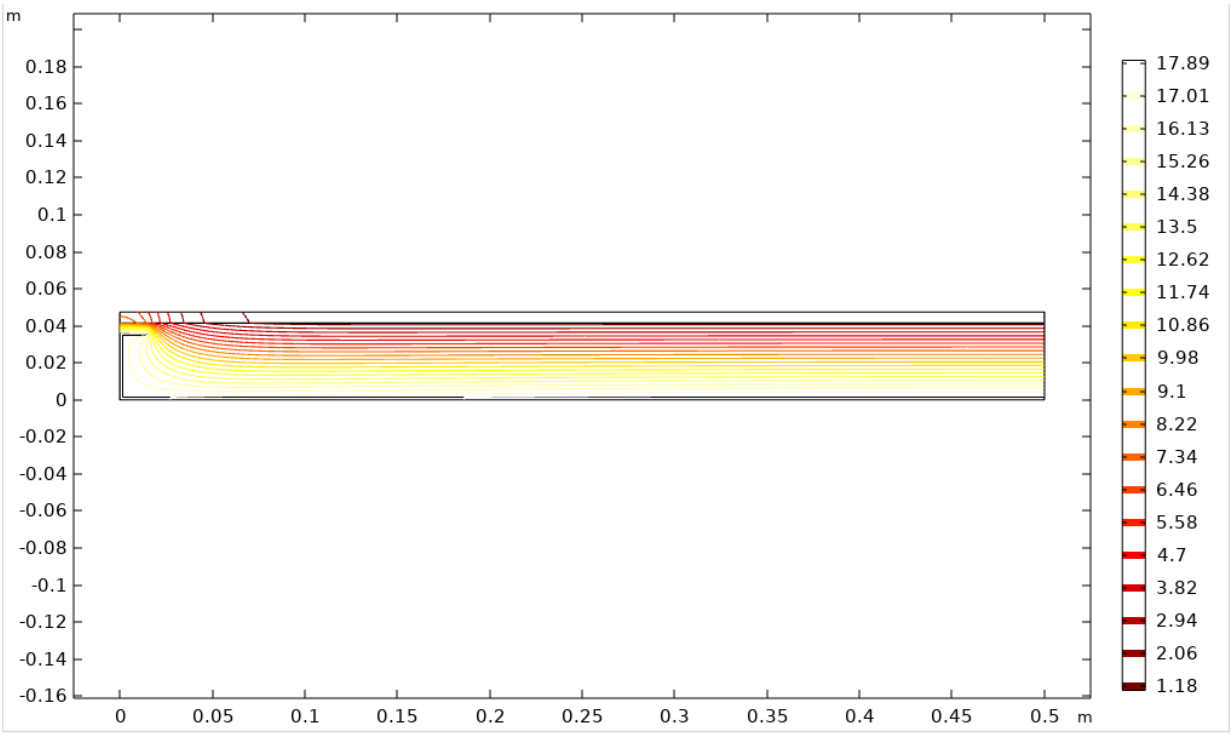

Figure A.6. Isothermal contours: second case study

Another set of results to evaluate for this case was the temperatures of some specific nodes in the wall. Also, Table A.5 summarizes these values, as well as the deviations, which must not exceed 0.1°C.

Table A.5. Temperature values of the selected nodes: second case study

X coordinate (mm)	Y coordinate (mm)	Expected result (°C)	Numerical result (°C)	Deviation (°C)
0	47.5	7.1	7.065	**0.035**
0	41.5	7.9	7.899	**0.001**
0	36.5	16.4	16.408	**0.008**
0	0	16.8	16.767	**0.033**
15	41.5	6.3	6.272	**0.028**
15	36.5	16.3	16.334	**0.034**
500	47.5	0.8	0.761	**0.039**
500	41.5	0.8	0.827	**0.027**
500	0	18.3	18.334	**0.034**

A.3. Third case study

In this case, a three-dimensional geometry shown in Figure A.7 is considered, which represents a floor-wall junction as part of the building envelope system. As can be observed, the geometry is divided into three environments: an upper inner environment, β, a lower inner environment, α, and the outside environment, γ. In addition, Figure A.8 illustrates the cross sections of the geometry, and Table A.6 represents the corresponding dimensions.

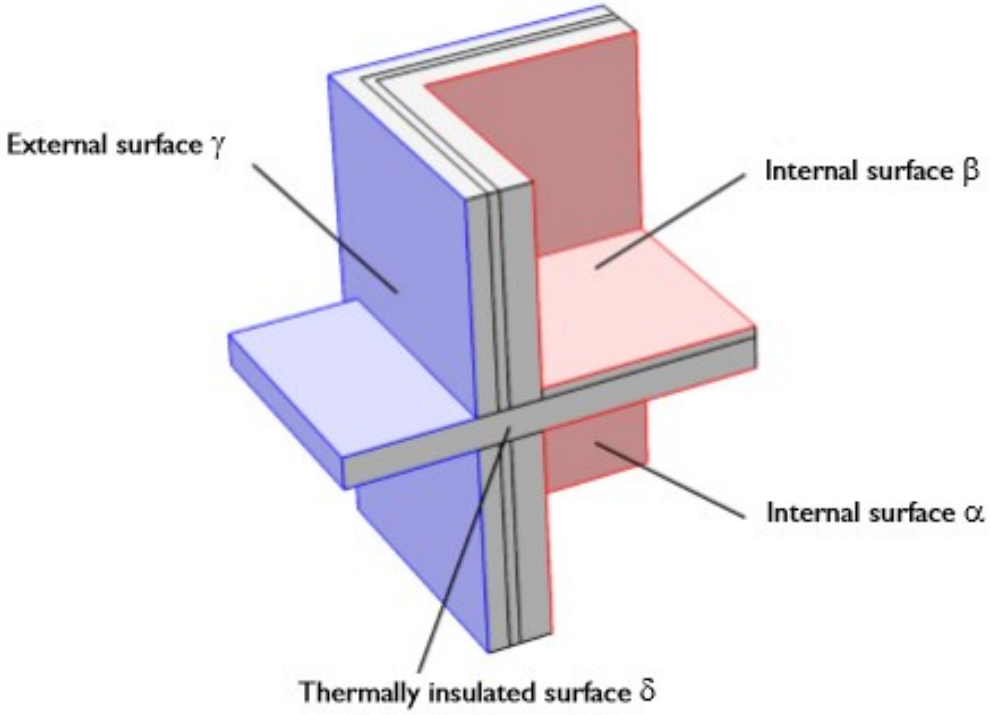

Figure A.7. Geometry: third case study [62]

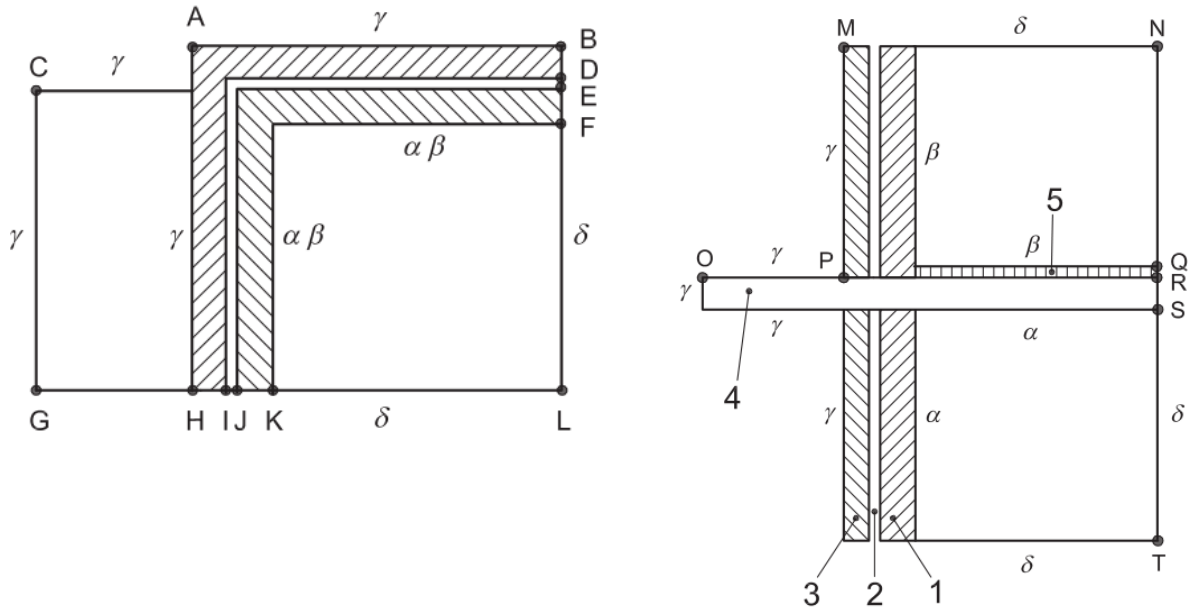

Horizontal section Vertical section

Figure A.8. Cross section views: third case study [62]

Table A.6. Corresponding dimensions for the geometry: third case study

Side	Dimension (mm)
AB	1300
BD=HI	100
DE=IJ	50
EF=JK	150
FL=KL	1000
CG	1150
GH	600
MP=ST	1000
QR	50
RS	150
NQ	950
OP	600

Four different materials with homogeneous thermal conductivities are intended for the geometry, the properties of which have been presented in Table A.7.

Table A.7. Material properties: third case study

Domain	Thermal Conductivity (W/m.K)	Density (kg/m^3)	Specific heat capacity (J/kg.K)
Floor slab	2.5	5000	600
Interior wall	0.7	1700	800
Exterior wall	1	2000	1000
Insulation	0.04	200	1000

The internal upper surface was kept at a constant temperature of 15°C and the corresponding convective heat resistance was 0.20 m^2.K/W, while the internal lower surface's boundary condition was another constant temperature of 20°C and a convective heat transfer resistance of 0.20 m^2.K/W. The outside temperature was 0°C and the convective heat transfer resistance was 0.05 m^2.K/W. The other boundaries were isolated.

There were two considerations for the results of these cases, which were minimum surface temperatures and heat fluxes through surfaces. The ISO 10211 standard provides a procedure for manually calculating the minimum surface temperatures, which is based on the concept of temperature factor. The definition of the temperature factor in ISO 10211 standard is as follows:

"*Difference between internal surface temperature and external temperature, divided by the difference between internal temperature and external temperature, calculated with a surface resistance R_{si} at the internal surface*"

For the case under study, the temperature factors are presented in Table A.8.

Table A.8. Temperature factors: third case study

Environment	g_g	g_α	g_β
g	1.000	0.000	0.000
α	0.378	0.399	0.223
β	0.331	0.214	0.455

Figure A.9, Figure A.10, and Figure A.11 show temperature profile for the geometry considered. The minimum internal surface temperatures were calculated, which were 11.323°C and 11.103°C

for surfaces α and β, respectively. On the other hand, manual calculations of the minimum surface temperatures are as follows [62]:

$$\theta_{min} = g_g.\,\theta_g + g_\alpha.\,\theta_\alpha + g_\beta.\,\theta_\beta \tag{A.1}$$

$$\theta_{\alpha,min} = 0.378\times0 + 0.223\times15 + 0.399\times20 = 11.32°C \tag{A.2}$$

$$\theta_{\beta,min} = 0.331\times0 + 0.455\times15 + 0.214\times20 = 11.11°C \tag{A.3}$$

Given that the maximum allowable deviation from the values presented in the standard is 0.1°C, we can conclude that COMSOL © has successfully evaluated the parameters. Figure A.10 and Figure A.11 show the temperature distribution, as well as the minimum and maximum temperatures over surfaces α and β, respectively. As expected, the lowest surface temperatures in the environments α and β are in corners of both indoor environment, where the heat flow is not one-dimensional.

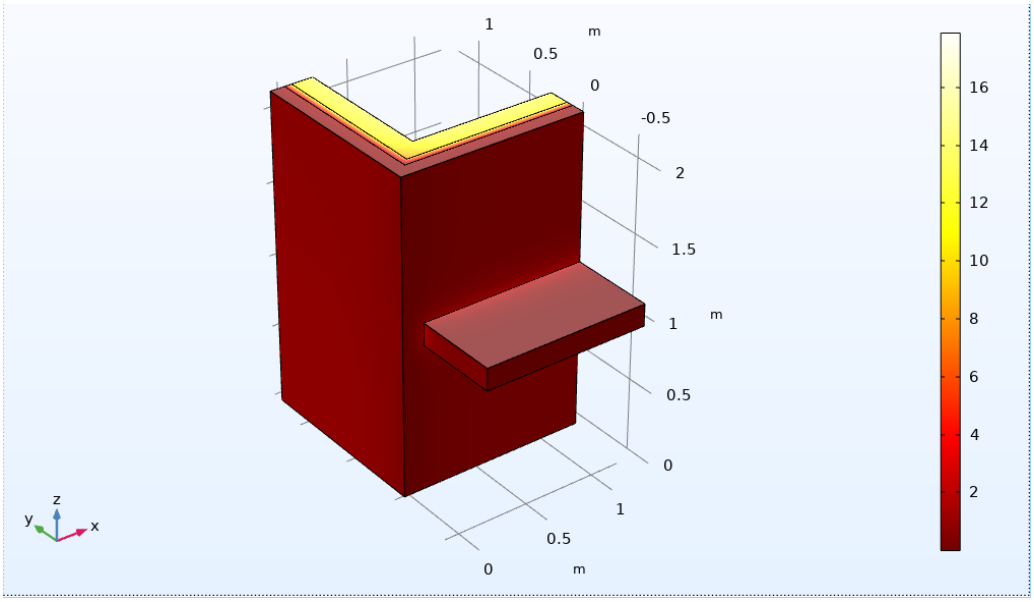

Figure A.9. Temperature profile: third case study

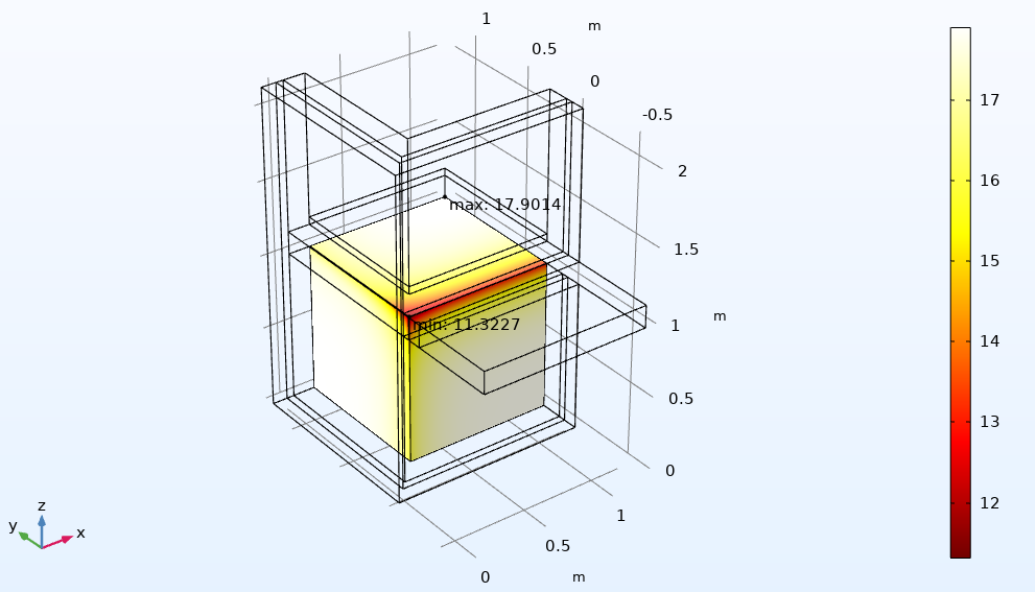

Figure A.10. Minimum surface temperature: α surface

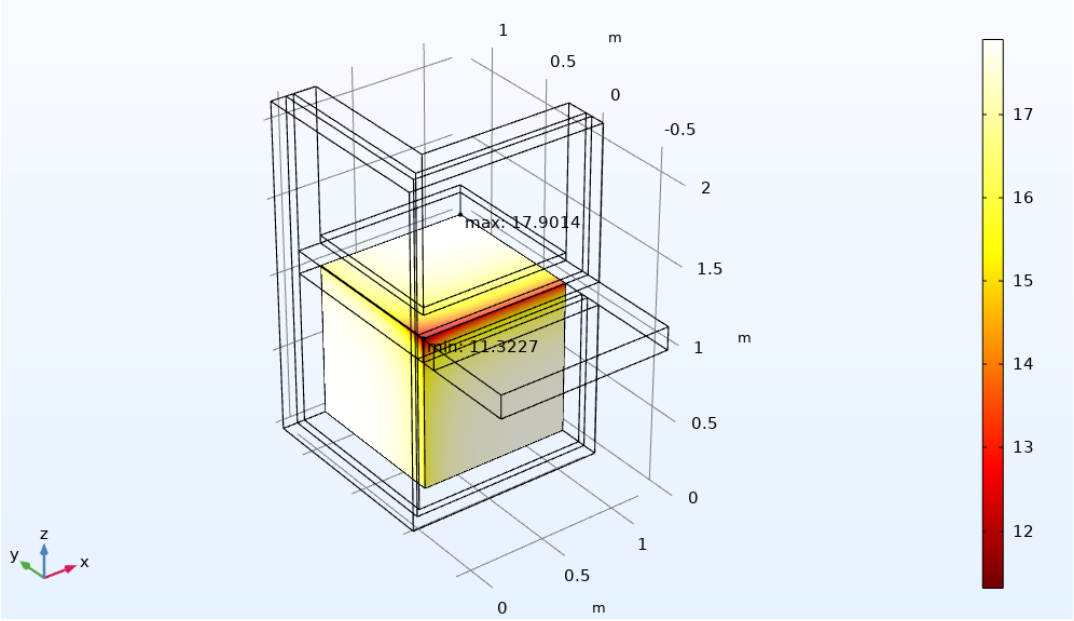

Figure A.11. Minimum surface temperature: β surface

The other parameter to evaluate was the heat flux through the surfaces. The method for manually calculating the heat fluxes is to utilize the concept of the thermal coupling coefficient, which is, as described by ISO 10211 standard, defined as follows [62]:

"*Heat flow rate per temperature difference between two environments which are thermally connected by the construction under consideration*"

Table A.9 gives the thermal coupling coefficients for the third case study.

Table A.9. Thermal coupling coefficients: third case study

Environment	g	α	β
g	-	1.781 (W/K)	1.624 (W/K)
α	1.781 (W/K)	-	2.094 (W/K)
β	1.624 (W/K)	2.094 (W/K)	-

As a result, the heat flux between the environments are calculated as follows:

For β and γ:

$$\Phi_{\beta,g} = L_{\beta,g} \,.\, D\theta_{\beta,g} = 1.624 \times (15\text{-}0) = 24.36 \text{ W} \quad \text{(A.4)}$$

For β and α:

$$\Phi_{\beta,\alpha} = L_{\beta,\alpha} \,.\, D\theta_{\beta,\alpha} = 2.094 \times (15\text{-}20) = -10.47 \text{ W} \quad \text{(A.5)}$$

For α and γ:

$$\Phi_{\alpha,g} = L_{\alpha,g} \,.\, D\theta_{\alpha,g} = 1.781 \times (20\text{-}0) = 35.62 \text{ W} \quad \text{(A.6)}$$

The heat transfer from indoor to outdoor is then:

$$\Phi_{\beta,g} + \Phi_{\alpha,g} = 24.36 + 35.62 = 59.98 \text{ W} \quad \text{(A.7)}$$

Another value to calculate was the total heat transferred from environments β and α:

$$\Phi_{\beta,g} + \Phi_{\beta,\alpha} = 24.36 - 10.47 = 13.89 \text{ W} \quad \text{(A.8)}$$

$$\Phi_{\alpha,g} + \Phi_{\alpha,\beta} = 35.62 + 10.47 = 46.09 \text{ W} \quad \text{(A.9)}$$

It was mentioned in the standard that the maximum acceptable difference is 1%. Table A.10 presents the numerical results from COMSOL Multiphysics © software, as well as the reference values mentioned in ISO 10211 standard [62]. It can be concluded that COMSOL Multiphysics © is able to generate satisfying results for this case, as well.

Table A.10. Numerical and reference heat flux values: third case study

Parameter	Manually calculated valies (W)	Numerical result (W)	Difference (%)
Heat flux through α	46.09	46.192	0.22%
Heat flux through β	13.89	13.924	0.25%
Heat flux through g	59.98	60.116	0.23%

A.4. Fourth case study

The geometry of interest for this case represents a point thermal bridge that was created by an iron bar puncturing the insulation of a wall, as shown in Figure A.12.

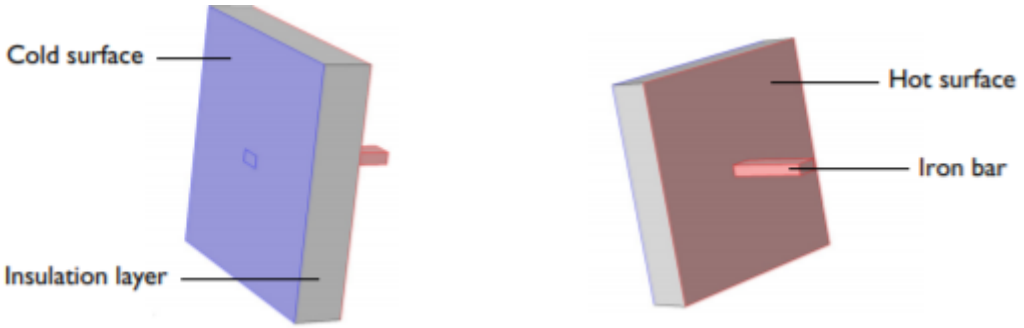

(a) (b)

Figure A.12. Views of an iron bar puncturing an insulation level: (a) Back-side view, (b) Front-side view [62]

The details and dimensions of the geometry are described in Figure A.13 and Table A.11.

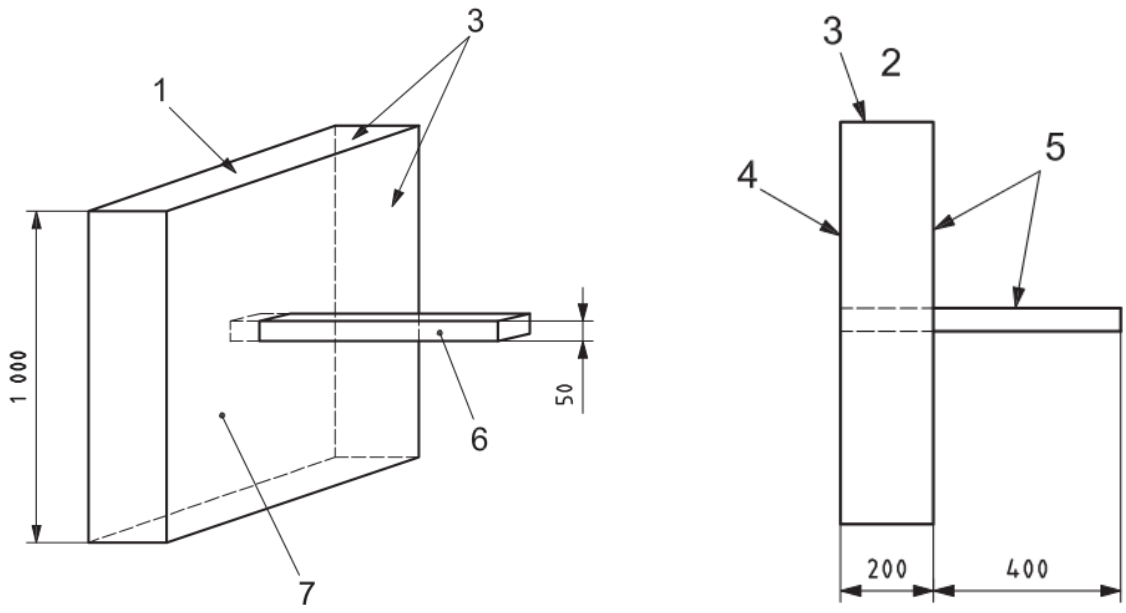

Key

1 top
2 top view
3 adiabatic cut-off planes
4 external surface
5 internal surface
6 iron bar
7 insulation

Figure A.13. Details and dimensions: fourth case study

Table A.11. Corresponding dimensions: fourth case study

Component	Dimension (mm)
Insulation	1000 × 1000 × 200
Iron bar	600 × 100 × 50

The material properties for the fourth case study are summarized in Table A.12. Both materials have homogeneous k-values and their characteristics are independent of the temperature.

Table A.12. Thermophysical properties of materials: fourth case study

Component	Thermal conductivity (W/m.K)	Density (kg/m^3)	Specific heat capacity (J/kg.K)
Insulation	0.1	500	1700
Iron	50	7800	460

The warm side of the geometry was kept at the constant temperature of 1°C, with the convective heat transfer resistance being 0.1 m^2.K/W. The cold side had a constant temperature of 0°C and a convective heat transfer resistance of 0.1 m^2.K/W. The boundary condition for other boundaries was adiabatic (zero heat flux).

Figure A.14 illustrates the temperature distribution over the intended geometry. It can be seen that near the thermal bridge, the cold side temperature increases, which means that a higher heat flux is expected in this area.

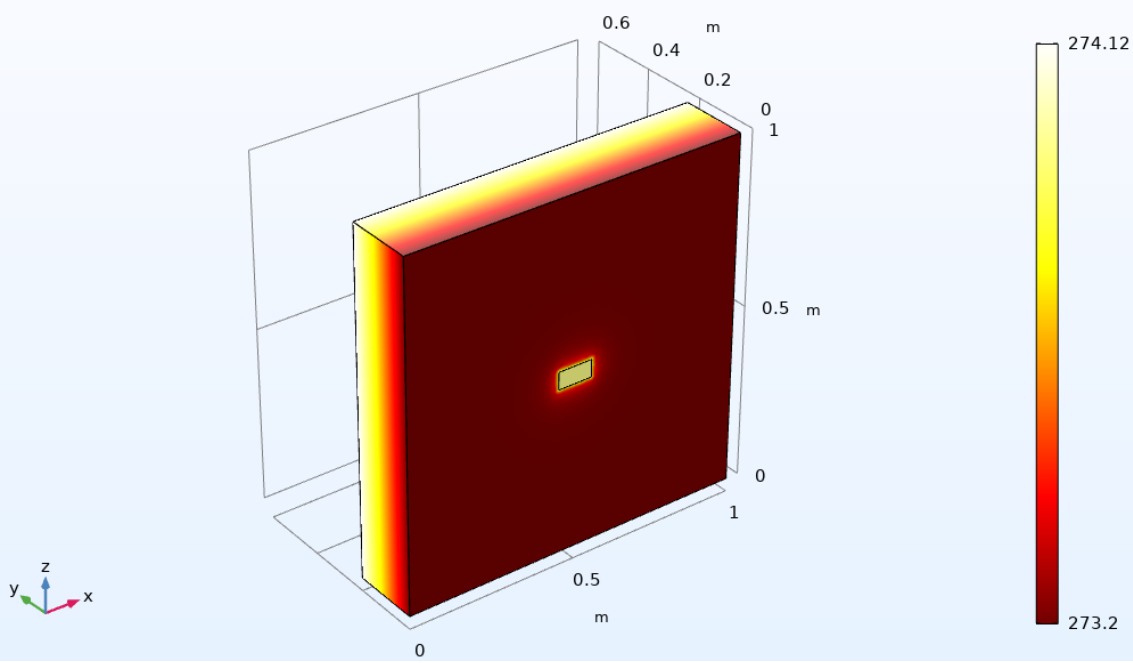

Figure A.14. Temperature distribution: fourth case study

Other parameters that were evaluated and compared with those presented in the ISO 10211 standard [62] were the heat flow from the interior side to the exterior side and the maximum temperature on outside surface. Table A.13 shows the comparison results. Given that the maximum

allowable difference was 1%, the results of the COMSOL Multiphysics © simulation for this case can be considered valid.

Table A.13. Numerical and reference heat flux and maximum exterior surface temperature values: fourth case study

Parameter	ISO standard values	Numerical result	Difference
Maximum temperature on cold side surface (°C)	0.805	0.8015	3.5×10^{-3}
Heat flux	0.540 W	0.5415 W	0.30%

A.5. Summary

Considering that COMSOL Multiphysics © software was able to generate satisfying results for the cases presented in ISO 10211 standard [62], it is concluded that the software is capable of performing simulations for the assessment of thermal bridging effect. In the following section, the methodology for assessing the effects of thermal mass and wall configurations on the transient thermal performance of three case study walls will be presented.